ORGANIZATION AND DYNAMICS OF CYTOSKELETAL NETWORKS OF FTSZ AND ITS CROSSLINKERS

by

Paulo Caldas

September, 2020

A thesis presented to the Graduate School of the
Institute of Science and Technology Austria, Klosterneuburg, Austria
in partial fulfillment of the requirements for the degree of
Doctor of Philosophy

The thesis of Paulo Caldas titled *Organization and Dynamics of Treadmilling Filaments in Cytoskeletal Networks of FtsZ and its Crosslinkers*, is approved by:

Supervisor

Martin Loose, IST Austria, Klosterneuburg, Austria

Signature: _____

Committee Member

Anna Kicheva, IST Austria, Klosterneuburg, Austria

Signature: _____

Committee Member

Julie Plastino, Institut Curie, Paris, France

Signature: _____

Defense Chair:

Edouard Hannezo, IST Austria, Klosterneuburg, Austria

Signature: _____

(signed page is on file)

ISBN: 978-3-99078-009-1

IST Austria Thesis, ISSN: 2663-337X

I hereby declare that this thesis is my own work and that it does not contain other people's work without this being so stated; this thesis does not contain my previous work without this being stated, and the bibliography contains all the literature that I used in writing the dissertation. I declare that this is a true copy of my thesis, including any final revisions, as approved by my thesis committee, and that this thesis has not been submitted for a higher degree to any other university or institution. I certify that any republication of materials presented in this thesis has been approved by the relevant publishers and co-authors.

Signature: _____

Paulo Caldas

September, 2020

(signed page is on file)

Abstract

During bacterial cell division, the tubulin-homolog FtsZ forms a ring-like structure at the center of the cell. This so-called Z-ring acts as a scaffold recruiting several division-related proteins to mid-cell and plays a key role in distributing proteins at the division site, a feature driven by the treadmilling motion of FtsZ filaments around the septum. What regulates the architecture, dynamics and stability of the Z-ring is still poorly understood, but FtsZ-associated proteins (Zaps) are known to play an important role.

Advances in fluorescence microscopy and *in vitro* reconstitution experiments have helped to shed light into some of the dynamic properties of these complex systems, but methods that allow to collect and analyze large quantitative data sets of the underlying polymer dynamics are still missing.

Here, using an *in vitro* reconstitution approach, we studied how different Zaps affect FtsZ filament dynamics and organization into large-scale patterns, giving special emphasis to the role of the well-conserved protein ZapA. For this purpose, we use high-resolution fluorescence microscopy combined with novel image analysis workflows to study pattern organization and polymerization dynamics of active filaments. We quantified the influence of Zaps on FtsZ on three different spatial scales: the large-scale organization of the membrane-bound filament network, the underlying polymerization dynamics and the behavior of single molecules.

We found that ZapA cooperatively increases the spatial order of the filament network, binds only transiently to FtsZ filaments and has no effect on filament length and treadmilling velocity. Our data provides a model for how FtsZ-associated proteins can increase the precision and stability of the bacterial cell division machinery in a switch-like manner, without compromising filament dynamics.

Furthermore, we believe that our automated quantitative methods can be used to analyze a large variety of dynamic cytoskeletal systems, using standard time-lapse movies of homogeneously labeled proteins obtained from experiments *in vitro* or even inside the living cell.

Acknowledgments

First and foremost, I would like to thank my supervisor, Martin Loose, for the opportunity that he gave me to work with his favorite protein and build my phd project on top of his most-relevant findings. I'm grateful for his guidance, his encouraging words during frustrating moments and above all, the flexibility he gave me to organize my own agenda and shift my work towards a more computational field as my interests changed along the way. I was able to acquire a wide range of skills and get the gist of what it is to be a scientist.

Secondly, I want to acknowledge all the support from the Boehringer Ingelheim Fonds (BIF). I'm still amazed at how thoughtful the BIF team is and how much they care about their fellows. Besides their support to travel abroad and attend conferences, their "fellow seminars" were extremely helpful to improve our soft skills, explore career options, create a worldwide network and ultimately grow as a scientist. Being awarded with this PhD fellowship was definitely one of the highlights of my PhD.

I should also express my gratitude to the bioimaging facility at IST Austria, for their assistance with the TIRF setup over the years, and especially to Christoph Sommer, who gave me a lot of input when I was starting to dive into programming. Likewise, I would like to thank Daniel Pierce, from the University of Geneva, for his help with my spatial data analysis, his insight and criticism on my work in general, which helped me to improve my first manuscript significantly. Also, a word of appreciation to all Loose group members, for their helpful input over the years during our lab meetings, and specially to Mar, who was a key player in virtually all projects in the lab and the person to talk to during times of struggle.

Finally, more on a personal note, I would like to address my family and friends at home - who supported me in many aspects of my life even thousands of miles away - Patricia Rodrigues - not only for her help when she was a rotation student in our lab, but mainly for her friendship and for making home less distant over the last 2 years - and of course, my CrossFit buddies in Vienna - who have helped me to find an escape from work and preserve my mental health over the years. They definitely made the whole journey much more pleasant.

About the Author

Paulo Caldas completed his BSc and MSc in Biochemistry at the Faculty of Sciences, University of Lisbon, before joining IST Austria in September 2015. During his MSc studies, he carried out classic biochemistry experiments involving spectroscopy and quantitative data analysis, working on a project focused in amyloid cytotoxicity mechanisms. For his PhD, he joined Martin Loose lab to continue with biochemistry and molecular biology experiments and get into fluorescence microscopy.

His PhD project concerned the spatial regulation of the Z-ring, an essential structure that guides cell division in most bacteria. His main goal was to reconstitute *in vitro* the dynamic behavior of different cytoskeletal proteins and study how they work together to increase the precision of cell division in bacteria. His work involved extensive quantitative image analysis and statistical modeling often requiring employing custom-made scripts in programming languages.
For the duration of his PhD, Paulo was a recipient of a Boehringer Ingelheim Fonds (BIF) PhD Fellowship. He presented and discussed his results at several international conferences and two papers came out of his PhD.

List of Publications

1. Paulo Caldas, Mar López-Pelegrín, Daniel J. G. Pearce, Nazmi Burak Budanur, Jan Brugués and Martin Loose (2019). **Cooperative ordering of treadmilling filaments in cytoskeletal networks of FtsZ and its crosslinker ZapA.** Nature Communications. Vol 10, p. 5744.
   https://doi.org/10.1038/s41467-019-13702-4
   [Caldas *et al.*, 2019]

2. Paulo Caldas, Philipp Radler, Christoph Sommer and Martin Loose (2020). **Computational analysis of filament polymerization dynamics in cytoskeletal networks.** Methods in Cell Biology. Vol 158, p. 145-161.
   https://doi.org/10.1016/bs.mcb.2020.01.006
   [Caldas *et al.*, 2020]

3. Keisuke Ishihara, Franziska Decker, Paulo Caldas, James F. Pelletier, Martin Loose, Jan Brugués, Timothy J. Mitchison. **Spatial Variation of Microtubule Depolymerization in Large Asters Suggests Regulation by MAP Depletion.** BioRxiv.
   https://www.biorxiv.org/content/10.1101/2020.06.26.172783v2
   [Ishihara *et al.*, 2020]

Table of Contents

Abstract i

Acknowledgments iii

About the Author v

List of Publications vii

List of Figures xiv

List of Tables xv

List of Movies xvii

List of Abbreviations xxi

1 Introduction 1

1.1 Towards *in vitro* Reconstitution of Bacterial Cytokinesis 2

1.2 Overview of the Bacterial Cell Division Machinery 3

1.2.1 Spatial Regulation: Finding the Center 6

1.2.2 Temporal Regulation: Assembling the Complex 7

1.2.3 Depicting Z-ring Architecture and Dynamics 9

1.3 A Brief History of the Bacterial Cytoskeleton 10

1.3.1 The Z-ring and Other Cytoskeletal Elements 10

1.3.2 Understanding FtsZ Polymerization 12

1.3.3 GTP Hydrolysis and Mechanical Force 15

1.3.4 The Treadmilling Era 16

1.4 The Architecture of a Robust Signaling Hub 18

1.4.1 Bundling FtsZ Filaments 19

1.4.2 Crosslinking FtsZ Filaments 20

1.4.3 Shaping the Signal Across the Membrane 24

2 Scope of this Work 27

3 Quantification of the Large-Scale Organization of Cytoskeletal Networks of FtsZ Filaments **29**

3.1 Bundle Thickness Estimation and the Effect of ZapA 31

3.2 Architecture Analysis and the Effect of ZapA 34

3.2.1 Curvature of the FtsZ Filaments Network 36

3.2.2 Spatial Order of the FtsZ Filaments Network 37

3.3 Re-organization Dynamics and the Effect of ZapA 39

3.4 Large-Scale Organization of FtsZ Filaments in the Presence of ZapB, ZapC and ZapD 41

3.4.1 Inhibitory Effect of ZapB on ZapA Activity 41

3.4.2 The Effect of ZapC and ZapD on FtsZ Filaments 43

4 Analysis of Filament Polymerization Dynamics in Cytoskeletal Filament Networks **47**

4.1 Differential Imaging Protocol 49

4.2 FtsZ Treadmilling Velocities in the Presence of ZapA 52

4.3 FtsZ Filament Polarity in the Presence of ZapA 54

4.4 Spatial Regulation of Microtubule Depolymerization 56

5 Behavior of Single Molecules in Cytoskeletal Networks of FtsZ Filaments **59**

5.1 Turnover Rate of FtsZ Filaments in the presence of ZapA 59

5.2 Turnover Rate of ZapA when Binding to FtsZ Filaments 61

5.3 Underlying FtsZ Dynamics in the Presence of ZapC 62

6 Material & Methods **67**

6.1 Reagents and Chemicals 67

6.2 Protein Biochemistry 67

6.2.1 Purification of FtsZ 67

6.2.2 Purification of FtsA 68

6.2.3 Purification of ZapA and Mutants 69

6.2.4 Purification of ZapB 70

6.2.5 Purification of ZapC 71

6.2.6 Purification of ZapD 72

6.3 Self-organization assay and Imaging 74

6.3.1 Preparation of small unilamellar vesicles 74
6.3.2 Preparation of reaction chamber 74
6.3.3 Preparation of supported lipid bilayers and experiments 75
6.3.4 Fluorescence Microscopy 76
6.4 Lifetimes Estimation 76
6.4.1 Fluorescence Recover After Photo Bleaching (FRAP) 76
6.4.2 Single Molecule Tracking (SMT) 77
6.5 Image Analysis and Code Availability 78
6.5.1 Bundle Width Estimation 78
6.5.2 Architecture Analysis 79
6.5.3 Image Autocorrelation Analysis 79
6.5.4 Quantification of Filament Polymerization Dynamics 80
6.6 Modeling and Bootstrapping Confidence Intervals 81
6.7 Statistical Analysis 83

7 Discussion **87**

List of Figures

1.1 *In vitro* reconstitution approaches 2
1.2 Bacterial cytokinesis overview 5
1.3 Organization of the divisome 8
1.4 Architecture of Z-ring *in vivo* 10
1.5 Three conformations of FtsZ proto-filaments *in vitro* 14
1.6 Treadmilling FtsZ filaments are coupled to the cell wall synthesis . . 18
1.7 Bundling and crosslinking of FtsZ filaments 20
1.8 Macromolecular structures of Zap proteins in *Escherichia coli* 21
1.9 ZapA effect on FtsZ filament organization *in vitro* and *in vivo* 24

3.1 ZapA modulates FtsZ filament network organization *in vitro* 30
3.2 ZapA induces bundling of membrane-bound FtsZ filament bundles . . 32
3.3 Tetramerization is essential for ZapA function 33
3.4 ZapA changes the architecture of FtsZ filament bundles 35
3.5 ZapA stabilizes FtsZ filament bundles 40
3.6 ZapB prevents ZapA activity 42
3.7 ZapC shows a distinct architecturethen ZapA 44
3.8 ZapD pellets FtsZ but has no effect on the self-organization assay . . 46

4.1 Treadmilling speed quantification using kymographs 48
4.2 Treadmilling analysis protocol 51
4.3 ZapA does not change treadmilling speed of FtsZ filaments 54
4.4 ZapA does not change orientation nor length of FtsZ filaments 55
4.5 Measurement of MTs dynamics using differential image protocol . . . 58

5.1 ZapA binds only transiently to FtsZ filaments. 60
5.2 ZapC decreases the treadmilling speed of FtsZ bundles 64

6.1 FRAP experiments 77
6.2 Single molecule tracking experiments 78
6.3 Orientation field and curvature of FtsZ filament network 80
6.4 Hill coefficients and bootstrapping 82

7.1 Influence of ZapA and its role for Z-ring maturation 90

List of Tables

5.1 Pattern quantification with WT or Cy5-labelled ZapA 62
5.2 Summary of ZapA effect on FtsZ filament network 63

6.1 Hill coefficients and bootstrapping parameters for ZapA titrations . . 83
6.2 Statistical significance matrix for ZapA quantifications 84
6.3 Statistical significance matrix for ZapC quantifications 85

List of Movies

Movie Repository:
https://figshare.com/s/fb5b7dea2115ab3eb036

Movie 1 Time-lapse movie (raw data) of our self-organization assay showing FtsZ (gray) pattern emerging from its interaction with FtsA (unlabeled) alone. The architecture of these FtsZ/FstA co-filaments is typically characterized by dynamic networks of curved filament bundles, forming streams and vortexes. All the components were added to the reaction buffer (50mM Tris-HCl pH=7.5, 150mM KCl, 5mM $MgCl_2$) prior to the addition of 4mM of GTP, which triggers FtsZ polymerization. Images were acquired using a TIRF microscope setup (typically one image every 2 seconds). See Fig. 3.1 for more details regarding the experimental setup.

Movie 2 Time-lapse movie (raw data) of our self-organization assay showing FtsZ pattern emerging from its interaction with FtsA and 6μM ZapA. FtsZ network organized into a network of thicker and longer filament bundles seemingly more aligned and straightened when compared with FtsZ alone. See Movie 1 caption for more details.

Movie 3 Time-lapse movie (raw data) of our self-organization assay showing FtsZ pattern emerging from its interaction with FtsA in the presence of 0.5μM (left), 1.5μM (center) or 3.0μM (right) ZapA. Increasing concentrations of ZapA progressively increased the thickness of the FtsZ filament bundles and decreased its curvature. See Movie 1 caption for details.

Movie 4 Time-lapse movie (raw data) of our self-organization assay showing FtsZ pattern emerging from its interaction with FtsA in the presence of 6μM ZapA R46A (left) and 6μM ZapA I83E (right). Mutants had no significant effect on the architecture and dynamics of FtsZ filament bundles. See Movie 1 caption for details.

Movie 5 Time-lapse movies (raw data) showing the inhibitory effect of ZapB on ZapA. Top row shows the effect of 1μM, 2μM and 6μM ZapB on 3μM ZapA (from

left to right). Bottom row shows the effect of 3μM, 6μM and 12μM ZapB on 6μM ZapA (from left to right). ZapB prevented ZapA effect when [ZapB] >> [ZapA]. See Fig. 3.6 for details.

Movie 6 Time-lapse movie (raw data) of our self-organization assay showing FtsZ pattern emerging from its interaction with FtsA and 1μM ZapC. FtsZ network organized into a carpet-like network of filament bundles seemingly more aligned and straightened, although with a different architecture than the one observed for ZapA (Movie 2). See Fig. 3.7 for details.

Movie 7 Time-lapse movie (raw data) of our self-organization assay showing FtsZ pattern emerging from its interaction with FtsA, 1μM ZapC and 3μM ZapA. The architecture of FtsZ filament bundles emerged as a combination of ZapA and ZapC effects when alone. See Fig. 3.7 for details.

Movie 8 Time-lapse movie (raw data) of our self-organization assay showing FtsZ pattern emerging from its interaction with FtsA and 6μM ZapD. ZapD had no effect on the FtsZ filament network. See Fig. 3.8 for details.

Movie 9 Time-lapse movie of raw image (gray) overlaid with fluorescent spots (resultant from our differential imaging protocol) corresponding to growing (green) and shrinking (magenta) ends of FtsZ/FtsA filament bundles. Differential imaging allows to visualize and track FtsZ polymerization dynamics. See section 4.1 and Fig. 4.2 for more details.

Movie 10 Time-lapse movie of raw image (gray) overlaid with fluorescent spots (resultant from our differential imaging protocol) corresponding to growing (green) and shrinking (magenta) ends of FtsZ/FtsA filament bundles in the presence of 6μM ZapA. Speed of treadmilling filaments remained unchanged when compared to FtsZ/FtsA alone. See section 4.1 and Fig. 4.2 for more details.

Movie 11 TIRF time lapse movie of microtubules containing Alexa647-labelled tubulin (gray) localized at the interior of the FOV. Differential imaging allows to visualize and track growing (cyan) and shrinking (red) events during aster growth. See Fig. 4.5 and section 4.1 for more details.

Movie 12 TIRF time lapse movie of microtubules containing Alexa647-labelled tubulin (gray) localized at the periphery of the FOV. Differential imaging allows to visualize and track growing (cyan) and shrinking (red) events during aster growth. See Fig. 4.5 and section 4.1 for more details.

Movie 13 Typical FRAP experiments on FtsZ filament network (gray) without (left) and with (center) 6μM ZapA. FRAP experiments performed directly on Cy5-labelled ZapA (magenta, right) revealed a much faster recovery time. See Fig. 5.1 and Fig. 6.1 for more details.

Movie 14 Typical Singe-molecule tracking (SMT) experiments on FtsZ (red) without (left) and with (center) 6μM ZapA. SMT experiments performed with Cy5-labelled ZapA (magenta, right) revealed a much shorter lifetime. See Fig. 5.1 and Fig. 6.2 for more details.

Movie 15 Dual-color time lapse movie showing FtsZ (Alexa488-FtsZ, gray) co-localization with ZapA (ZapA-Cy5, magenta). See Fig. 5.1 for more details.

Movie 16 Dual-color time lapse movie showing FtsZ (Alexa488-FtsZ, gray) co-localization with ZapC (ZapC-GFP, green). See Fig. 5.2 for more details.

List of Abbreviations

ADP: Adenosine Diphosphate

ATP: Adenosine Triphosphate

DOPC 1,2-dioleoyl-sn-glycero-3-phosphocholine

DOPG 1,2-dioleoyl-sn-glycero-3-phospho-(1‘-rac-glycerol)

DTT Dithiothreitol

EDM Eucledean Distance Mapping

FRAP Fluorescence Recovery After Photobleaching

FRET Fluorescence Resonance Energy Transfer

Fts Filamentous Temperature Sensitive

GDP Guanosine Diphosphate

GMPCPP Guanylyl-(alpha, beta)-methylene-diphosphonate

GTP Guanosine Triphosphate

GUVs Giant Unilamellar Vesicles

IPTG Isopropyl-”-D-1-thiogalactopyranosid

$MgCl_2$ Magnesium Chloride

MSD Mean Square Displacement

MTs Microtubules

MTOC Microtubules Organizing Center

PALM Photo Activated Localization Microscopy

PIPES Piperazine-N,N’-bis (ethanesulfonic acid)

SLBs Supported Lipid Bilayers

SMT Single Molecule Tracking

STED STimulated Emission Depletion microscopy

SUVs Small Unillamelar Vesicles

SUMO protein Small Ubiquitin-related MOdifier protein

Ter Macrodomain Termination of DNA replication

TIRF Total Intern Reflection Fluorescence

Tris-HCl tris(hydroxymethyl)aminomethane hydrochloride

Ulp1 Ubiquitin-like-specific protease 1

Chapter 1

Introduction

Bacteria are everywhere. They have been around for 3.5 billion years, they are the oldest living organism on the planet and the most abundant life form on Earth. They exist on almost every environment, soils, plants, ocean depths, on the food that we eat and inside our gut. Hundreds of different bacteria species are living inside of us right now. They can be harmful or extremely beneficial for many life forms on the planet, including ours. They come in different shapes and flavors according to their abilities. We have known them for roughly 400 years now, since there were first seen by Antoni van Leeuwenhoek on samples of pond water and saliva. However, only recently we have begun to understand how bacteria influence everything that surrounds us and how they support life on earth. Better understanding how bacteria divide and multiply is of great interest, not only to help fight the harmful species, but also to benefit as much as possible from the good ones.

Bacteria have a simple life. They have a single piece of DNA spread in the cytosol, typically involved in a soft cell membrane and a rigid cell wall composed of peptidoglycan. They spend most of their lifetime absorbing nutrients from their surroundings to duplicate their size and genetic material so that they can cut themselves in half and generate two nearly-equal daughter cells. For efficient cell division, bacteria must accomplish the challenging task of continuously maintaining their structural integrity while the cellular membrane constricts and new cell wall material is inserted. Regardless of their seemingly simple internal organization, it is now clear that these microorganisms rely on a highly structured yet dynamic intracellular architecture to perform essential biological functions, including cytokinesis. This complexity was primarily thought to be limited to eukaryotic cells, but advances in fluorescence microscopy and the use of fluorescent fusion proteins during the past three decades completely changed the way we look at bacteria.

1.1 Towards *in vitro* Reconstitution of Bacterial Cytokinesis

Understanding the mechanisms underlying complex intracellular biological processes is often hard to decipher when studied inside living cells, particularly for tiny cells such bacteria. The intrinsic complexity of regulatory protein networks and redundancies inside cells can substantially limit their functional characterization. Inhibiting or deleting specific components can often be compensated by other components with overlapping functions or by an additional backup system, which masks relevant functions of potential key players. Besides, fluorescence labelling can perturb the functionality or localization of proteins *in vivo* in some situations. [Fletcher and Geissler, 2009; Liu and Fletcher, 2009].

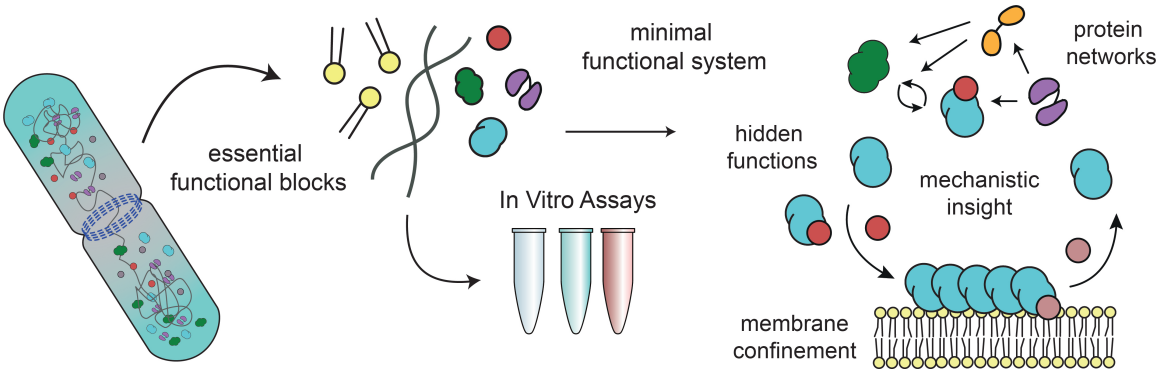

Figure 1.1: *In vitro* reconstitution approaches. Biochemical *in vitro* reconstitution approaches rely on purified components, such as proteins and DNA, and can be used to study protein network interactions in great detail, helping to shed light into complex underlying mechanisms, probe hidden functionalities and test hypothesis.

In the last two decades, reconstitution approaches have overcome some of these limitations and provided remarkable insight in understanding dynamic protein-protein interactions that give rise to different cellular functions, both in prokaryotic and eukaryotic cells (Fig. 1.1). Cell-free systems can be used to study the behavior of a single protein in solution or build up to much more complex reaction vessels containing multiple proteins, nucleic acids and biomimetic membranes. This approach provides an ideal platform to find the minimal number of components required for a specific cellular function, elucidate the specific role of individual molecular players and to identify additional unknown functions or interaction partners.

Besides, *in vitro* reconstitution studies are often more suitable to meticulous quantitative analysis and mathematical modelling and for that reason can provide a level of detailed understanding that is often difficult to obtain from *in vivo* experiments

alone [Fletcher and Geissler, 2009; Liu and Fletcher, 2009].

Together with the advances in high resolution microscopy techniques, *in vitro* reconstitution of the bacterial cell division machinery have been particularly helpful due to its high dynamics and membrane-associated nature. Structural organization supported by artificial membranes can be study in nanoscopic detail using a variety of fluorescence microscopy techniques and atomic force microscopy (AFM) [Martos *et al.*, 2012]. The dynamic interaction between single molecules, either lipids or subunits of protein complexes, can be explored by techniques such as fluorescence after photobleaching (FRAP) and fluorescence resonance energy transfer (FRET), which are extremely informative methods, specially when combined with total internal reflection fluorescence (TIRF).

Significant demonstrations of the power of these bottom-up approaches include the reconstitution of protein dynamics related to the eukaryotic and bacterial cytoskeleton, such as the observation of dynamic instability of microtubules [Mitchison and Kirschner, 1984], microtubule transport driven by the molecular motor kinesin-1 [Howard *et al.*, 1989], DNA segregation mechanism by the actin homologue ParM [Garner *et al.*, 2007] or the ATP-driven self-organization of *Escherichia coli* Min proteins on supported lipid bilayers [Loose *et al.*, 2008; Loose and Schwille, 2009]. Recent studies have been able to reconstitute even more complex systems aiming towards the full reconstitution of a mitotic spindle [Roth *et al.*, 2019] or bacterial cell division [Martos *et al.*, 2012].

Many more experiments have been fundamental to our current understanding of the molecular processes underlying the cellular organization of the bacterial division machinery, otherwise hidden in the complexity of the living cell. Overall, *in vitro* reconstitution experiments have proven to be a valuable and complementary tool to address biological questions and to confirm or refine our mechanistic understanding of complex biological phenomena.

1.2 Overview of the Bacterial Cell Division Machinery

In most bacteria, cell division is performed by the divisome, a large multi-protein complex that assembles at mid-cell and spans from the cytosol to the outer membrane.

The mature divisome contains more than 30 known components in *Escherichia coli* that work together to regulate nucleoid segregation, peptidoglycan synthesis and septation. Divisome assembly is guided by a dynamic ring of FtsZ filaments, the so-called Z-ring (Fig.1.2). This structure forms at mid-cell early during the cell cycle, where it persists during the inward growth of the cell septum until it disassembles just before division is completed [Bi and Lutkenhaus, 1991; de Boer, 2010; Pichoff and Lutkenhaus, 2002; Soderstrom *et al.*, 2014; Coltharp and Xiao, 2017]. Polymeric FtsZ is anchored to the inner side of the cytoplasmic membrane by proteins such as FtsA, and stabilized by regulatory proteins such as ZapA during its assembly into a ring-like structure. This initial proto-ring functions as a signaling-hub to recruit of all the downstream late divisome components to the division site and form the mature divisome [Aarsman *et al.*, 2005; de Boer, 2010; Goehring and Beckwith, 2005; Margolin, 2005; Coltharp and Xiao, 2017] (Fig. 1.2). The composition of this cytokinetic apparatus varies across species, but a significant number of components and interactions are conserved. In *Escherichia coli*, at least 10 of these proteins are essential for cytokinesis as cells deprived of one of them fail to divide.

Importantly, FtsZ polymerization is GTP-dependent and powers the motion of filaments around the cell circumference by treadmilling [Loose and Mitchison, 2014; Bisson-Filho *et al.*, 2017; Yang *et al.*, 2017]. Furthermore, this treadmilling motion was found to guide the distribution of late division proteins involved in septal peptidoglycan (PG) synthesis to incorporate new cell wall material homogeneously around the septum [Bisson-Filho *et al.*, 2017; Yang *et al.*, 2017]. This is arguably the most remarkable feature of the divisome and has received special attention during the last couple of years.

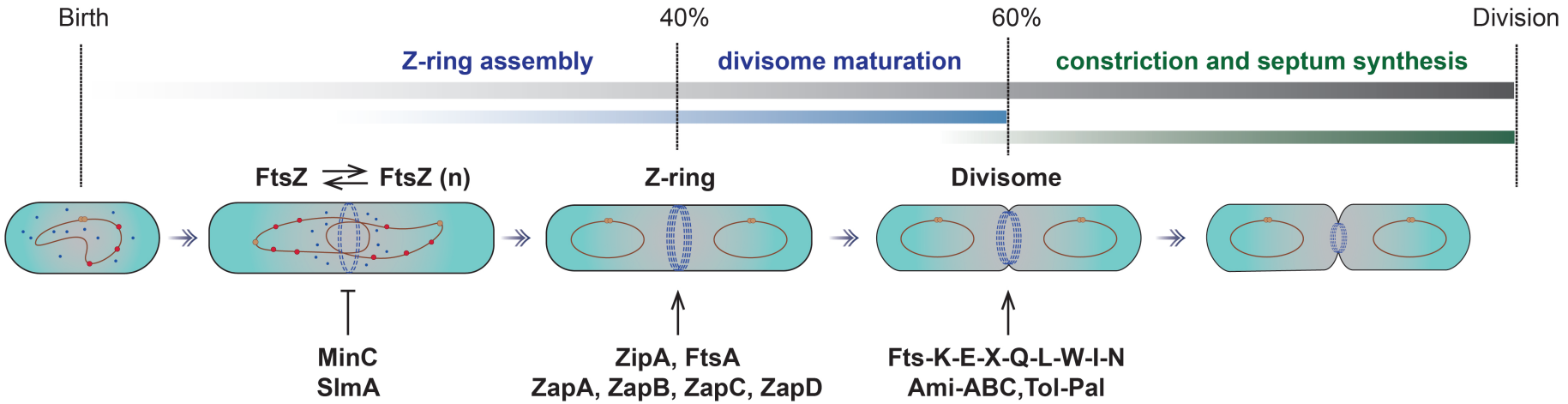

Figure 1.2: Bacterial cytokinesis overview. FtsZ localizes at midcell together with its membrane tethers, FtsA and ZipA, and self-organizes into a proto-Z-ring. MinC (MinCDE system, cyan gradient) and SlmA (NO system, red circles) ensure the correct position at the division site, preventing FtsZ polymerization at the cell poles and at the vicinity of the bacterial chromosome, respectively. Shortly after, Zap proteins are recruited to the division site and contribute to increase the stability of the Z-ring and the precision of cell division. Later, the remaining divisome components (late divisome proteins) are recruited to form the mature divisome. These include proteins such as FtsK, involved in chromosome segregation, FtsI, involved in cell wall synthesis, and regulatory proteins such as AmiA and AmiC, involved in the cleavage of septal peptidoglycan.

1.2.1 Spatial Regulation: Finding the Center

In *Escherichia coli*, two complementary regulatory mechanisms control the position of the Z-ring assembly: the MinCDE system [de Boer *et al.*, 1989; Pichoff and Lutkenhaus, 2001] and the nucleoid occlusion (NO) system [Bernhardt and De Boer, 2005; Wu and Errington, 2004]. Proteins of the Min system self-organize into a spatiotemporal oscillator to prevent polymerization of FtsZ at the cell poles, allowing Z-ring formation only at the cell center, where the concentration of MinC is poor (Fig. 1.2, cyan gradient). The nucleoid occlusion system is mediated by the DNA-binding protein and FtsZ polymerization inhibitor SlmA, which prevents ring assembly in the vicinity of the bacterial chromosome (Fig. 1.2, red circles). Overexpression of SlmA (or its homologue in *Bacillus subtilis*, Noc) produces elongated cells and its knockout leads to the formation of the Z-rings over unsegregated nucleoids, cutting the chromosome in two [Bernhardt and De Boer, 2005; Wu *et al.*, 2009]. These two negative regulatory systems give rise to a remarkable precision of FtsZ-ring formation, which happens at midcell position ± 2%.

Interestingly, protein homologues or a nucleoid occlusion system has not been observed in *Caulobacter crescentus*. Alternatively, an ATPase called MipZ binds to the chromosomal replication origin (oriC) and connects FtsZ polymerization to the initiation of chromosome at mid-cell [Espéli *et al.*, 2012]. In fact, this type of direct guidance where the chromosome itself provides positional information is also observed in *Escherichia coli* and *Bacillus subtilis* by a protein called MatP, a DNA binding protein that binds to the DNA replication terminus binding-site (Ter macrodomain) of the nucleoid [Mercier *et al.*, 2008; Rodrigues and Harry, 2012; Buss *et al.*, 2015]. Upon division, daughter cells quickly localize the Ter region to mid-cell, MatP organizes it into a specific macrodomain [Mercier *et al.*, 2008] and connects it to the Z-ring by the early division protein ZapA [Buss *et al.*, 2015]. This Ter-linkage produces a positive spatial regulation for the Z-ring positioning that may provide cytokinesis precision even in the absence of the two main negative regulatory systems, Min system and NO [Rodrigues and Harry, 2012].

1.2.2 Temporal Regulation: Assembling the Complex

In *Escherichia coli* and *Bacillus subtilis* the recruitment of divisome components occurs in two distinct temporal steps separated by a time lag of 10-20 min: (i) the arrival of early divisome proteins to midcell, e.g FtsZ, FtsA, ZipA and the regulatory protein ZapA, and (ii) the recruitment of late divisome components, e.g FtsK, FtsQLB, FtsW, FtsI (PBP3) and FtsN (Fig. 1.2). Each protein requires the localization of upstream factors for its localization, revealing an extensive network of protein-protein and protein-membrane interactions existent within the divisome [Aarsman *et al.*, 2005; Gamba *et al.*, 2009]. In *Caulobacter crescentus* the pathway appears to be less linear as proteins are recruited to midcell as a series of functional modules, but most of the components are still conserved [Goley *et al.*, 2011].

The ability of FtsZ to assemble into a functional Z-ring relies on membrane anchors. In *Escherichia coli*, these are FtsA, an actin-homolog that binds to the membrane surface via C-terminal amphiphatic helix, and ZipA, a bitopic transmembrane protein [Pichoff and Lutkenhaus, 2002] (Fig. 1.3). FtsA is also conserved in *Bacillus subtilis*, *Caulobacter crescentus* and *Streptococcus pneumoniae*, but ZipA is restricted to gammaproteo bacteria [Alexeeva *et al.*, 2010; Du *et al.*, 2016; Pichoff *et al.*, 2018]. However, several other protein anchors may replace the role of ZipA, such as EzrA and SepF in *Baccilus subtilis* and FzlC in *Caulobacter crescentus* [Duman *et al.*, 2013; Haeusser *et al.*, 2007; Meier *et al.*, 2016].

Simultaneously, a variety of FtsZ-associated proteins (Zaps) interact with FtsZ proto filaments and are thought to contribute to the precision of cell division by modulating Z-ring stability and architecture [Ortiz *et al.*, 2015] (Fig. 1.3). These proteins are ZapA, ZapB, ZapC and ZapD in *Escherichia coli* [Durand-Heredia *et al.*, 2011; Durand-Heredia *et al.*, 2012; Gueiros-Filho and Losick, 2002], but only ZapA is conserved in other species such as *Bacillus subtilis*, *Caulobacter crescentus* and *Streptococcus pneumoniae* [Goley *et al.*, 2011; Gueiros-Filho and Losick, 2002; Maggi *et al.*, 2008].

Late divisome proteins arrive at midcell with different time lags (Fig. 1.2). These include regulatory lipoproteins, e.g LpoA and LpoB, amidases involved in the cleavage of septal peptidoglycan, e.g AmiA, and AmiC, and enzymes required to synthesize septal cell wall, e.g PBP1B and PBP3 [Pazos *et al.*, 2018]. These components do

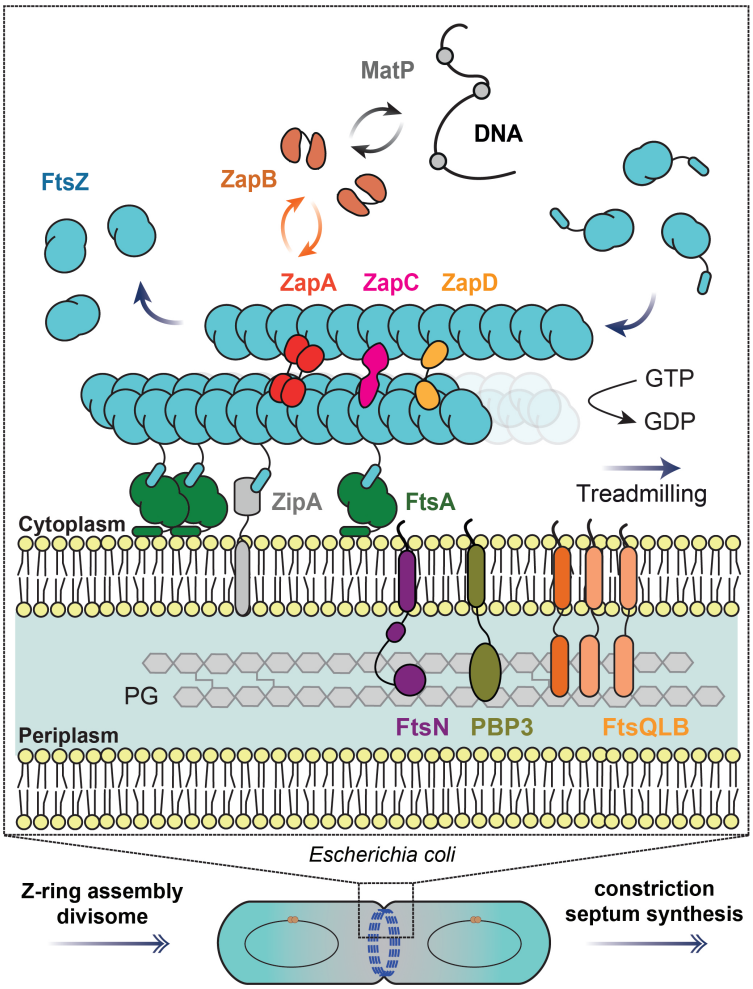

Figure 1.3: Organization of the divisome. Illustration of the protein network involved in bacterial cytokinesis. For simplicity, only a few components are depicted. ZipA and FtsA tether treadmilling FtsZ protofilaments bundles to the membrane using flexible linkers, either a transmembrane segment (in the case of ZipA) or an amphipathic helix (in the case of FtsA). Zap proteins promote stability of the Z-ring by crosslinking protofilaments. MatP, ZapB and ZapA are organized in multiple layers that span the region between the nucleoid and the cytoplasmic membrane. This system seem to prevent the formation of a Z-ring at midcell as long as the nucleoid resides at this cellular location. The arrival of FtsN at the septum activates PG synthesis, which results from a complex interaction between the FtsN and other divisome components, including FtsA and FtsQLB.

not interact with FtsZ directly. Septal PG synthases interact with each other and with other divisome components such as FtsN and FtsW. FtsN has special interest as it seems to have an important role in the activation of the divisome by integrating different signals from the cytoplasmic and periplasmatic proteins [Corbin *et al.*, 2004; Rico *et al.*, 2004]. FtsN and FtsQ can be recruited by FtsA [Alexeeva *et al.*, 2010; Busiek *et al.*, 2012; Baranova *et al.*, 2020] and ZipA interacts directly with PBP1b [Pazos *et al.*, 2018], suggesting that these two proteins can function as linkers between early and late divisome proteins. Moreover, FtsQ interacts with large number of other cell division proteins FtsA, FtsK, FtsL, FtsW, FtsI, FtsN FtsQ, providing another structural link between the two steps of divisome assembly [Karimova *et al.*, 2005].

FtsK, also widely conserved, acts as a double-strand DNA translocase to regulate chromosome segregation. It binds FtsZ directly and evidence suggests that stabilizes the divisome before septation [Sherratt *et al.*, 2010]. Most of these proteins contain a transmembrane helix and a periplasmic domain.

Several interactions between these and other proteins create a complex protein network that connects the inner and outer membrane, coordinating the invagination of the envelope layers. However, the role of many of these interactions as well as the specific function of most of these components are still elusive.

1.2.3 Depicting Z-ring Architecture and Dynamics

Over the past decade, advances in high resolution imaging have changed our understanding of the Z-ring. In contrast to what was observed by conventional fluorescence microscopy (Fig. 1.4A,B), FtsZ filaments are not packed into a continuous ring [Bi and Lutkenhaus, 1991; Erickson *et al.*, 1996] but rather organized into discontinuous loosely associated disordered FtsZ clusters [Buss *et al.*, 2013; Fu *et al.*, 2010; Li *et al.*, 2007] (Fig. 1.4C). This was first observed in *Caulobacter crescentus* using Cryo-EM, where a few irregular spaced arcs of FtsZ were detected but no complete Z-rings [Li *et al.*, 2007], and later in *Escherichia coli* using super resolution microscopy, where the Z-ring appeared as a discontinuous structure made of heterogeneously clusters around the cell waist [Fu *et al.*, 2010; Lyu *et al.*, 2016]. Since then, several other super-resolution microscopy methods have confirmed this nanoscale organization of the Z-ring in different bacteria [Biteen *et al.*, 2012; Buss *et al.*, 2013; Holden *et al.*, 2014; Huecas *et al.*, 2017; Lyu *et al.*, 2016; Rowlett and Margolin, 2014]. Furthermore, other studies have shown that a complete Z-ring is not required for constriction in some species [Leisch *et al.*, 2016; Yao *et al.*, 2017]. In this scenario, short dynamic FtsZ filaments are enough to drive peptidoglycan synthesis and constriction.

Together, these findings portray cell division in bacteria as a highly dynamic process guided by the polymerization of FtsZ, which is tightly regulated in space and time by a variety of proteins (Fig. 1.2 and Fig. 1.3). FtsZ filaments are organized into patches (Fig. 1.4) that treadmill around the septum to assist cell wall synthesis (discussed later on).

It has become clear that sophisticated biochemical networks are involved in each one of these steps, but we still have to uncover most of the underlying mechanistic principles. Central questions remained to be answered, in particular how different players modulate the properties of the Z-ring and how the signal is integrated and transmitted across the membrane to guide PG enzymes.

In the next section, we briefly describe how our knowledge have evolved over the years to shape our current view of the Z-ring structure and dynamics, highlighting the importance of *in vitro* reconstitution experiments for that purpose.

1.3 A Brief History of the Bacterial Cytoskeleton

1.3.1 The Z-ring and Other Cytoskeletal Elements

In the late 60s, light microscopy studies in *Escherichia coli* revealed that dividing bacterial cells formed a septum at mid-cell triggered by an invagination of the cytoplasmic membrane and ingrowth of the cell wall [Hirota *et al.*, 1968; Van De Putte *et al.*, 1964]. Following this observation, researchers used conditional alleles that blocked septum formation at high temperatures to identify the proteins required for cell division [Hirota and Matthieu, 1973; Lutkenhaus *et al.*, 1980]. These experiments allowed to obtain a long list of proteins specifically involved in cell division based on the observation that cells lacking one of these genes failed to divide and formed mult-

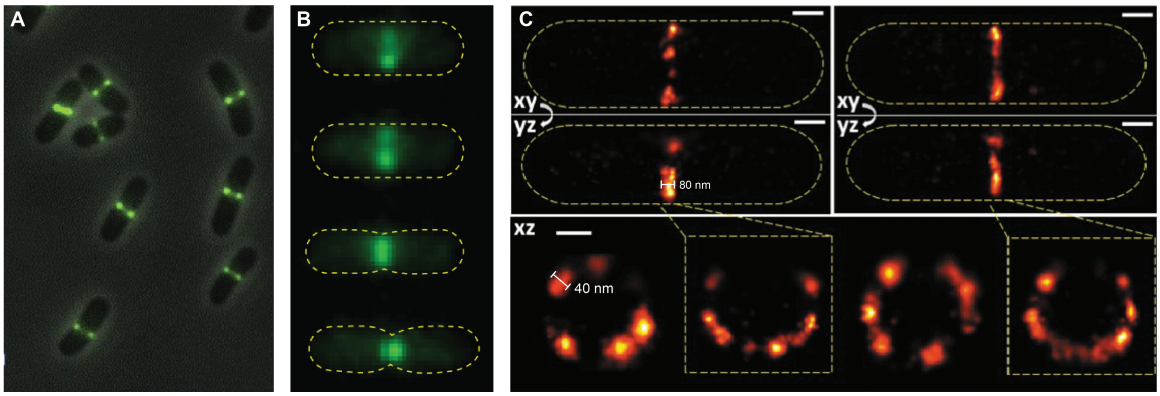

Figure 1.4: Architecture of Z-ring *in vivo*. **(A)** Images of FtsZ–GFP in wild type *E. coli* cells. The filaments are presumed to be aligned in parallel based on the directional movement seen in bundles and patches. Adapted from [Du and Lutkenhaus, 2019]. **(B)** Fluorescence images of FtsZ-GFP (green) in live *E. coli* cells. Cell outlines are approximated by yellow dashed lines. Adapted from [McQuillen and Xiao, 2020]. **(C)** Representative 3D PALM images of two-dimensional projections of live *Escherichia coli* cells expressing FtsZwt-mEos. Upper, xy-plane and yz-plane projections. Lower, xz-plane projections (cross-section). Cell outlines are approximated by yellow dashed lines in the top panel, with the corresponding Z-rings outlined in dashed boxes in the panel below. scale bar = 200 nm. Adapted from [Lyu *et al.*, 2016].

inucleated filamentous cells, even when chromosome segregation and replication was still possible. Among these genes, ftsZ was of great interest. It was essential for cytokinesis, acting before any other component and restricting the frequency of cell division [Bi and Lutkenhaus, 1991]. Later, electron microscopy in conjunction with immunogold staining revealed that FtsZ product was distributed in a ring-like arrangement and localized at the leading edge of the division septum [Bi and Lutkenhaus, 1991], subsequently referred to as the Z-ring. This ring-like architecture was confirmed later in GFP-labelling studies with FtsZ and FtsA [Addinall and Lutkenhaus, 1996; Ma *et al.*, 1996; Ma and Margolin, 1999]. These studies also showed that FtsA has a similar arrangement and position than the one observed for FtsZ, which presented the first evidence for the interaction between these two proteins.

These findings were a breakthrough in the field as they not only provided a functional role for FtsZ as the key regulator in bacterial cytokinesis, but also suggested for the first time that bacteria also contain cytoskeletal elements to regulate morphogenesis, a feature that was thought to be exclusive to eukaryotic cells. Several years later, this idea was strengthened when FtsZ and FtsA crystal structures were solved, revealing a remarkable structural similarity with tubulin and actin, respectively [Löwe and Amos, 1998; Van den Ent *et al.*, 2002] despite their limited sequence conservation. However, significant differences exist in their organization, for instance FtsZ was not capable of assembling microtubules or showing dynamic instability [Mitchison and Kirschner, 1984]. Interestingly, FtsZ is also present in some chloroplasts and mitochondria [Beech *et al.*, 2000; Osteryoung and Vierling, 1995]. In fact, a variety of other bacterial proteins share the actin fold and its conformational plasticity, such as ParM and MreB [Ozyamak *et al.*, 2013]. Likewise, characteristics that are typically from eukaryotic intermediate filaments can also be found in bacteria, crescentin in *Caulobacter crescentus* [Ausmees *et al.*, 2003] and FilP in *Streptomyces* [Bagchi *et al.*, 2008] are two well-known examples, both with an important role in cell shape and integrity. Moreover, other types of spatial organization such as cell patterning and polarity were also discovered in bacteria [Dworkin, 2009; Treuner-Lange and Søgaard-Andersen, 2014]. All these traits have proven that bacteria, as their eukaryotic descendants, also own cytoskeletal elements and most likely a primitive eukaryotic cytoskeleton structure first arose in bacteria. Together, these findings led us to abandon the dogma that bacteria were simple tiny bags of floating

biomolecules and spatial organization was exclusively a eukaryotic feature. A new way to look at bacteria had begun.

These experiments have identified the genes and respective individual proteins involved in cytokinesis, as well as a first portrait of the molecular organization of the Z-ring. However, the underlying organization the proto-filaments and their interaction with other regulatory proteins remained difficult to study unambiguously using only *in vivo* experiments. As a result, over the years several cell-free experiments were crucial to help us answer some fundamental questions concerning the assembly of the Z-ring, namely the underlying polymerization dynamics of FtsZ filaments.

1.3.2 Understanding FtsZ Polymerization

Early *in vitro* reconstitution approaches, mostly electron microscopy and sedimentation assays, have shown that purified FtsZ is able to polymerize into proto-filaments [Bramhill and Thompson, 1994; Erickson *et al.*, 1996; Mukherjee and Lutkenhaus, 1998; Wang *et al.*, 1997]. Individual subunits of FtsZ interact longitudinally to form single strand proto-filaments in a head-to-tail fashion and can adopt a straight or a sharply curved conformations [Erickson *et al.*, 1996; Wang *et al.*, 1997; González *et al.*, 2003; Lu *et al.*, 2000; Mingorance *et al.*, 2001; Popp *et al.*, 2009] (Fig. 1.5A-D). These proto-filaments assemble into higher order structures such as tubes, sheets and mini rings, including protofilament pairing and formation of bundles. Straight conformations contained about 30 to 50 subunits with roughly 100-200 nm in length and circular structures 16 subunits with a 23-degree bend at each interface. The type of structures formed was dependent on protein concentration, pH, presence of divalent cations (calcium and magnesium), crowding agents [Popp *et al.*, 2009] and the type of nucleotide present [Lu *et al.*, 2000].

Assembly was still possible with either GMPCPP (nonhydrolyzable GTP) or GDP indicating that nucleotide hydrolysis is not required, however GTP hydrolysis was dependent on polymerization [Löwe and Amos, 2000; Lu *et al.*, 2000]. Further experiments showed that FtsZ tubes could be converted into sheets after exchange GDP with GTP. This provided the first evidence for a more favorable GTP-bound state when filaments are in a straight conformation, and a more favorable GDP-bound state when filaments are in a curved conformation [Lu *et al.*, 2000].

Some of these studies have suggested that FtsZ polymers could exchange nucleotides along the whole filament [Mingorance *et al.*, 2001] but GDP dissociation was shown to be much slower than polymer disassembly [Huecas *et al.*, 2007], suggesting that exchange occurs only at the filament ends and not within the polymer.

Importantly, at concentrations below 1μM FtsZ polymers were not detected, but after a small increase in this concentration, polymerization and GTP hydrolysis initiated abruptly [Mukherjee and Lutkenhaus, 1998; Oliva *et al.*, 2003; Romberg *et al.*, 2001]. This sharp critical concentration and unfavorable nucleation showed that FtsZ exhibits cooperative assembly. Later, several groups suggested that this cooperative behavior could be explained by the existence of two different conformations, one with high affinity for the polymer (open) and other with high affinity to maintain a monomeric state [Huecas *et al.*, 2008; Lan *et al.*, 2008]. More recently, X-ray crystallography provided structural evidence for existence of these two conformations, T (Tense) for high affinity and R (Relaxed) for low affinity [Matsui *et al.*, 2014; Fujita *et al.*, 2017]. The proposed mechanism suggests that FtsZ bound to GDP in solution can switch from the R to the T conformation after binding to GTP enabling the formation of straight filaments. Then the GTP hydrolysis forces the molecule to return to the relaxed state and form a curved filament. Together, these findings explain the cooperativity of FtsZ polymerization and the plasticity of the proto-filaments that experience cycles of assembly, GTP hydrolysis, disassembly, and nucleotide exchange.

The atomic structure of FtsZ was first determined using FtsZ from the thermophillic archaeon *Methanococcus jannaschii* and revealed a similar structural fold and GTP-binding site to tubulin [Löwe and Amos, 1998; Nogales *et al.*, 1998] (Fig. 1.5E). In both proteins, the catalytic domain is formed during filament assembly by the addition of a sequence region called T7 loop from the incoming subunit [Löwe and Amos, 1998; Oliva *et al.*, 2004] (Fig. 1.5D). This 40 kDa polypeptide contains a disordered N-terminal region (NTP), a globular core and a flexible highly charged C-terminal peptide (CCTP). The CCTP is subdivided into a highly conserved region (CTC) and a C-terminal variable (CTV) region [Wang *et al.*, 1997; Sossong *et al.*, 1999; Erickson *et al.*, 2010; Huang *et al.*, 2016b]. The globular core contains the nucleotide binding site and the essential alpha helix loop H7 [Wang *et al.*, 1997].

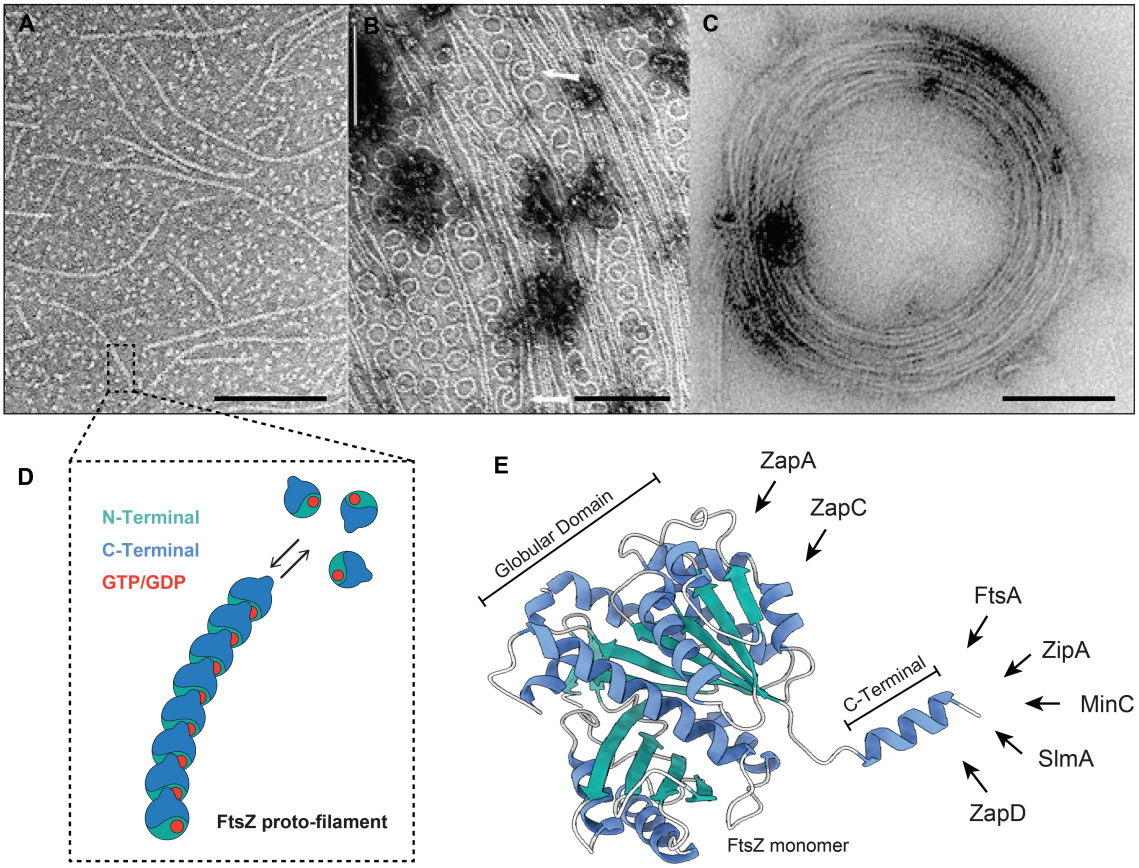

Figure 1.5: Three conformations of FtsZ protofilaments *in vitro*. **(A)** Proto-filaments assembled in the presence of GTP are mostly straight, although some have intermediate curvature. scale bar = 100 nm. **(B)** Proto-filaments assembled in the presence of GDP on a cationic lipid monolayer, show a highly curved miniring-like conformation (white arrows), mixed with straight conformations. scale bar = 500 nm. **(C)** A closer look at the architecture of rings in B. scale bar = 200 nm. Adapted from [Popp *et al.*, 2009]. **(D)** Illustration of one FtsZ proto-filament. FtsZ polymerizes in a head-to-tail fashion with GTP in the interface between subunits **(E)** Crystal structure of the *Methanocaldococcus jannaschii* FtsZ monomer bound to GTP (PDB: 1fsz). Different colors are respective to their secondary structure: helices in bue, β strands in green, and loops in gray. On the right are some of the proteins that interact with the C-terminal peptide of FtsZ to modulate its properties.

The C-terminal acts a central pivot able to interact with several division-related proteins [Buske and Levin, 2012; Huang *et al.*, 2016a]. These include players such as the membrane anchors FtsA and ZipA [Mosyak, 2000; Pichoff and Lutkenhaus, 2002], the inhibitors of FtsZ polymerization MinC and SlmA [Hu and Lutkenhaus, 1999; Pichoff and Lutkenhaus, 2001; Lutkenhaus, 2007], the crosslinking protein ZapD [Durand-Heredia *et al.*, 2012; Huang *et al.*, 2016a] and the ClpX moiety of the ClpXP protease involved in FtsZ degradation [Buczek *et al.*, 2016]. These proteins modulate FtsZ polymerization properties, inhibiting or promoting bundling of FtsZ, regulating Z-ring formation in space and time (Fig. 1.5E).

1.3.3 GTP Hydrolysis and Mechanical Force

The observation that GTP hydrolysis could power the transition from a straight to a highly curved conformation was key to suggest that FtsZ could convert this energy into mechanical forces [Lu *et al.*, 2000]. According to this idea, GTP hydrolysis would drive shortening and bending of membrane-attached polymers, generating a pinch on the inner side of the membrane [Li *et al.*, 2007; Lu *et al.*, 2000]. The rationale was supported by the fact that motor proteins are lacking in bacteria and most of the accessory division-related proteins are not highly conserved. Thus, the most conserved divisome component, FtsZ, should be critical to create an inward force to constrict the membrane.

Later other reconstitution *in vitro* experiments supported this idea by showing that an autonomously membrane-binding version of FtsZ was able to induce membrane deformations when captured inside tubular liposomes [Osawa *et al.*, 2008]. In this synthetic version of FtsZ, the C-terminal binding region for FtsA and ZipA was replaced with a membrane targeting sequence (MTS) from MinD, which made possible to bypass the need to native membrane anchors. The position of the membrane invaginations correlated with the position of FtsZ rings and rapidly relaxed when the system run out of GTP. This synthetic version of FtsZ was also able to produce multiple concave distortions when added to the outside of spherical liposomes [Osawa *et al.*, 2009]. Interestingly, when the MTS was attached to the N-terminal instead, convex protrusion were observed, in agreement with the idea of a bending force being generated in the direction of the outside curvature (front of the filament). More recently, encapsulation of native FtsZ inside giant liposomes with a hyperactive mutant of FtsA also showed vesicles contracting sporadically in a GTP-depend manner [Osawa and Erickson, 2013] and a similar observation was also made in vesicles containing ZipA-FtsZ filaments [Cabré *et al.*, 2013].

These studies have shaped the foundation for a model of membrane contraction where FtsZ drives the main inward force [Erickson and Osawa, 2010]. However, these experiments do not handle the fact that membrane anchors could influence the assembly dynamics of the proto-ring, due to the use an artificial membrane tether. In addition, membrane deformations were also observed in liposomes without FtsZ-rings - potentially caused by a crowing effect alone - and disappeared over time with no final

scission of the liposome. Moreover, other studies have shown that curvature of FtsZ filaments would not allow complete fission of a typical *Escherichia coli* cell diameter and their stiffness cannot generate enough force to pull the membrane inwards [Lan *et al.*, 2008; Lan *et al.*, 2009].

An alternative mechanism was later suggested, where FtsZ filaments could slide relative to one another to shrink the diameter of the ring [Szwedziak *et al.*, 2014]. In fact, this mechanism is not necessarily independent of the iterative-bending mechanism. Increasing lateral interaction between filaments should be thermodynamically advantageous, but kinetically unfavorable as all lateral bonds need to break and bind again as the filament slides. In disagreement with both models, FtsZ was found to disassemble from the division site before compartmentalization and mutants with impaired GTPase activity had no impact on cytokinesis rate [Coltharp *et al.*, 2016; Söderström *et al.*, 2016], showing that the GTPase activity of the Z-ring is not a limiting factor to achieve full constriction. Conversely, impairing cell wall synthesis via mutation to the enzyme FtsI (PBP3) substantially reduced the rate of constriction [Coltharp *et al.*, 2016].

Together, these findings pointed to a model where FtsZ filaments could potentially produce some degree of mechanical force to pinch the inner membrane, but cell wall synthesis seem to play the main role to achieve full septation.

1.3.4 The Treadmilling Era

Later, seeking to elucidate how membrane anchors could influence the assembly dynamics of proto-filaments, FtsZ polymerization mediated by native protein anchors, FtsA and ZipA, was reconstituted *in vitro* on supported lipid bilayers [Loose and Mitchison, 2014]. FtsZ was shown to self-organize into highly dynamic cytoskeletal patterns of FtsZ filament bundles in the presence of its membrane anchor FtsA. The dynamics reported there showed a collective behavior of FtsZ filaments moving directionally on the surface, reminiscent of effects observed on motor-driven microtubules [Howard *et al.*, 1989; Schaller *et al.*, 2010]. Remarkably, single-molecule experiments revealed that the fast moving streams and rotating vortexes of FtsZ bundles were driven by treadmilling dynamics and not filament sliding as previously proposed from *in vivo* experiments with *Escherichia coli* and *Caulobacter crescentus*

[Szwedziak *et al.*, 2014]. Treadmilling is a distinctive feature of polar filaments, such as actin and microtubules, where the balanced turnover of monomers at the front and back of a filament produces directional motion [Bugyi and Carlier, 2010].

Shortly after, treadmilling filaments of FtsZ were also observed *in vivo*, where FtsZ polymers displayed periodic cycles of assembly and disassembly in *Escherichia coli* and *Bacillus subtillis* [Bisson-Filho *et al.*, 2017; Yang *et al.*, 2017]. Treadmilling motion was shown to be proportional to the rate of GTPase activity, revealing a new functional role of GTP hydrolysis: driving the movement of treadmilling filaments around the septum.

Notably, the two different conformations adopted by FtsZ, open as a monomer in solution and closed when incorporated into straight filaments, explained not only filament polymerization cooperativity, as discussed before, but also the treadmilling dynamics of the filaments [Wagstaff *et al.*, 2017]. Early FRAP studies showed that FtsZ subunits inside the Z-ring rapidly exchanging with those in the cytoplasm (half-time of around 8-10 seconds) in both *Escherichia coli* and *Bacillus subtilis* [Anderson *et al.*, 2004; Stricker *et al.*, 2002]. The arrangement of FtsZ filaments via treadmilling appears as an additional mode of dynamics on a longer timescale (around 100 seconds) [Bisson-Filho *et al.*, 2017; Loose and Mitchison, 2014; Yang *et al.*, 2017].

Remarkably, the movement of PBP3/FtsI in *Escherichia coli* and PBP2b in *Bacillus subtilis* were shown to be dependent on the FtsZ treadmilling movement of around the septum, suggesting that FtsZ filaments are able to actively move transmembrane proteins in the plane of the membrane [Bisson-Filho *et al.*, 2017; Yang *et al.*, 2017] (Fig. 1.6). Interestingly, the rate of treadmilling was found to control the rate of peptidoglycan synthesis in *Bacillus subtilis* but not in *Escherichia coli*, perhaps due to the different thickness of cell wall in these species [Schoenemann and Margolin, 2017]. How exactly the signal is transmitted across the membrane is not known. FtsN is a strong candidate for this role as it has been implicated in triggering septal PG synthesis, is the last essential protein recruited to the divisome and interacts directly with FtsA [Gerding *et al.*, 2009; Busiek *et al.*, 2012; Baranova *et al.*, 2020].

Together, these findings support a model were the Z-ring is a highly dynamic structure made of treadmilling filaments of FtsZ, constantly remodeling itself to control assembling and disassembling rates. This filament motion is coupled to the cell wall

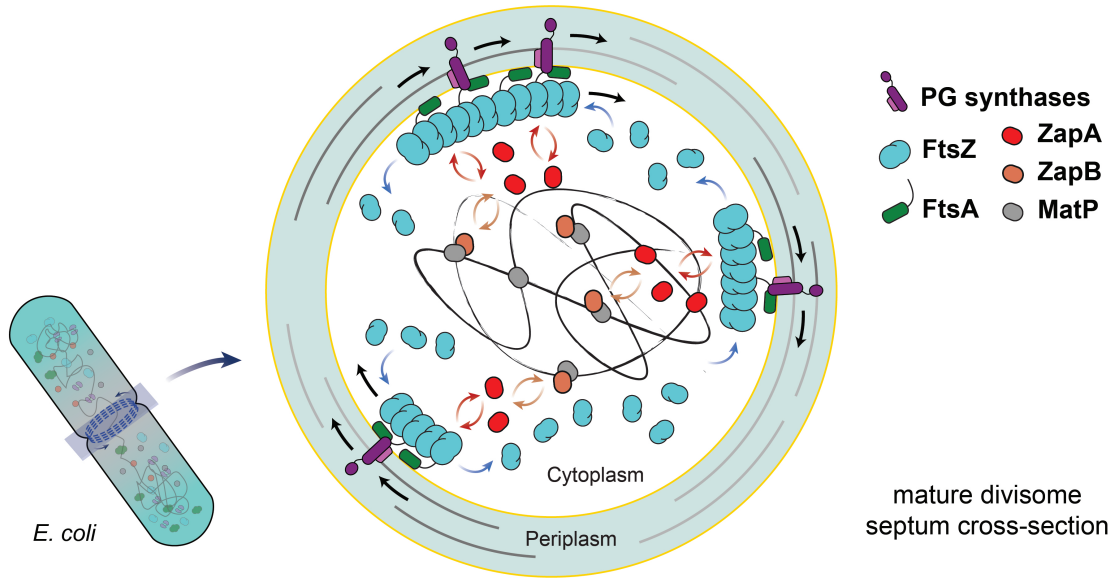

Figure 1.6: Treadmilling FtsZ filaments are coupled to the cell wall synthesis Illustration of a cross-sectional view of the division septum during treadmilling-coupled dynamics. The Z-ring contains multiple FtsA-FtsZ filaments that treadmill around the division plane to distribute coupled PG synthases around the septum, resulting in symmetrical incorporation of PG. In addition to the Min System and NO system, assembly at mid cell is aided by the interaction between MatP-ZapB complex and ZapA bound to FtsZ filaments. Crosslinking of FtsZ filaments by ZapA most likely contributes to the overall stability of the Z-ring.

machinery to provide spatiotemporal control over cytokinesis [Xiao and Goley, 2016; Coltharp and Xiao, 2017] (Fig. 1.6). However, despite these amazing breakthroughs, what exactly drives constriction is still not clear. The more reasonable assumption is that the incorporation of new material during the expansion of the septal peptidoglycan exerts some force on other parts of the cell envelope [Coltharp and Xiao, 2017], but how exactly FtsZ filaments communicate with the cell wall machinery is not known. The Z-ring most likely works as a central hub that integrates a variety of signals from different players to define the composition and the morphology of PG machinery [Xiao and Goley, 2016; Squyres *et al.*, 2020]. Understanding how these regulators modulate the plasticity of dynamic FtsZ polymers and their influence on signal transduction is key to fully understand septation in bacteria.

1.4 The Architecture of a Robust Signaling Hub

As discussed, evidence suggests that the Z-ring is a discontinuous patchy structure made of FtsZ assemblies that treadmill circumferentially at the division site and are coupled to the septal PG machinery. Even though the *in vivo* nanoscale organization of the Z-ring has not been well defined, evidence suggests that FtsZ cannot form a

functional Z-ring on its own and lateral interactions between proto-filaments play an important role to achieve a successful cell division. [Bramhill and Thompson, 1994; Erickson *et al.*, 1996; Löwe and Amos, 1999; Oliva *et al.*, 2003; Dajkovic *et al.*, 2008; Szwedziak *et al.*, 2014; Guan *et al.*, 2018; Squyres *et al.*, 2020]. According to this idea, FtsZ clusters inside the Z-ring presumably contain multiple FtsZ filaments associated by lateral bundling. However, how filaments are organized in patches and the functional relevance of the lateral interfaces is still under debate.

1.4.1 Bundling FtsZ Filaments

Several FtsZ mutants have given prominent insight into the importance of lateral interactions in cell division. One such mutant, FtsZ L169R can enhance proto-filament bundling *in vitro*, reduce GTP hydrolysis rate and resist several FtsZ inhibitors [Haeusser *et al.*, 2015]. Cells expressing this mutant assemble spiral-shaped FtsZ structures causing abnormal shaped division septa, suggesting that hyper bundling has a negative effect on Z-ring stability (Fig. 1.7). Other gain of function mutations have shown a similar phenotype [Encinar *et al.*, 2013; Jaiswal *et al.*, 2010; Stricker and Erickson, 2003]. Other mutants such as K121L, D304L and R174D are defective for lateral interactions and their expression results in cells with elongated phenotype, unable to constrict and divide [Guan *et al.*, 2018; Koppelman *et al.*, 2004]. Interestingly, the toxicity of R174D can be compensated by L169R [Haeusser *et al.*, 2015], suggesting that a balanced amount filament bundling is required for cell viability.

Overexpression of FtsZ *in vivo* makes the Z-ring more homogenous with no changes in its thickness, width or density, suggesting that these additional FtsZ protofilaments progressively occupies existent empty spaces within the structure [Lyu *et al.*, 2016]. However, other studies have observed an increasing density towards the end of the division [Lan *et al.*, 2009; Coltharp *et al.*, 2016]. As intracellular levels of FtsZ stay constant over the cell cycle [Si *et al.*, 2013] an higher number of lateral interactions between FtsZ filaments could explain density fluctuations with a constant concentration of FtsZ monomers overtime [Lan *et al.*, 2009]. According to this evidence, regulation of Z-ring formation and cell division occurs at the level of filament assembly.

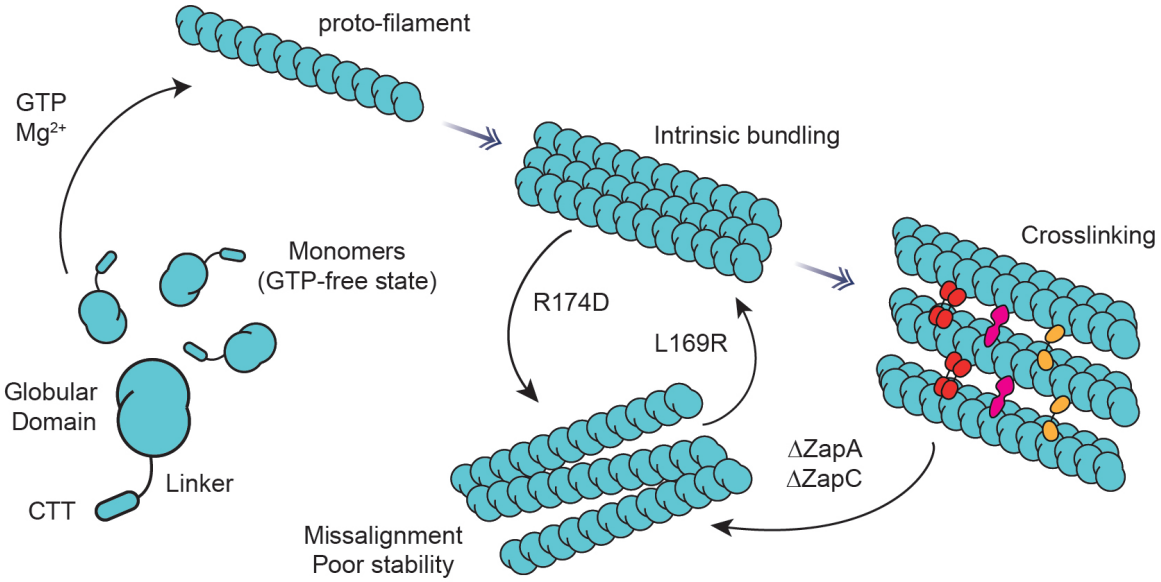

Figure 1.7: Bundling and crosslinking of FtsZ filaments. FtsZ filaments are presumed to be aligned in parallel inside Z-ring clusters. In the absence of crosslinking proteins, such as ZapA and ZapC, cells are elongated and contain spiral Z rings, most likely due to the misalignment of the filaments. Overexpression of FtsZ, or the presence of hyper bundling mutants such as L169R, may lead to increased bundling that compensates for the loss of Zap proteins. Mutants deffective for lateral interactions such as R174D show a similar phenotype than the one observed for Zap mutants. These observations suggest that cell viability depends on a tight regulation of lateral-lateral interactions.

Membrane anchors, such FtsA and ZipA, also seem to play a role in bundling FtsZ filaments. FtsA has been shown to recruit FtsZ to the membrane and simultaneously prevent bundling of FtsZ filaments [Geissler *et al.*, 2003; Loose and Mitchison, 2014; Krupka *et al.*, 2017; Krupka *et al.*, 2018]. On the other hand, a mutant of FtsA that bypasses the need for ZipA *in vivo* (FtsA*) promotes FtsZ polymerization [Pichoff *et al.*, 2018]. As FtsA* is less oligomeric and able to enhance the interaction with downstream proteins, the current view is that during proto-ring assembly FtsA antagonizes the bundling of FtsZ filaments, blocking the recruitment of downstream proteins. As the cell cycle proceeds, FtsA becomes less oligomeric and able to activate PG machinery.

1.4.2 Crosslinking FtsZ Filaments

In addition to the intrinsic ability of FtsZ filaments to self-associate, lateral interactions between filaments can also be facilitated through accessory proteins termed FtsZ associated proteins (Zaps) (Fig. 1.8). In *Escherichia coli* these proteins are ZapA, ZapB, ZapC and ZapD [Gueiros-Filho and Losick, 2002; Ebersbach *et al.*, 2008; Durand-Heredia *et al.*, 2011; Durand-Heredia *et al.*, 2012]. They all co-localize with

the Z-ring at early stages during division and have the ability to crosslink FtsZ filaments *in vitro* (Fig. 1.9A-C). Cells with individual knockouts of these proteins are still viable, but show poor survival rates and elongated phenotype [Durand-Heredia *et al.*, 2011; Durand-Heredia *et al.*, 2012; Buss *et al.*, 2013]. When more than one Zap is knockout at once this effect is synergetic and cell viability drops drastically [Durand-Heredia *et al.*, 2011; Durand-Heredia *et al.*, 2012].

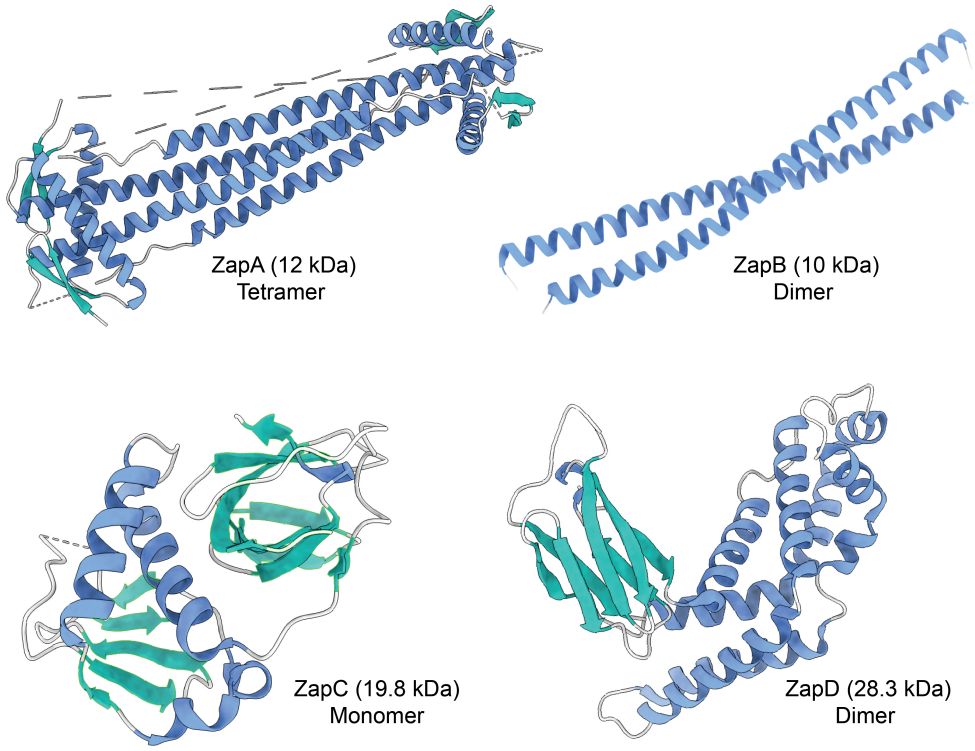

Figure 1.8: Macromolecular structures of Zap proteins in *Escherichia coli*. Ribbon diagrams of ZapA (a dimer of dimers with two binding sites), ZapB (a dimer with two binding sites), ZapC (a monomer with two biding sites) and ZapD (a dimer with two binding sites). Different colors are respective to their secondary structure: helices in bue, β strands in green, and loops in gray. These proteins have an overlapping crosslinking function to promote the association of FtsZ proto-filaments, increasing Z-ring stability *in vivo*.

ZapA was discovered in *Bacillus subtilis* as an antagonizing factor for MinCD [Gueiros-Filho and Losick, 2002], is arguably the best characterized FtsZ-associated protein and widely conserved, in contrast to the other Zaps, which appear to be restricted to gammaproteobacteria [Durand-Heredia *et al.*, 2011; Durand-Heredia *et al.*, 2012]. Cells containing knockouts of ZapA often have FtsZ dispersed in the cytosol rather than aligned at midcell, an elongated phenotype, multiple irregular invaginations and abnormal septa [Galli and Gerdes, 2010; Buss *et al.*, 2013] (Fig. 1.9B,C).

This small cytoplasmic protein (12 kDa) forms a pseudosymmetric tetramer with two distal pairs of FtsZ-binding domains oligomerized via a central four-helix bundle [Low

et al., 2004; Mohammadi *et al.*, 2009] (Fig. 1.8). ZapA exists in a dimer/tetramer equilibrium *in vitro* but the tetramer is likely the most relevant arrangement for the *in vivo* situation in *Escherichia coli* [Pacheco-Gómez *et al.*, 2013; Roach *et al.*, 2014; Roseboom *et al.*, 2018]. These reports show that the tetrameric structure of ZapA is required for substantial bundling *in vitro*, although the dimer can still bind to FtsZ, and for a proper midcell localization *in vivo*. However, this might be different for other species as the coiled-coil domain lengths vary among species.

This crosslinking effect of ZapA have been reported for *Bacillus subtilis*, *Escherichia coli* and *Pseudomonas aeruginosa*, and it is correlated with an apparent reduction of GTPase activity in several studies [Gueiros-Filho and Losick, 2002; Low *et al.*, 2004; Small *et al.*, 2007; Mohammadi *et al.*, 2009; Pacheco-Gómez *et al.*, 2013]. This would suggest that ZapA could slow down treadmilling dynamics and consequently the distribution of cell wall synthases at the division site [Bisson-Filho *et al.*, 2017; Yang *et al.*, 2017], which would be inconsistent with ZapA role on Z-ring stability and cell division precision (Fig. 1.6). However, others studies have reported only a minor effect on the GTPase activity of ZapA and show that the observed effect may vary in different buffer conditions, such as pH and divalent cation concentration [Mohammadi *et al.*, 2009].

ZapB does not bind FtsZ directly, but it is recruited to the divisome via its interaction with ZapA. Mutants for ZapB show a similar phenotype as the one observed for ZapA with widely-dispersed FtsZ clusters through the cytoplasm and abnormal septa formation [Galli and Gerdes, 2010; Buss *et al.*, 2013; Busiek and Margolin, 2015]. ZapB is also a small cytoplasmic protein (10 kDa) containing a coiled coil dimer and interacts with the C-terminal coiled-coil domain of ZapA via its N-terminal region [Galli and Gerdes, 2012] (Fig. 1.8). Evidence suggests that ZapA and ZapB are in equimolar concentrations with FtsZ inside the cells [Galli and Gerdes, 2012; Mohammadi *et al.*, 2009]. *In vitro* ZapB also forms polymers itself, in a divalent cation-dependent manner [Ebersbach *et al.*, 2008], and in high concentrations disrupts the interaction of FtsZ and ZapA, suggesting a sequester mechanism where ZapB modulates ZapA effect on FtsZ.

This ZapA-ZapB complex may also contribute to promote cytokinesis efficiency by an alternative bundling-independent mechanism. ZapB has been found to interact with MatP, a DNA-binding protein involved in condensation and segregation of the

terminus macrodomain of the chromosome [Mercier *et al.*, 2008; Bailey *et al.*, 2014; Buss *et al.*, 2015].

This evidence suggests an attractive model where a protein network formed by FtsZ, ZapA, ZapB and MatP form a physical link between the membrane and the ter region of the chromosome that may act to prevent undesirable chromosome fission, increase the accuracy of Z-ring placement and provide additional stability by assisting the midcell localization of ZapA [Buss *et al.*, 2013]. Interestingly, in *Caulobacter crescentus* ZapA does not affect the GTPase activity, protofilament assembly, or bundling of FtsZ under any conditions tested *in vitro*, but still promotes midcell positioning of the Z-ring [Woldemeskel *et al.*, 2017].

ZapC and ZapD are less studied, but they also localize and interact with the Z-ring, independently of ZapA and ZapB, and promote bundling of FtsZ filaments *in vitro* [Durand-Heredia *et al.*, 2011; Durand-Heredia *et al.*, 2012], suggesting an overlapping role on the stabilization of the Z-ring. However, these proteins differ considerably from each other. ZapC is a 19.8 kDa monomer with two FtsZ binding sites [Schumacher *et al.*, 2016] while ZapD forms 28.3 kDa dimers [Schumacher *et al.*, 2017] (Fig. 1.8). In addition, ZapC binds to the globular core of FtsZ like ZapA [Schumacher *et al.*, 2016], while ZapD interacts with the C-terminal tail of FtsZ [Schumacher *et al.*, 2017], similar to its membrane anchors FtsA and ZipA in *Escherichia coli*.

Overall, it is generally accepted that these proteins have an overlapping crosslinking function to promote the association of FtsZ proto-filaments and contribute to increase Z-ring stability and cell division efficiency *in vivo* (Fig. 1.9), but the molecular mechanism for how these Zap proteins organize and stabilize FtsZ filaments is still poorly understood (Fig. 1.7). There is no amino acid sequence homology among Zaps and their molecular dimensions and binding sites differ significantly. This raises the possibility that these diverse features may modulate the dynamics of FtsZ filaments in distinct manners that classic studies using transmission electron microscopy, sedimentation assays and light scattering overlooked.

Moreover, the reason why *Escherichia coli* has conserved so many components with overlapping functions is unclear. Perhaps the abundance of FtsZ bundlers compensates for a relatively weak inherent bundling capacity of FtsZ in *Escherichia coli*, as most bacteria species only contain one of these crosslinkers. Another interesting possi-

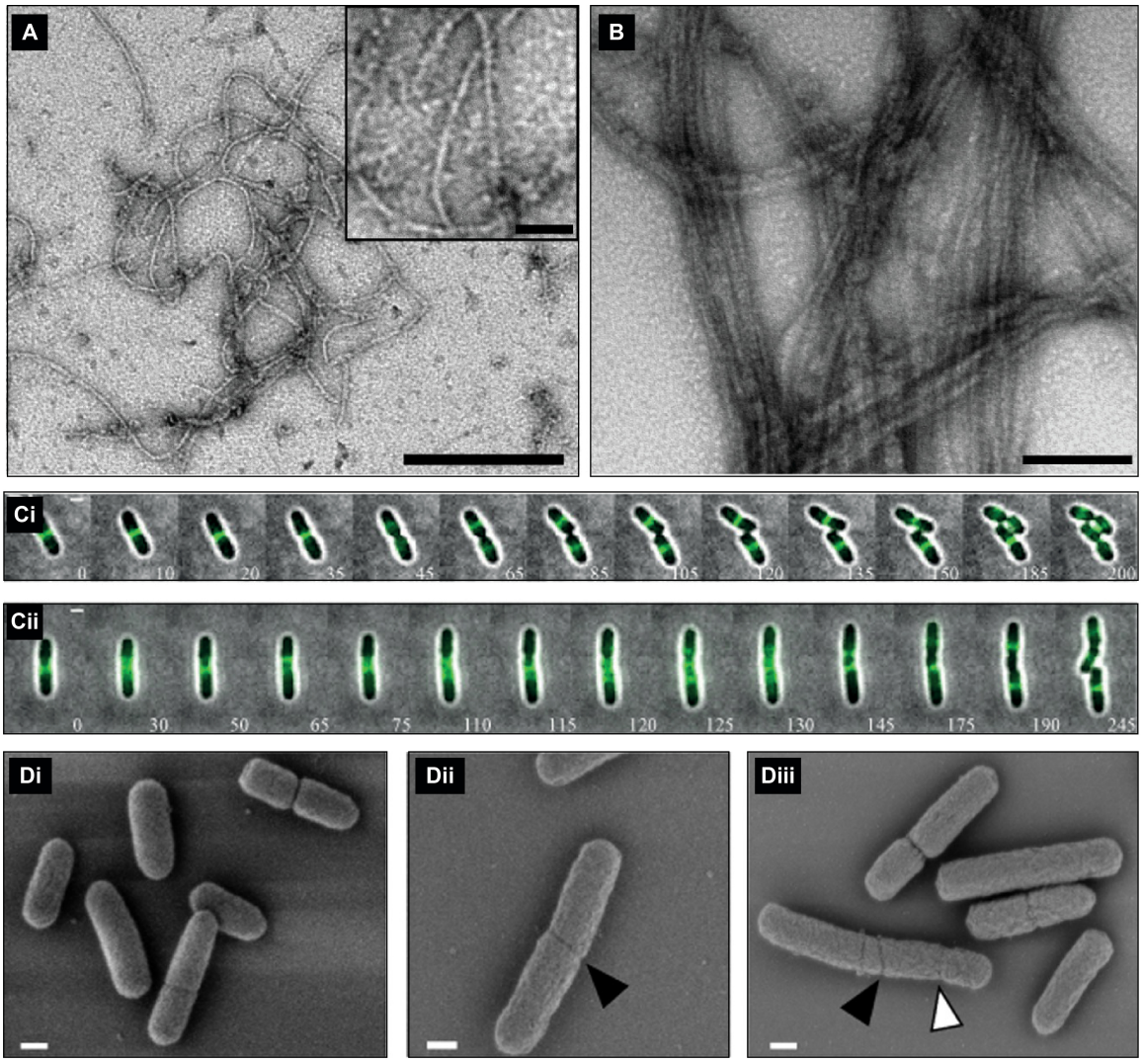

Figure 1.9: ZapA effect on FtsZ filament organization *in vitro* and *in vivo*. **(A)** Purified FtsZ filaments with 1 mM GTP in the absence of ZapA. Scale bar = 250 nm, inset bar = 25 nm. Data from [Roach *et al.*, 2014]. **(B)** FtsZ filaments in the presence of 4.8 mM of purified ZapA. Scale bar = 100 nm. **(C)** Montages from time-lapse movies of WT cells (upper panel) and mutats for ZapA (lower panel) expressing FtsZ–GFP during cell division. At each time point, the fluorescence image (green) was overlaid with the corresponding bright-field image (grey) with the time (min) indicated in the bottom corner. Data from [Buss *et al.*, 2013]. **(D)** Scanning electron micrographs of dividing *E.coli* cells. WT cells (i) show single, midcell septa oriented perpendicular to the cells long axes. In ZapA mutants (ii, iii), slanted, non-midcell, and multiple septa are observed (arrows). Scale bars = 500 nm. Data from [Buss *et al.*, 2013].

bility is that Zap proteins may be regulated under different environmental conditions and enhance ring stability under specific critical circumstances to the host.

1.4.3 Shaping the Signal Across the Membrane

Direct evidence for the existence of intrinsic bundling *in vivo* is still lacking, but the role of crosslinking by Zaps on Z-ring stability seems to be well established. Nevertheless, evidence suggests that these two traits are tightly coupled and can compensate for the loss of one another and other regulatory systems (Fig. 1.7).

For instance, ZapA can suppress the inhibitory effect of MinC [Dajkovic *et al.*, 2008], compensating the destabilizing effect of the Min system. The gain-of-function mutant L169R can prevent aberrant septa formation in ZapA and ZapC mutants [Stricker and Erickson, 2003; Krupka *et al.*, 2018]. Moreover, hyper bundled mutants of FtsZ [Stricker and Erickson, 2003; Haeusser *et al.*, 2015; Krupka *et al.*, 2018] or excess of ZapA or ZapC [Krupka *et al.*, 2018] cause cells to divide abnormally, showing a similar phenotype as the one observed for FtsZ mutants defective for lateral interactions or Zaps knockouts. Importantly, this shows that augmented stability has the same negative effect on cell viability as inhibiting bundling.

The exact function of these lateral interactions inside the Z-ring is still not clear. They may simply improve the recruitment of more FtsZ to the membrane or help to organize FtsZ filaments in the right orientation towards the center of the cell. A more attractive hypothesis suggests that a fine-tune between intrinsic bundling and crosslinking might help to incorporate a greater density of components into its structure. This would help to create a higher capacity signaling hub and properly shape the output signal to the downstream proteins. Many more studies, both *in vivo* and *in vitro*, will be needed to elucidate if this is the case.

Chapter 2

Scope of this Work

The main goal of this thesis was to investigate **how FtsZ-associated proteins (Zaps) contribute to the stability of the Z-ring and precision of cell division at the molecular level**, while establishing a set of **quantitative methods to characterize the large-scale architecture and dynamics of FtsZ filaments** in a cell-free system. Accordingly, this work can be divided into two main tasks - even though they move in parallel:

- Establish an *in vitro* system based on purified proteins, supported lipid bilayers and high-resolution microscopy to visualize the self-organization of FtsZ-FtsA co-filaments in the presence of different bacterial crosslinkers.

  This approach should allow us to study dynamic interactions between proteins of interest on top a membrane surface, mimicking the physiological conditions of the living cell. Here, we have total control over protein concentrations, the lipid composition of the membrane, and the components inside the reaction vessel. Furthermore, by using total internal reflection fluorescence (TIRF) microscopy, we benefit from higher spatiotemporal resolution than inside living cells to simultaneously visualize the self-organization of FtsZ and its crosslinkers.

- Develop a set of quantitative tools to characterize the large-scale architecture and the underlying dynamics of membrane-bound FtsZ filaments, enabling comparative studies across different conditions.

  Robust automation of image data analysis to extract information from large amounts of bioimages is still one of the main bottlenecks in scientific productivity. Therefore, not only robust experimental assays are required, but also a set of automatic methods for image analysis that do not require parameter tweaking and can be used in an wide range of studies, both *in vitro* and *in vivo*.

In the end, we have established a set of novel image analysis tools to quantify the influence of different Zaps on the FtsZ filament network on three different spatial

scales: First, we analyzed the large-scale organization of the membrane-bound filament network (chapter 3); next, we studied the underlying polymerization dynamics (chapter 4), and finally, we quantified the behavior of single molecules (chapter 5).

We describe our quantitative methods and experimental approaches in detail (chapter 6) and conclude this thesis by discussing how our work has contributed to shed new light on the self-organizing properties of the bacterial cytoskeleton (chapter 7).

Chapter 3

Quantification of the Large-Scale Organization of Cytoskeletal Networks of FtsZ Filaments

The best characterized FtsZ-associated protein is ZapA, widely conserved across Gram-positive and Gram-negative bacteria. Previous *in vitro* experiments using only purified FtsZ and ZapA showed that ZapA promotes the formation of stable FtsZ filament bundles when incubated together in solution, consistent with a crosslinking activity (Fig. 1.9). This is also supported by its molecular structure, a pseudosymmetric tetramer with two distal pairs of FtsZ-binding domains oligomerized via a central four-helix bundle [Low *et al.*, 2004; Roach *et al.*, 2014; Mohammadi *et al.*, 2009] (Fig. 1.8). The symmetry of the ZapA tetramer appears to be compatible with an antiparallel orientation of filaments within FtsZ bundles.

Together, these findings have led to a model where ZapA stabilizes the Z-ring by promoting antiparallel bundling of filaments [Low *et al.*, 2004; Galli and Gerdes, 2012]. However, a direct demonstration of these effects has not yet been possible.

To study the effect of ZapA on the architecture and dynamics of the FtsZ filament network, we took advantage of an *in vitro* system based on supported lipid bilayers and purified proteins (Fig. 3.1A; see section 6.3 for more details). This setup mimics the dynamic interaction of proteins with the cytoplasmic face of the inner cellular membrane, since phospholipid mobility is well preserved and the reaction buffer reflects the intracellular environment [Loose and Schwille, 2009; Loose and Mitchison, 2014]. Here, we used the purified proteins FtsZ, ZapA and FtsA, the natural membrane anchor of FtsZ (see section 6.2 for details on protein purification). These proteins were labelled with a variety of fluorescent dyes, enabling multi-color experiments and co-localization studies.

As reported previously [Loose and Mitchison, 2014], FtsZ and FtsA form treadmilling filaments on supported membranes when incubated in the presence of ATP and GTP and at a concentration ratio similar to that found in the living cell (FtsZ:FtsA = 1.5μM:0.5μM). These filaments further self-organize into dynamic networks of curved filament bundles (Fig. 3.1B; Movie 1).

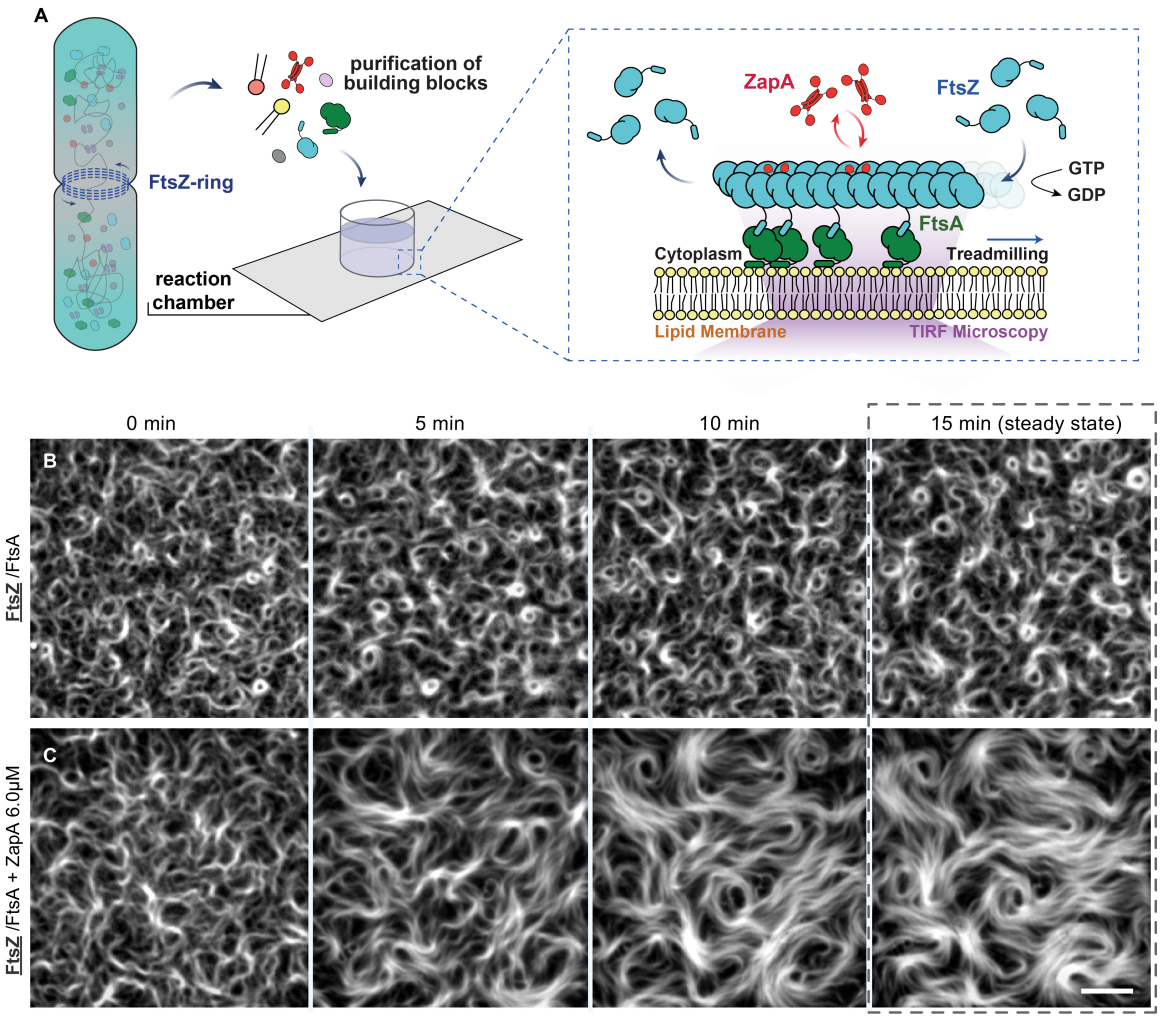

Figure 3.1: ZapA modulates FtsZ filament network organization *in vitro*. **A** A plastic ring is glued to a glass coverslip to build a reaction chamber. A supported lipid bilayer is formed on the glass surface by fusion of small lipid vesicles. All the components are added to the reaction buffer (50mM Tris-HCl pH=7.5, 150mM KCl, 5mM $MgCl_2$) prior to the addition of 4 mM of GTP, which triggers FtsZ polymerization. Images are acquired using a TIRF microscope setup (typically one image each 2 seconds). **(B)** Snapshots of FtsZ pattern emerging from its interaction with FtsA alone and **(C)** in the presence of 6μM ZapA. Concentrations of FtsZ (30% Cy5-labelled) and FtsA were kept constant for all experiments (1.5μM and 0.5μM, respectively). Scale bars = 5μm.

Next, we performed this experiment in the presence of defined concentrations of ZapA. We first used a concentration of 6μM, about four times higher than *in vivo* [Small *et al.*, 2007], and found that FtsZ filaments organized into a network of thicker and longer filament bundles seemingly more aligned and straightened (Fig. 3.1C; Movie 2). The dynamics of the travelling streams of filaments was preserved, but the characteristic ring-like architecture was lost. This effect became more pronounced over time until the system assembled into a stable steady state after about 15min, with an architecture that strongly differed from the pattern found in the absence of ZapA (Fig. 3.1B,C).

Next, we sought to establish a set of analytical tools that would allow us to quantify these observations. The main challenge was to overcome the great variability of the background and isolate specific features from the net of overlapping filaments. In the end, we analyzed the large-scale organization of the membrane-bound filament network using four different parameters: apparent bundle width (δ), curvature (κ), correlation length (ρ) and correlation time (τ). All these parameters are pixel-based and the information of each pixel is used by unsupervised methods (i.e does not require human intervention) for some sort of mathematical computation.

3.1 Bundle Thickness Estimation and the Effect of ZapA

To characterize the large-scale organization of FtsZ filament network, we first built a simple automated method that could track the apparent width of filament structures on the membrane. For this aim, we used an image segmentation approach followed by Euclidean distance mapping (Fig. 3.2A-C). This transformation resulted in a grey scale map, where each pixel represents the shortest distance to the nearest pixel in the background. Accordingly, bundle widths correspond to the local peak intensities multiplied by two. The mean bundle width of each frame was calculated by scanning each row and column of pixels and identifying the peak intensities using a custom script (Fig. 3.2D; see section 6.5.1 for more details). The mean value could then be plotted as a function of time (δ) and the characteristic bundle width was obtained by taking the time-average at steady state (δ_{ss}).

For bundles of membrane-bound FtsZ filaments in the absence of ZapA, our analysis found a mean width of $\delta_{(t=0)} = 0.63 \pm 0.03\mu$m, which stayed roughly constant over time ($\delta_{ss} = 0.70 \pm 0.05\mu$m, $n = 10$; Fig. 3.2E, blue). In contrast, in the presence of 6.0μM ZapA, the FtsZ bundle width continuously increased until it plateaued at a slightly higher value of $\delta_{ss} = 0.77 \pm 0.05\mu$m ($n = 10$, Fig.3.2E, red) at steady state ($t > 15$min). This is in agreement with previous observations showing that ZapA promotes lateral interactions between FtsZ protofilaments and the formation of filament bundles when incubated together in solution [Mohammadi *et al.*, 2009; Galli and Gerdes, 2012; Pacheco-Gómez *et al.*, 2013].

Next, we investigated how varying concentrations of wild-type ZapA affect the FtsZ filament pattern (Fig. 3.2F; Fig. 3.3A,B,G; Movie 3).

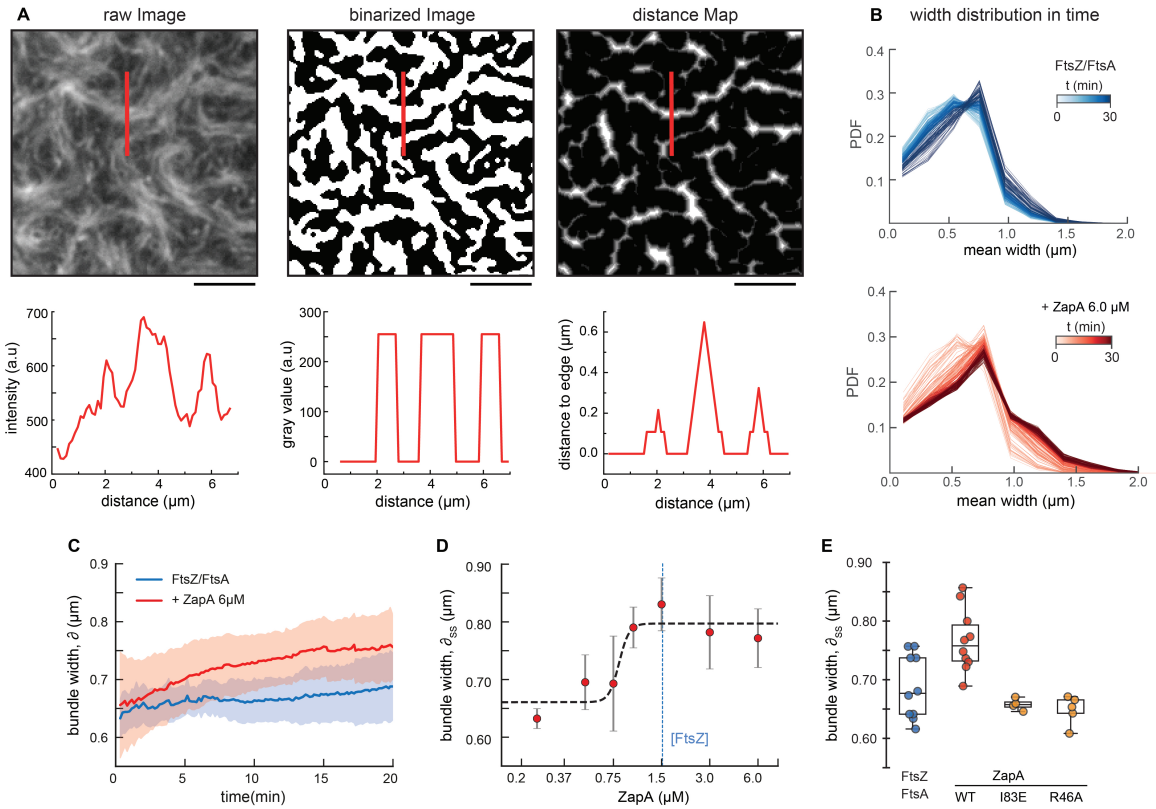

Figure 3.2: ZapA induces bundling of membrane-bound FtsZ filament bundles. To estimate bundle width, each frame in the raw data **(A)** was binarized by adaptive threshold **(B)** before the Euclidean distance was calculated for every pixel in that frame **(C)**. Local peaks in the final gray scale image correspond to half of the bundle width (orange line). **(D)** Mean bundle width over time was given by the peak of widths distribution of each frame without (top, light to dark blue) and with ZapA (bottom, light to dark red). **(E)** Estimated mean bundle width, δ, over time for FtsZ/FtsA filament pattern (blue) and with $6\mu M$ ZapA (red). Curves depict the mean and the standard deviation (std) as shaded error bands of independent experiments (FtsZ, $n = 10$, ZapA, $n = 10$). **(F)** Change in δ_{ss} with varying concentrations of ZapA. Data shown corresponds to the average bundle width measured between t = 15min and t = 20min (mean $\pm$ std). Black line corresponds to Hill equation fit with $n_H = 13.86$ and $EC_{50} = 0.81\mu$M with 90% confidence intervals of [13.86 - 94.68] and [0.71, 0.98], respectively, obtained from asymmetric bootstrap distributions (see section 6.6 for details). **(G)** Mean bundle width, δ_{ss}, of membrane-bound FtsZ filaments is increased in the presence of 6μM ZapA (red) ($p = 0.004$) while it was unchanged in the presence of ZapA I83E and ZapA R46A (orange) ($p > 0.05$).

Up to a concentration of ZapA = 0.75μM, the observed bundle width at steady state was below 0.70μM and did not change significantly (Movie 3, left). However, at ZapA concentrations higher than 1.0μM (Movie 3, right) we observed a rapid shift to structures thicker than 0.75μm. This value peaked at ZapA = 1.5μM before it slightly decreased (Fig. 3.2F). Interestingly, the observed plateau point occurs at an equimolar stoichiometry of FtsZ and ZapA, matching the concentration ratio found *in vivo* [Mohammadi *et al.*, 2009]. These forms of switch-like transitions above a critical threshold are common in biology and are often analyzed by fitting a Hill equation (see section 6.6 for more details).

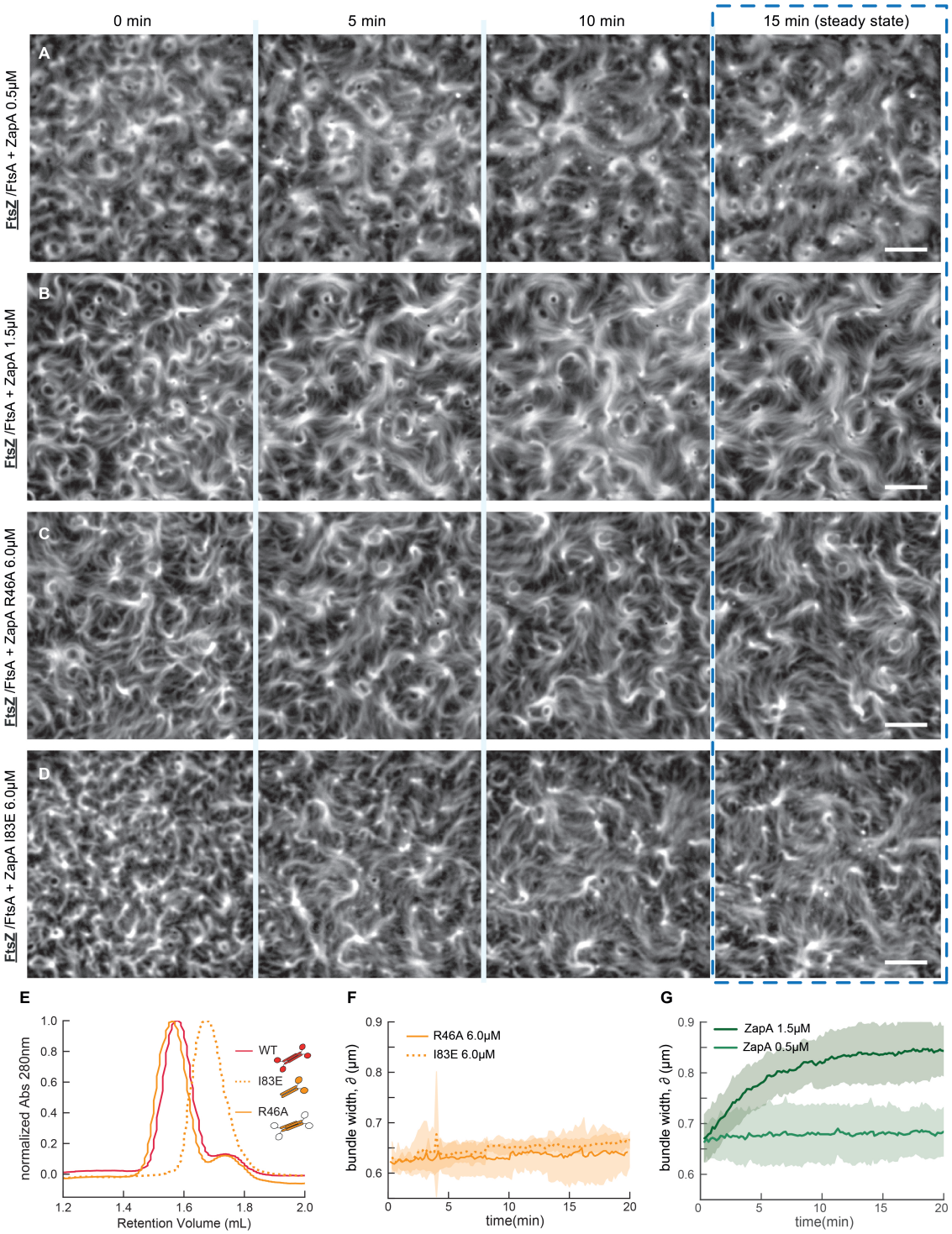

Figure 3.3: Tetramerization is essential for ZapA function. Snapshots of FtsZ pattern emerging from its interaction with FtsA and 0.5μM ZapA **(A)**, 1.5μM ZapA **(B)**, 6μM ZapA R46A **(C)** or 6μM ZapA I83E **(D)**. Scale bars = 5μm. **(E)** Size-exclusion chromatography results for ZapA wild type (WT) and mutants (ZapA I83E and ZapA R46A). **(F,G)** Estimated δ over time for FtsZ/FtsA filament pattern in the presence of 6μM ZapA I83E (orange solid line, $n = 4$), 6μM ZapA R46A (orange dashed line, $n = 5$), 0.5μM ZapA (green, $n = 4$); and 1.5μM ZapA (dark green, $n = 11$). Curves depict the mean and standard deviation (shaded error bands) of independent experiments.

This analysis confirmed a cooperative transition of the system towards thicker FtsZ bundles with a Hill coefficient (n_H) much larger than 1 and $EC_{50} = 0.81\mu$M (90% confidence interval (CI): 0.71 - 0.98).

All together, we found that ZapA is able to increase the apparent width of FtsZ filament bundles, even when they are recruited to the membrane by FtsA. Furthermore, being able to define specific protein concentrations in our *in vitro* experiments, we were able to show that ZapA acts on FtsZ in a highly cooperative manner.

As a control, we studied the behavior of two mutants in our assay (Fig. 3.3C,D,F; Movie 4), ZapA R46A, a mutant with an inactive FtsZ binding site [Roach *et al.*, 2014] and ZapA I83E, a mutant where the dimer-dimer interaction is disrupted [Pacheco-Gómez *et al.*, 2013] (Fig. 3.3E). As expected, adding ZapA R46A up to a concentration of 6μM did not change the FtsZ filament pattern and bundles had the same average width as in the absence of ZapA (Fig. 3.2G; $p = 0.080$). In the presence of ZapA I83E, the appearance of FtsZ filaments slightly changed (Fig. 3.3D) but we did not observe a significant increase of bundle thickness as found for the wild-type protein (Fig. 3.2G ; $p = 0.131$). Accordingly, we confirmed that only tetrameric ZapA with two pairs of FtsZ binding sites has a significant effect on FtsZ filaments, in agreement with previous observations showing that tetramerization of ZapA is essential for its function [Pacheco-Gómez *et al.*, 2013].

3.2 Architecture Analysis and the Effect of ZapA

Bundling of FtsZ filaments does not fully characterize the influence of ZapA, as we also observed a dramatic shift in the overall architecture of the filament network. In the absence of ZapA, the filament bundles were highly curved, often forming ring-like structures on the membrane. The addition of ZapA gave rise to a pattern of straighter filament bundles, where ring-like structures were missing (Fig. 3.1B,C). Thus, to better characterize the biochemical activity of ZapA and its influence on FtsZ filament organization, we established a method to obtain a mathematical representation of the filament network (Fig. 3.4A). Our approach is based on the computation of structure tensors. This involves dividing each image into small regions with roughly the size of the feature we aim to quantify and assigned an unitary vector $u_\theta = (cos\theta, sin\theta)$ to which one of those regions.

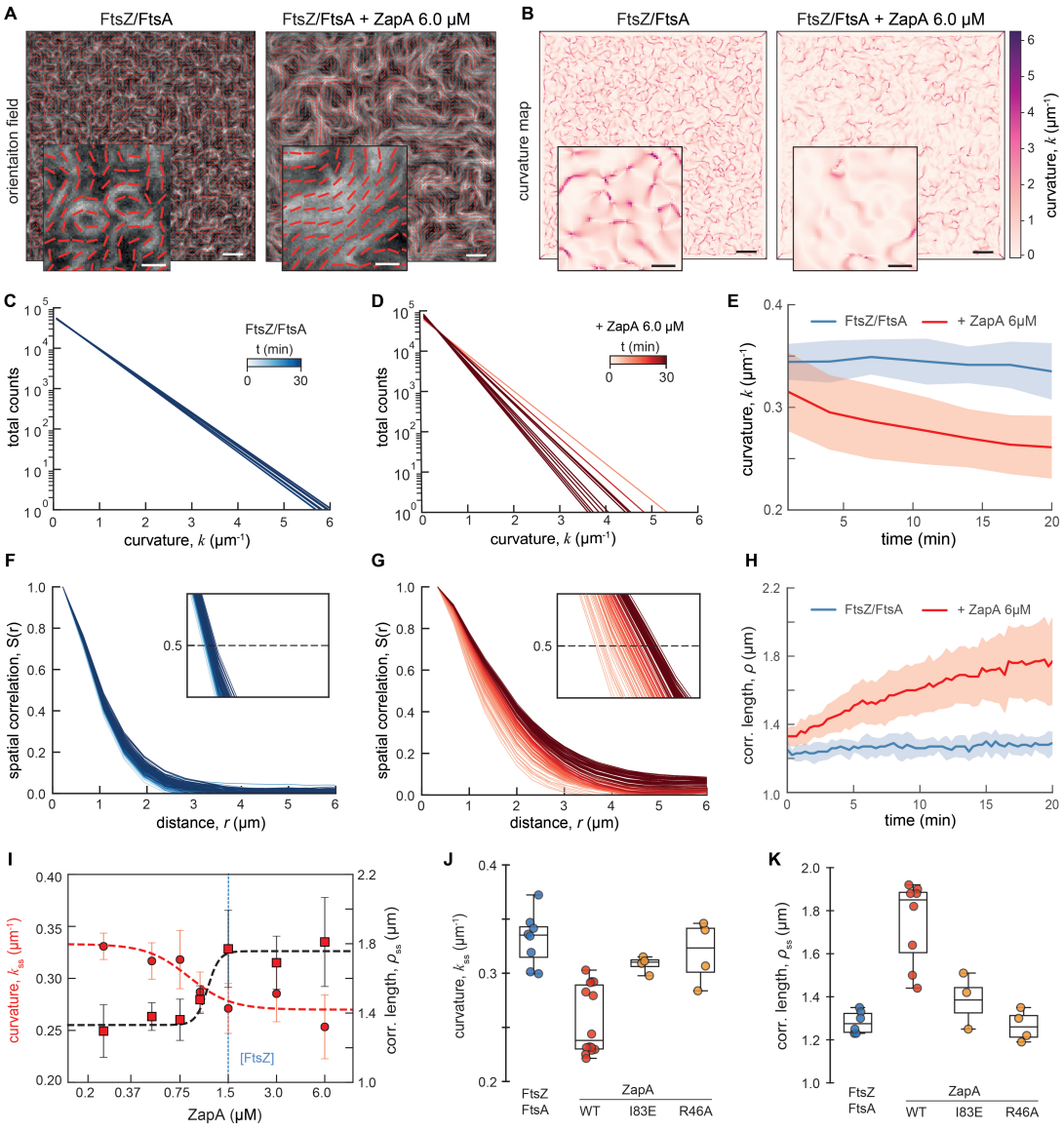

Figure 3.4: ZapA changes the architecture of FtsZ filament bundles. (A) Orientation fields (red lines) for FtsZ filament network without (left) or with 6.0μM ZapA (right) overlaying the corresponding fluorescence micrographs. **(B)** Curvature maps of the orientation fields in A. White areas correspond to spots with no curves (straight filament bundles), while the purple gradient describes the degree of curvature in the orientation field at a given position. Scale bars, large image = 5μm, small image = 2μm. **(C)** Time-dependent decrease of curvature for FtsZ filaments alone (blue gradient, light to dark) and **(D)** with 6μM ZapA (red gradient, light to dark) (Y-axis in log scale). **(E)** The mean curvature, κ, at each time point was given by the characteristic length scale of an exponential fit to the curvature distributions in C,D. Curves depict the mean and std as shaded error bands of independent experiments (FtsZ, $n = 10$, ZapA, $n = 10$). **(F)** Typical time-dependent spatial correlation function, $S(r)$, for an FtsZ filament network without (blue gradient, light to dark) and **(G)** with 6μM ZapA (red gradient, light to dark). Without ZapA, the curves overlapped in time, but in its presence a shift to higher correlation lengths is observed. **(H)** Correlation length, ρ, was given by the intersection line where $S(r) = 0.5$ (insets in F,G) and shows that ρ remained constant for FtsZ alone (blue) over time, but continuously increased with 6μM ZapA (red). Curves show the mean and std as shaded error bands of independent experiments (FtsZ, $n = 6$, ZapA, $n = 8$). **(I)** κ and ρ with varying concentrations of ZapA. ZapA induced a switch-like behavior for k_{ss} and ρ_{ss} ($n_H = 3.28$ and $IC_{50} = 0.84\mu M$; $n_H = 12.04$ and $IC_{50} = 1.05$, respectively) with a saturation point close to equimolar concentrations with FtsZ. Dots depict the mean with standard deviation of independent experiments (FtsZ, $n = 6$, ZapA, $n = 8$). The 90% confidence intervals for n_H and k_H obtained from boostramping are shown in Table 6.1. **(J,K)** Mean values for ZapA I83E and R46A (orange) are similar to the one observed for FtsZ alone (blue).

The directional derivative for each unitary vector is then measured:

$$D_{u_\theta} f(x,y) = u_\theta^T \nabla f(x,y) = u_\theta^T [\frac{\delta f(x,y)}{\delta x}, \frac{\delta f(x,y)}{\delta y}]$$

where $f(x,y)$ is the local grey value and $\nabla f(x,y)$ is the corresponding gradient in x and y. The algorithm then finds the direction u_ϕ, where the derivative is maximized over the region of interest:

$$u_\phi = argmax \|D_{u_\theta} f(x,y)\|_w^2 \qquad and \qquad \|u_\theta\| = 1$$

where $w(x,y) \geq 0$ is related with the function that describes the region of interest. Thus, the magnitude of each vector is proportional to the image contrast in a given direction and the average local direction is given by a weighted sum of all the vectors. A Gaussian filter, with a variance σ, governs the effective region of interest in which the orientation should be projected, i.e. the approximate dimension (in pixels) of the local structures in the image. A range of different σ was tested to find the best orientation field that could describe our data. This parameter was settled as 4 pixels for the analysis. From a standard inner-product manipulation we get:

$$\|D_{u_\theta} f(x,y)\|_w^2 = \langle u_\theta^T \nabla f(x,y), \nabla f(x,y)^T u_\theta \rangle = u_\theta^T \hat{P} u_\theta$$

where the first eigenvector of the structure tensor matrix, $\hat{P} = \langle f(x,y), \nabla f(x,y)^T \rangle$, defines the local dominant orientation. The final output is a two-dimensional orientation field, $\phi(x,y)$, where each pixel has been replaced by unit vectors (Fig. 3.4A). This can be applied to every frame within a movie and the time-dependent changes in each orientation field can then be analyzed to compute two independent parameters: the curvature, κ (μm^{-1}) (Fig. 3.4B-E), given by the rate of change in the local orientation at each pixel position, and the mean correlation length, ρ (μm) (Fig. 3.4F-H), given by the spatial correlation of the angles as a function of an increasing distance.

3.2.1 Curvature of the FtsZ Filaments Network

To estimate the curvature (k) of the orientation field, we used the definition from [van Ginkel *et al.*, 1999], where curvature is described as the rate of change in the

local orientation in the direction perpendicular to that orientation:

$$k(x,y) = \frac{\delta\phi(x,y)}{\delta c} = -sin\phi(x,y)\frac{\delta\phi(x,y)}{\delta x} + cos\phi(x,y)\frac{\delta\phi(x,y)}{\delta y}$$

where c corresponds to the axis perpendicular to the orientation. From this, we generated a color map (white to purple) containing every $k[x_j, y_i]$, which represents the magnitude of the absolute curvature in ϕ at position x, y (Fig. 3.4B and Fig. 6.3). As a result, this method identifies how much the orientation of a bundle is changing (to left or right) at every pixel using an arbitrary reference point. The degree of this 'kink' in the orientation field is depicted by the increasing intensity of the purple color on the heatmap, where white spaces correspond to straight filaments, i.e no kinks/curves are identified.

In sum, the magnitude of the local curvature at each time point is illustrated in a heatmap and proportional to the intensity of the purple color. (Fig. 3.4B). Accordingly, the abundance of white spaces in the presence of 6μM ZapA qualitatively describes the lower curvature of the filament bundles.

The distribution of curvatures was shown to be exponentially distributed across all samples and time points (Fig. 3.4C,D). The mean curvature of the filament network at each time point, $\kappa(t)$, was then given by the characteristic scale of an exponential fit to the curvature distribution (Fig. 3.4E). In the absence of ZapA, FtsZ filaments showed a constant mean curvature of $\kappa_{ss} = 0.33 \pm 0.06 \mu m^{-1}$ (Fig. 3.4E, blue, $n = 10$). In contrast, in the presence of $6\mu M$ ZapA, $\kappa(t)$ decreased over time by about 20% with a plateau at $\kappa_{ss} = 0.25 \pm 0.03 \mu m^{-1}$ (Fig. 3.4E, red, $n = 10$), confirming that the presence of ZapA results in straighter bundles of FtsZ on the membrane.

Similar as for the bundle width (Fig. 3.2F),increasing concentrations of ZapA induced a switch-like transition between two states with a Hill coefficients of $n_H = 3.28$ and a $EC_{50} = 0.84\mu$M (Fig. 3.4I). Furthermore, neither R46A nor I83E had a significant effect on the FtsZ filament network (Fig. 3.4J,K; $p > 0.05$).

3.2.2 Spatial Order of the FtsZ Filaments Network

Next, we used the same orientation field to calculate the spatial order of the filament network, which is a measure for how the orientations of the filaments co-vary with one another across the observed membrane area. Specifically, we used the correlation

function, $S(r)$, which compares the relative orientation of each angle with all the surrounding angles separated by an increasing distance r:

$$S(r) = \langle cos(2\phi(r_{i,j})) - \phi(r_l)\rangle_{(|r_{i,j}-r_l|=r)}$$

Where $\phi(r_{i,j})$ is the orientation angle at the position $r_{i,j}$ and $\phi(r_l)$ corresponds to all the surrounding angles at the position r_l, given that $|r_{i,j} - r_l| = r$. The angular brackets indicate an average over the indicated range and the presence of the '2' in the correlation function reflects the nematic symmetry of the system $[-\pi/2, \pi/2]$. As a result, we describe the average distance range over which the angles share a common orientation in each image. Each correlation curve typically goes from 1, where r is small and correlation is higher, to zero, where the correlation decreases drastically as the r increases (Fig. 3.4F,G). Accordingly, more ordered arrangements will display a higher spatial correlation at higher correlation lengths. To better visualize fluctuations in this parameter we defined the correlation length as the distance r where $S(r) = 0.5$ as a function of time, and we use this parameter to track temporal changes in the spatial order of each system (Fig. 3.4H).

In the absence of ZapA, the correlation curves obtained for different time points overlapped with each other (Fig. 3.4F, light to dark blue gradient), showing that the spatial order stayed constant during the experiment. The presence of ZapA promoted a shift of the correlation curves to higher correlation lengths, an effect that became more pronounced with time, indicating that ZapA increases the spatial order of the system (Fig. 3.4G, light to dark red gradient). We quantified this time-dependent increase in spatial order by defining a characteristic correlation length, $\rho(t)$, which corresponds to the distance at which $S(r) = 0.5$ (Fig. 3.4F,G insets). We found that the presence of ZapA led to a continuous increase in spatial order from $\rho_{(t=0)} = 0.97 \pm 0.06\mu m$ to $\rho_{ss} = 1.81 \pm 0.26\mu m$ at steady state (Fig. 3.4H, red, $n = 8$), while ρ_t stayed constant for FtsZ and FtsA alone (Fig. 3.4H, blue, $n = 8$). Both values are similar to the dimensions of the *Escherichia coli* cell, consistent with the spatial scale at which the Z-ring is operating *in vivo*.

Again, we found an ultrasensitive transition between two states when using varying concentrations of ZapA ($n_H = 12.04$ and $EC_{50} = 1.05\mu M$) (Fig. 3.4I) and no effect upon addition of either ZapA R46A or I83E (Fig. 3.4K).

In summary, this analysis showed that the system exists in two states: a state of high curvature and low spatial order, at ZapA concentrations below 0.8μM, and a state of high spatial order and low curvature at higher concentrations. These observations are in agreement with the switch-like transition observed when measuring the apparent bundle width of the filaments.

3.3 Re-organization Dynamics and the Effect of ZapA

In cells lacking ZapA, Z-rings show loose filament arrangement and are highly dynamic, transitioning back and forth between multiple locations in the cell [Buss *et al.*, 2013]. In contrast, the Z-ring in wildtype cells usually persists at the same position during the cell cycle (Fig. 1.9C). Consistent with these observations, we realized that FtsZ filament bundles continuously reorganized in the absence of ZapA, but appeared much more static when ZapA was present (Fig. 3.5A).

To quantify the rate of reorganization in our experiments, we performed temporal autocorrelation analysis (Fig. 3.5B). This method measures the similarity of fluorescence images as a function of a time lag δt between different frames based on the Pearson cross-correlation coefficient (PCC). For highly dynamic patterns, the PCC typically decays rapidly with δt, but for persistent structures drops slowly. We defined the correlation time, τ, as the half-time of a mono-exponential fit to each curve, which was used to compare across a set of individual experiments.

Accordingly, we found that the corresponding autocorrelation function, $\Theta(\delta t)$, rapidly decayed in the absence of ZapA (Fig. 3.5B, blue curve), consistent with a rapidly rearranging pattern. In the presence of $6\mu M$ of ZapA, however, this decay was about 4-fold slower (Fig. 3.5B, red curve).

Similar to bundle width, curvature and correlation length, the characteristic correlation time, τ, displayed a two-state behavior as a function of varying concentrations of ZapA: below a critical concentration of ZapA the pattern showed fast reorganization and consequently short correlation times, but the system switched to slow reorganization and long correlation times at saturating ZapA concentrations with a Hill coefficient of 14.55 (90% CI: 9.22 - 69.27) and EC_{50} = 0.82 (90% CI: 0.76 - 0.87) (Fig. 3.5C). ZapA R46A, which does not bind to FtsZ, did not affect reorganization dynamics, while ZapA I83E increased slightly, but not-significantly the correlation

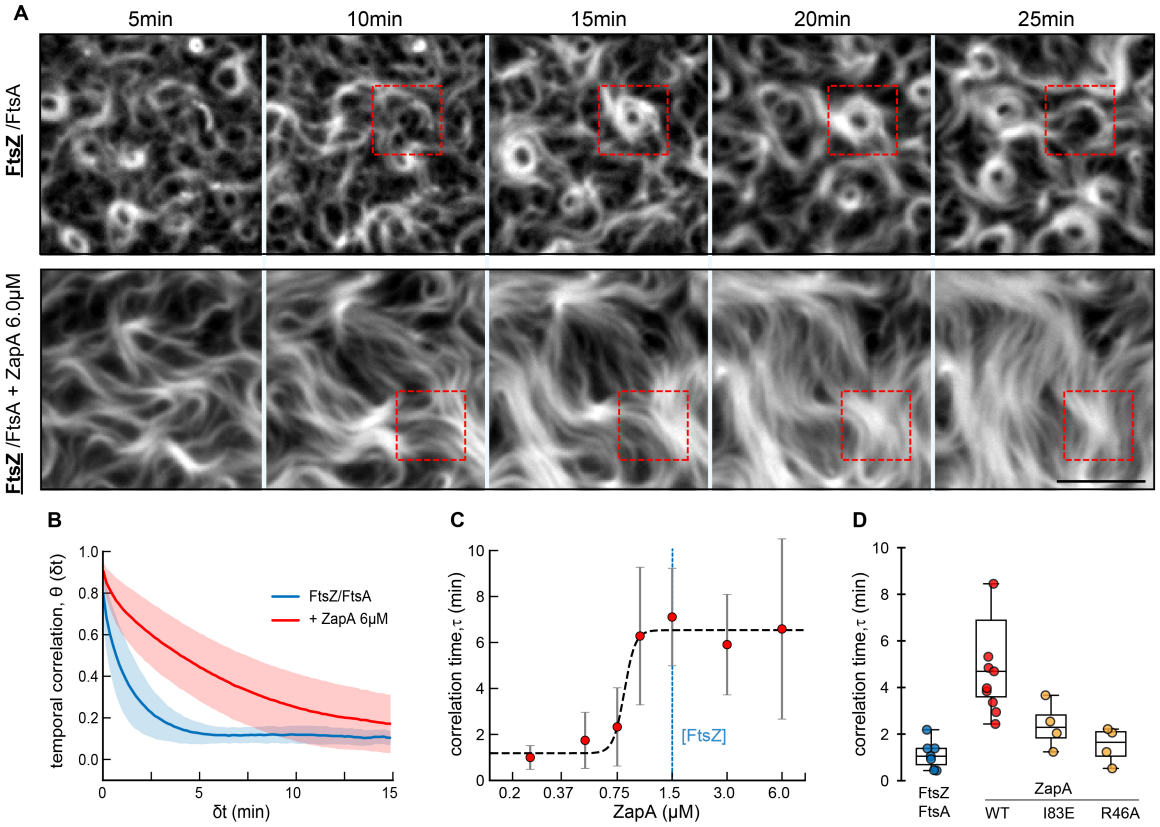

Figure 3.5: ZapA stabilizes FtsZ filament bundles. (A) In the absence of ZapA (upper panel), the FtsZ filament pattern constantly reorganized and ring-like structures formed only transiently (red dashed squares). In contrast, in the presence of ZapA (lower panel) FtsZ assemblies were much more persistent. Scale bars = $2\mu M$ **(B)** The temporal autocorrelation function of the FtsZ filament network decayed quickly without ZapA (blue), but slowly in the presence of $6.0\mu M$ (red). Each curve represents the mean ± std (error bands) of independent experiments (FtsZ, $n = 7$, ZapA, $n = 9$). **(C)** The characteristic correlation time, τ, as a function of ZapA concentration. The autocorrelation curves were fitted to a mono-exponential decay and τ was given by the half-time of each decay. Once again, ZapA induced a switch-like behavior showing a hill coefficient >> 4 and a $IC_{50} = 1.05$. Data shown corresponds do the average τ from individual experiments (mean ± std). **(D)** ZapA I83E and R46A (light red) did not change the persistence of FtsZ filament bundles ($p > 0.05$; Table 5.2).

time (Fig. 3.5D; $p = 0.427$ and $p = 0.084$, respectively). This shows that tetrameric ZapA not only affects the architecture of the membrane-bound filament network, but also its reorganization dynamics in a highly cooperative manner.

Together, our *in vitro* experiments and quantitative image analysis have identified an ultrasensitive switch in filament architecture and reorganization dynamics dependent on the concentration of ZapA. In all instances, this switch happens at ZapA concentrations between 0.75μM and 1.0μM, before the system saturates at ZapA concentrations equimolar to FtsZ at 1.5μM. Interestingly, this correlation is consistent with ZapA tetramers having four FtsZ binding sites and with their concentration ratio found *in vivo* [Low *et al.*, 2004; Mohammadi *et al.*, 2009].

3.4 Large-Scale Organization of FtsZ Filaments in the Presence of ZapB, ZapC and ZapD

Similar to ZapA, another three FtsZ associated proteins, ZapB, ZapC and ZapD, have been implicated in stabilizing the cytokinetic ring at midcell by bundling and binding to FtsZ filaments [Durand-Heredia *et al.*, 2012; Galli and Gerdes, 2012; Galli and Gerdes, 2010]. In contrast to ZapA, these Zaps are only found in Gammaproteobacteria bacteria [Durand-Heredia *et al.*, 2012; Hale *et al.*, 2011] but also dispensable for cell division, with mutants exhibiting similar mild phenotypes. However, strong synergistic division anomalies appear when more than one Zap protein is mutated [Durand-Heredia *et al.*, 2012; Hale *et al.*, 2011]. Here, we purified these three crosslinkers and investigated how they differ from ZapA using our *in vitro* reconstitution approach and our image analysis tools described previously.

3.4.1 Inhibitory Effect of ZapB on ZapA Activity

ZapB is recruited to midcell via its interaction with ZapA and MatP, a DNA-binding protein that condenses the Ter macrodomain of the chromosome [Ebersbach *et al.*, 2008; Espéli *et al.*, 2012; Buss *et al.*, 2013]. The absence of either ZapA or ZapB leads to widely-dispersed FtsZ clusters through the cytoplasm and abnormal septa formation [Buss *et al.*, 2013; Buss *et al.*, 2017; Galli and Gerdes, 2010; Galli and Gerdes, 2012] suggesting that ZapB can regulate the activity of ZapA. *In vitro*, high concentrations of ZapB were shown to disrupt the interaction of FtsZ and ZapA, which points to a sequester mechanism [Galli and Gerdes, 2012]. Therefore, we were interested to know if ZapB would show a similar effect on the activity of ZapA in our experimental assay.

First, we performed our standard self-organization experiment with FtsZ and FtsA in the presence of increasing concentration of ZapB up to 12μM. As expected, we observed no alteration of the standard FtsZ filament network architecture, since ZapB does not bind FtsZ directly [Ebersbach *et al.*, 2008]. Then, to probe if ZapB reduces the interaction of ZapA with FtsZ, we repeated this experiment in the presence of 3μM or 6μM ZapA (Fig. 3.6A; Movie 5). We found that with increasing concentrations of ZapB, FtsZ filaments self-organized back into a network of curved filament bundles, recapping the behavior of FtsZ alone (Fig. 3.6A, far-right).

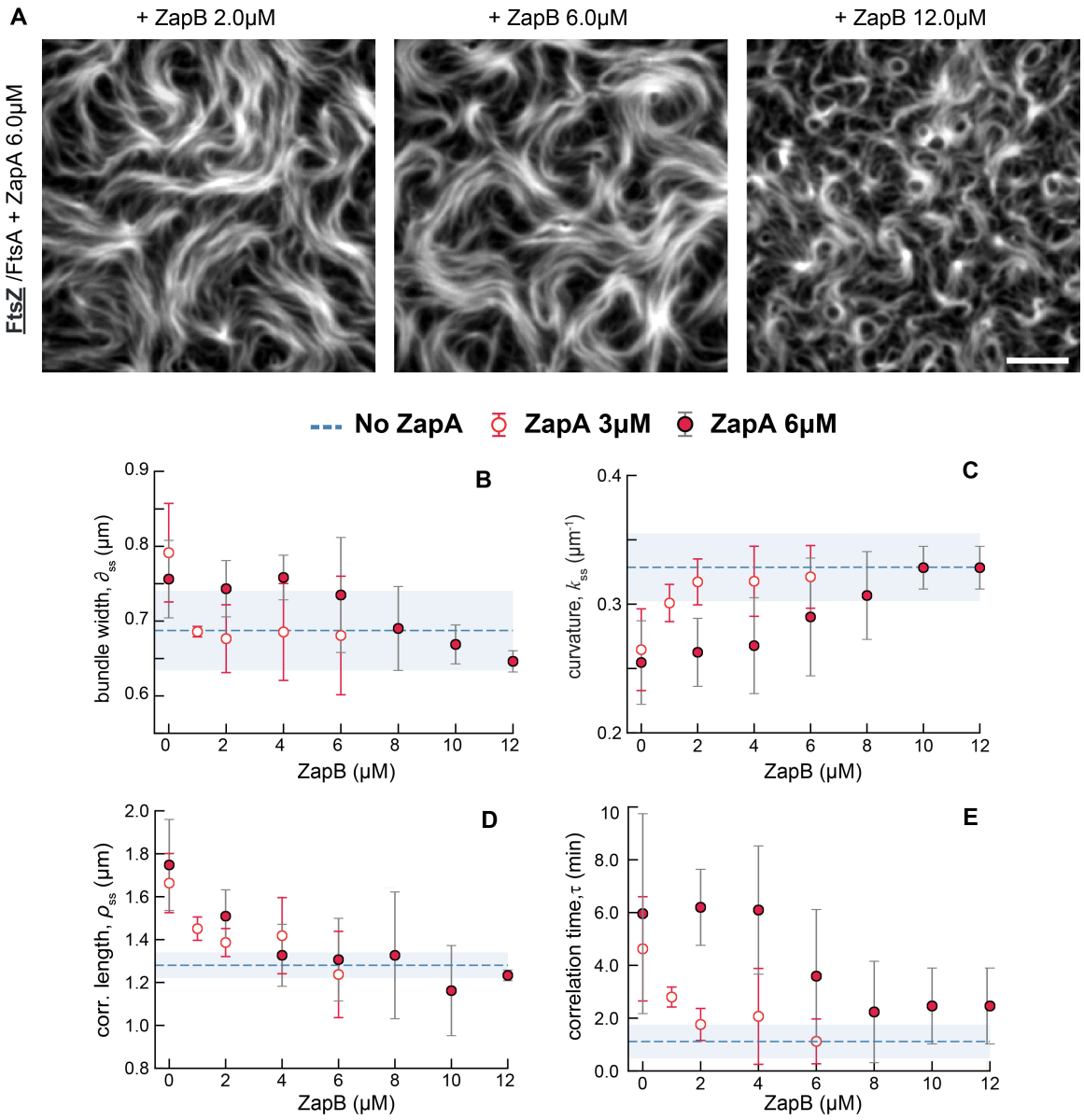

Figure 3.6: ZapB prevents ZapA activity. **(A)** Snapshots showing the inhibitory effect of increasing concentrations of ZapB (0-12μM) on the activity of 6μM ZapA (FtsZ = 1.5μM, FtsA = 0.5μM). Scale bars = 5μm. **(B)** ZapB counteracted the influence of ZapA on bundle width, curvature **(C)**, correlation length **(D)** and correlation time **(E)** in a concentration-dependent manner, causing a shift towards values typically observed for the FtsZ pattern alone (blue dashed line).

To quantify these observations, we measured all the parameters described before in the presence of ZapA (bundle width, curvature, correlation length and correlation time) and found that ZapB completely reversed the effect of ZapA in a concentration-dependent fashion (Fig. 3.6B-E). These values plateaued when the concentration of ZapB exceeded the concentration of ZapA. These results confirm the ability of ZapB to counteract the activity of ZapA on FtsZ, as formerly observed in other studies [Buss *et al.*, 2013; Buss *et al.*, 2017; Galli and Gerdes, 2012].

3.4.2 The Effect of ZapC and ZapD on FtsZ Filaments

Recent evidence has shown that ZapC and ZapD can bind FtsZ independently of FtsA, ZipA, ZapA and ZapB, and seem to have a similar effect to the one observed for ZapA, promoting filamentous structures of polymeric FtsZ in several *in vitro* studies [Durand-Heredia *et al.*, 2012; Hale *et al.*, 2011]. These studies relied on transmission electron microscopy, sedimentation assays and light scattering studies, which mask potential differences in the dynamics of these structures.

Opposing to the four binding site tetramer formed by ZapA, ZapC is a monomer (20 kDa) with two FtsZ binding sites [Schumacher *et al.*, 2016], while ZapD (28 kDa) organizes into a dimer with one binding site in each subunit [Schumacher *et al.*, 2017] (Fig. 1.8). All of these are in agreement with their ability to crosslink FtsZ filaments. In addition, these proteins also show unique binding properties: ZapD interacts with the C-terminal tail of FtsZ, similarly to its membrane anchors FtsA and ZipA, while ZapC and ZapA bind to the globular core of FtsZ [Schumacher *et al.*, 2016].

Therefore, despite having seemingly overlapping functions, it is possible that the different oligomerization states, molecular dimensions and binding sites of different Zaps contribute to modulate FtsZ filaments organization and dynamics in a different manner.

Therefore, we started by questioning if ZapC has a similar effect to the one observed for ZapA in our experimental assay. We performed our self-organization assay with FtsZ and FtsA (1.5μM and 0.50μM, respectively, as before) in the presence of increasing concentrations of ZapC up to 3.0μM. We found that ZapC induced filament re-organization into a network of more aligned and straighten filaments with an apparent increase in bundle width (Fig. 3.7A,B, Movie 6), similar to the effect observed for ZapA (Fig. 3.1B, Movie 2).

However, the architecture induced by ZapC is slightly different. FtsZ filament bundles display less local density and spread like a carpet, completely covering the membrane when in high concentrations ($>$ 1.0μM) or after long incubation times (>15min). For this reason, we considered only mild concentrations of ZapC for the quantitative analysis (0.5μM and 1.0μM) with short incubation times (10min). This allowed us to observe a significant re-organization of the pattern without completely saturate the membrane (Fig. 3.7B).

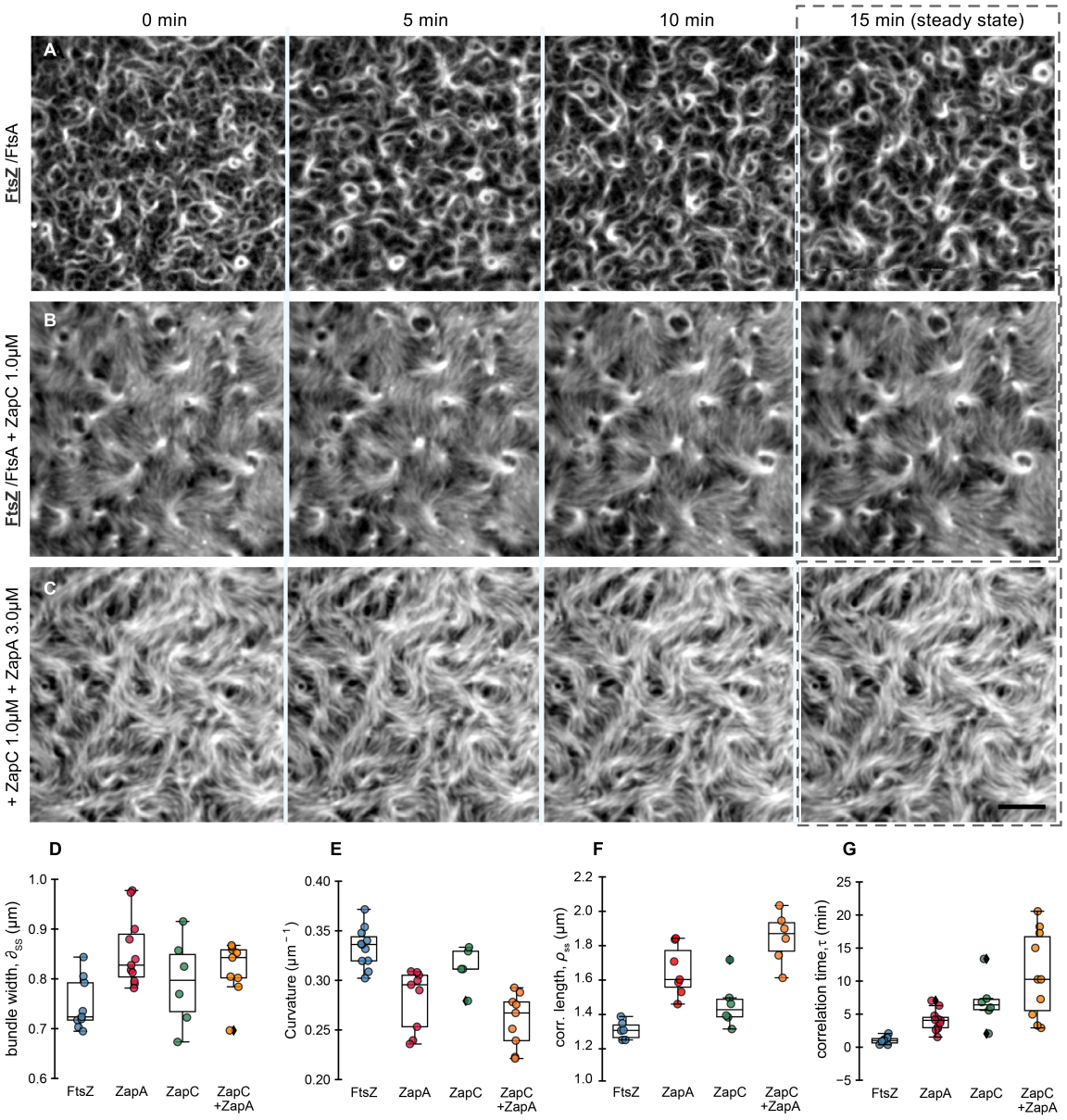

Figure 3.7: Bundles of membrane-bound FtsZ filaments show a distinct architecture in the presence of ZapC when compared with ZapA. Snapshots of FtsZ pattern emerging from its interaction with FtsA alone on SLBs **(A)**, in the presence of 1μM ZapC **(B)** or in the presence of 1μM ZapC in combination with 3μM ZapA **(C)**. Concentrations of FtsZ (30% Cy5-labelled) and FtsA were kept constant for all experiments (1.5μM and 0.5μM, respectively). Scale bars = 5μm; **(D)** Mean bundle width, δ_{ss}, of membrane-bound FtsZ filaments did not change significantly in the presence of 0.5/1μM ZapC alone (green, $p = 0.30$)), but showed an increase when ZapC was combined with 3μM ZapA (orange) ($p < 0.05$). Similarly, a combination of 0.5/1μM ZapC and 3muM ZapA showed a significant decrease in the curvature of the FtsZ filament network **(E)**, along with an increase of the correlation length **(F)** and correlation time **(G)** ($p < 0.05$, Table 6.3), showing that a combination of these two proteins increase the persistence and order of membrane-bound FtsZ filaments.

Next, we investigated how a combination of both ZapC and ZapA would affect the large-scale architecture of the FtsZ network. For this, we performed our self-organization assay with FtsZ, FtsA and 3μM of ZapA in the presence of ZapC, either in a final concentration of 0.5μM or 1μM (Fig. 3.7C; Movie 7).

The pattern emerged as a combination of ZapA and ZapC effects previously observed, rapidly forming high density filament bundles with the typical motile assemblies. Following these observations, we then used our image analysis tools to quantify the organization of membrane-bound FtsZ filaments in these conditions.

The quantification of the apparent bundle width in the presence of ZapC or ZapC combined with ZapA, was somewhat limited by the observed carpet-like effect, but our analysis was still able to track a slight increase compared to FtsZ alone (Fig. 3.7D). In the presence of ZapC alone, the mean curvature κ and the mean correlation length, ρ, of the filament network did not change significantly, but in combination with ZapA showed a more pronounced effect - lower curvature and higher correlation length - than ZapA alone (Fig. 3.7E,F; $p < 0.01$, Table 6.3). This is in agreement with a filament network containing more aligned and straighten filaments in the network. Lastly, our temporal autocorrelation analysis also showed a more pronounced effect when ZapC and ZapA were combined together than the effect of ZapA or ZapC alone (Fig. 3.7G; $p < 0.01$, Table 6.3). These results suggest that ZapC and ZapA have a synergistic effect in increasing order and persistence of the FtsZ filament bundles.

Finally, we tested the effect of ZapD under the same experimental conditions used up to this point. Interestingly, concentrations of ZapD up to 12μM showed no effect on the FtsZ/FtsA self-organization pattern (Fig. 3.8A,B; Movie 8). Although, FtsZ pellet was enriched in the presence of ZapD in our sedimentation assays (Fig. 3.8C,D), a method commonly used to demonstrate binding of proteins that interact directly with FtsZ filaments.

We also investigated if the presence of ZapD could have an impact on ZapA and/or ZapC behavior, but the filament network pattern observed remained intact irrespective to the amount of ZapD in solution (data not shown). A possible explanation for these observations is the fact that ZapD shares the binding for FtsZ with FtsA, while ZapC and ZapA bind to a different region of the backbone [Schumacher *et al.*, 2016], thus, FtsA might gain an advantage over ZapD when competing to bind the C-terminal domain in our assays. Further experiments are necessary to explore these observations in more detail.

We confirmed that ZapB has no direct effect on FtsZ filament network but can reverse the activity of ZapA. Surprisingly, ZapD had no influence on the organization or

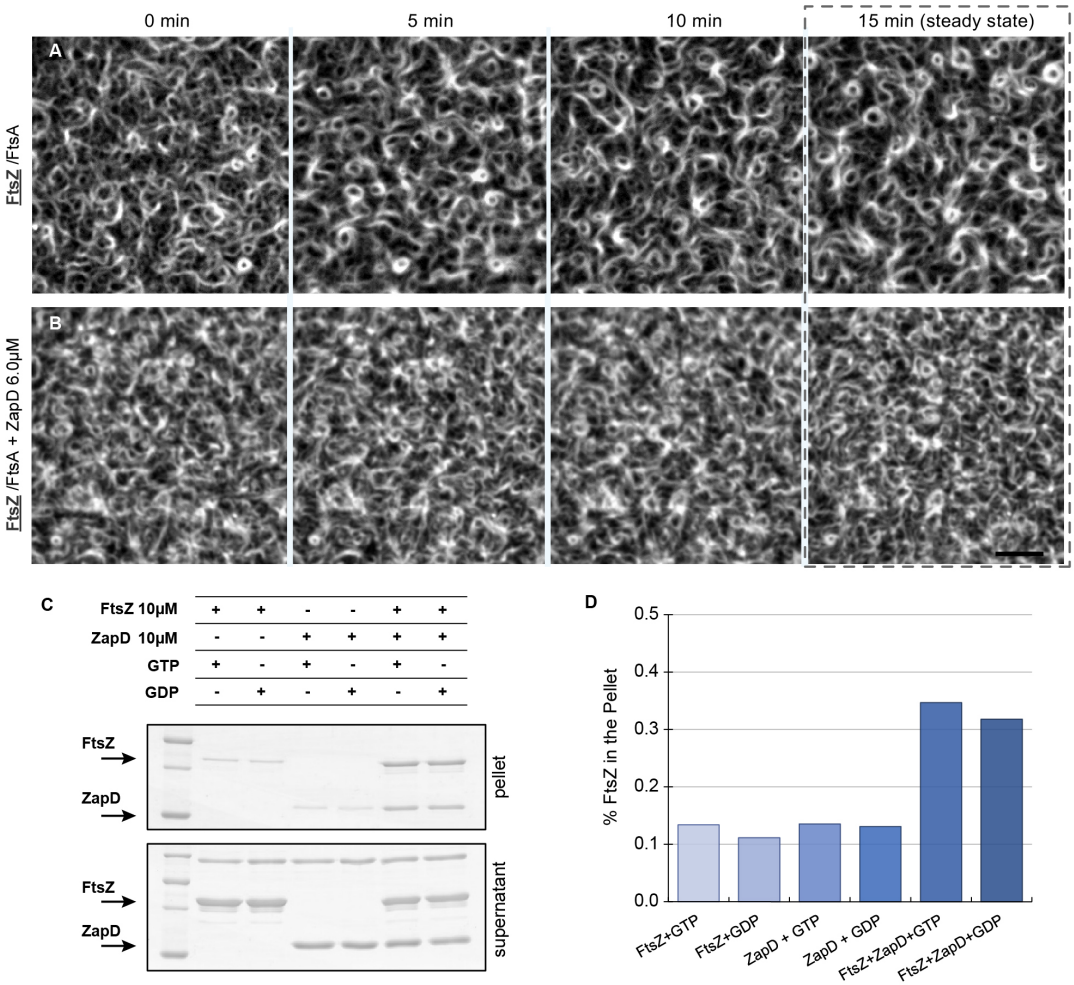

Figure 3.8: ZapD has no effect on FtsZ filament network but binds directly to FtsZ filaments. Snapshots of FtsZ pattern emerging from its interaction with FtsA alone on SLBs **(A)** and in the presence of 6μM ZapD **(B)**. Concentrations of FtsZ (30% Cy5-labelled) and FtsA were kept constant for all experiments (1.5μM and 0.5μM, respectively). Scale bars = 5μm; **(C)** Sedimentation of FtsZ and ZapD in equimolar concentrations. Reaction contained PIPES buffer (pH = 6.5), KCL 50mM, MgCl2 10mM and GTP or GDP in a final concentration of 4μM. **(D)** Protein percentages in each pellet were quantified based on band intensities of total protein present in the pellet and supernatant fractions.

dynamics of FtsZ filament bundles, either alone or in combination with other Zaps, despite being able to induce polymerization of FtsZ in sedimentation assays. Lastly, we found that ZapC increases the spatial order and persistence of membrane-bound FtsZ filaments, as observed for ZapA. However, the architecture of the pattern was considerably distinct.

Chapter 4

Analysis of Filament Polymerization Dynamics in Cytoskeletal Filament Networks

To understand the properties of cytoskeletal filaments and their role for the large-scale organization of the cell, it is essential to study their polymerization–depolymerization dynamics and how they are changed by regulatory proteins. This not only requires experimental assays that can visualize filament dynamics, but also reliable, quantitative methods to measure the rates of polymerization and depolymerization in a non-biased, high-throughput manner.

Despite recent advances in high-resolution fluorescence imaging in biology, kymographs are still the most commonly used approach to visualize dynamics, in particular of cytoskeletal structures. In kymographs, the intensity along a predefined path is plotted for every image of a time-lapse movie, which results in the profile at the spatial position of an object over time. This approach helps to visualize dynamic processes and allows for a direct read-out of speed and direction of a moving object by analyzing the slope of a corresponding diagonal line (Fig. 4.1). Due to their ease of use, kymographs have been routinely used to measure growth and shrinkage velocities of dynamic systems, including the treadmilling behavior of membrane-bound filaments of FtsZ [Loose and Mitchison, 2014; Ramirez-Diaz *et al.*, 2018]. However, using kymographs to quantify polymerization dynamics has serious drawbacks. Despite being assisted by image analysis software, kymographs are essentially a hand-tracking technique, which makes the collection of large data sets not only impractical but also subject to user bias.

Recently, a number of computational approaches have been developed aiming for an automated analysis of experimental data. In these cases, automatic tracking algorithms were designed to either follow the position of microtubules or actin filaments in filament gliding assays [Ruhnow *et al.*, 2011], an important tool to study molecular motors and microtubule polymerization dynamics [Kapoor *et al.*, 2019]. However, reliable single filament tracking is currently impossible within dense assemblies of homogeneously labelled filaments, such as in the actin cortex, mitotic spindle or

membrane-bound cytoskeletal networks of FtsZ. To overcome these difficulties, different alternative strategies relying on automated data collection and analysis have been developed. For instance, fluorescently labelled microtubule plus-end binding proteins have been used as markers for plus end-growth [Perez *et al.*, 1999]. These proteins specifically recognize a structural property of the growing end of the microtubule, where they form a characteristic comet-like fluorescence profile. These comets were first semi-manually tracked and analyzed [Gierke *et al.*, 2010], but later improved image analysis methods helped to fully computationally detect and track EB1 comets in space and time. This made possible to analyze large populations of microtubule ends in an unbiased manner even in the crowded environment of a mitotic spindle, microtubule asters in cells or cytoplasmic extracts [Applegate *et al.*, 2011; Matov *et al.*, 2010]. However, up to date the ability to use filament end binding proteins as a proxy for polymerization dynamics only exists for microtubules and is not available for other cytoskeletal systems. Furthermore, depolymerization velocities are not directly available with this method.

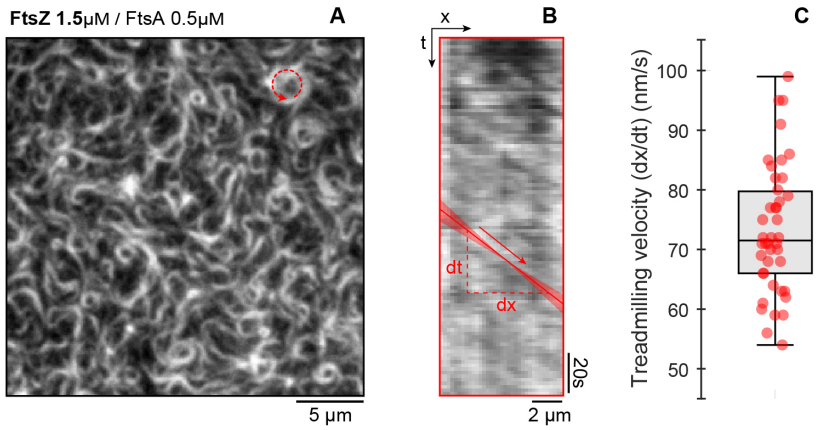

Figure 4.1: Treadmilling speed quantification using kymographs.(A) Snapshot of FtsZ (30% Cy5-labelled) pattern emerging from its interaction with FtsA, 15min after the addition of GTP and ATP to the reaction buffer. Scale bars = 5μm. **(B)** Representative kymograph of treadmilling dynamics taken along the contour of a rotating FtsZ ring (red line in A). The shaded red bar illustrates the imprecision associated with manually drawing the diagonal line to estimate velocity. Scale bars, x = 2 μm, t = 20s. **(C)** Example for the distribution of velocities obtained using kymographs. Red dots correspond to velocities obtained from individual rings in multiple experiments. Box plots encompass the 25–75th percentiles, whiskers indicate outliers and midlines indicate the median.

A more generally applicable approach was introduced with Fluorescent Speckle Microscopy, which has been proven to be valuable for analyzing *in vivo* dynamics of actin and microtubule sliding in living cells as well as cell extracts [Waterman-Storer *et al.*, 1998].

Here, small amounts of fluorescently labelled molecules are added to an endogenous dark background, producing a random distribution of fluorescent spots inside cytoskeletal structures. Intensity changes in these speckles disclose information regarding the turnover and binding constants of the subunits, while their motion can be computationally analyzed to retrieve an intracellular map of polymer dynamics. However, fluorescence speckle microscopy does not provide a direct readout of filament growth and shrinkage. Instead, in the case of actin, polymerization rates are derived from the quantification of retrograde polymer flow, while depolymerization is estimated from the decay of speckle number with time [Watanabe and Mitchison, 2002]. Accordingly, in the absence of polymer transport, a quantification of polymerization dynamics is not possible by Speckle Microscopy.

To address these limitations, we sought to develop a new image analysis workflow that would allow us to track polymerization dynamics in a more accurate and automated manner using time-lapse movies of homogeneously labeled filaments. This approach comprises three computational steps: (i) generation of dynamic fluorescent speckles by image subtraction; (ii) detection and tracking of fluorescent speckles to build treadmilling trajectories and (iii) analysis of trajectories to quantify velocity and directionality of filaments (Fig. 4.2). We use this approach to quantify the speed, directionality and orientation of treadmillling FtsZ filaments in our experiments, and later, the dynamic of microtubules in large asters, as a proof of concept.

4.1 Differential Imaging Protocol

To extract dynamic information from time-lapse movies, we took advantage of a background subtraction method also used for motion detection in computation-aided video surveillance [Singla, 2014]. By subtracting the intensity of two consecutive frames, a new image is created where persistent pixels are removed and only short-term intensity changes are kept. Thus, non-moving objects generate small absolute pixel values, while high positive and negative intensity differences correspond to fluorescent material being added or removed at a given position, respectively. When applying this procedure to our image sequences, we generate a new time-lapse movies containing moving fluorescent speckles that correspond to growing and shrinking filament ends within FtsZ bundles (Fig. 4.2A).

Accordingly, this process allows to visualize and quantify polymerization as well as depolymerization rates (Fig. 4.2B). While this process can be easily applied using the ImageJ ImageCalculator plugin, simple image subtraction is susceptible to noise and may generate stretched speckles when the sample acquisition rates are not ideal. Therefore, we incorporated a pre-processing step where we apply a spatiotemporal low-pass filter prior to image subtraction (Fig. 4.2A, I and II). This procedure uses a 3D Gaussian filter where the extent of the smoothing is defined by σ_{xy} and σ_t, representing a convolution in space and time, respectively. The spatial smoothing replaces each pixel value by the Gaussian-weighted average of its neighboring pixels, while the temporal filter replaces each pixel value by the averaged pixel intensity in the previous and subsequent frames. This spatiotemporal smoothing not only effectively removes acquisition noise, but also improves speckle detection and tracking in the next step.
In sum, this procedure generates two new time-lapse movies showing directionally moving fluorescent spots, either corresponding to growth or shrinkage of filaments at a given position (Fig. 4.2A, III).

Next, TrackMate (https://imagej.net/TrackMate) was used to follow hundreds of fluorescent spots generated per experiment and obtain detailed information regarding their displacement and velocity (Fig. 4.2B,C). Moving speckles were detected using the LoG (Laplacian Gaussian) detector with an estimated diameter of 0.8μm. We discarded all speckles with a signal-to-noise ration lower than 1. To build the final trajectories we used the "Simple LAP tracker" with a "Max Linking Distance" of 0.3μm, a "Maximal gap-closing distance" of 0µm and "Max frame Gap" of 0 frames. For the analysis, we only considered trajectories longer than 6sec.

Finally, these trajectories were further analyzed with a custom python script to obtain a quantitative information about speed and directionality (Fig. 4.2C; see section 6.5 for code availability). For each individual trajectory, we computed the mean-squared displacement (MSD) and fitted the resulting curve to a quadratic equation containing both a diffusion (D) and a constant squared velocity (V) term [Qian and Sheetz, 1991]:

$$MSD(\tau) = \langle (x(t+\tau) - x(t))^2 \rangle = 4Dt + V^2t^2$$

The velocity was determined by performing a weighted fit to only 50% of the track

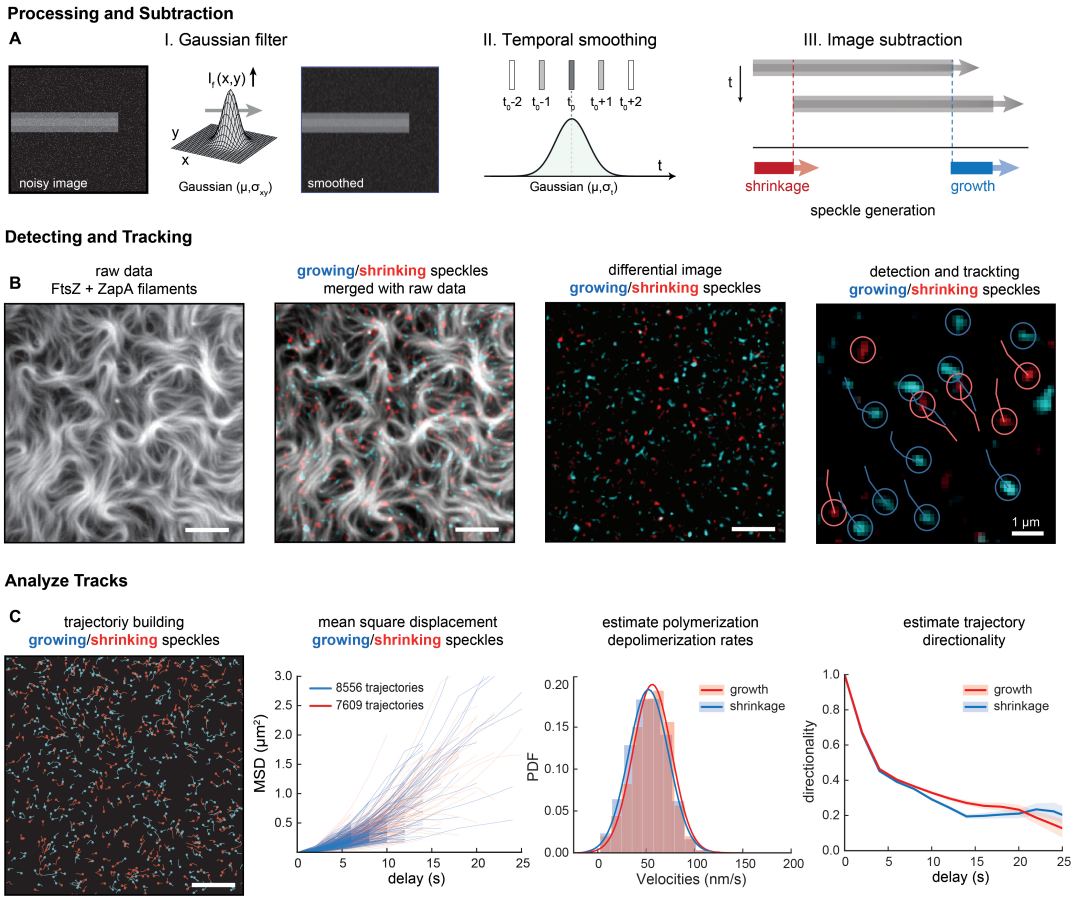

Figure 4.2: Treadmilling analysis protocol. (A) Illustration of the Gaussian filtering step in space (I) and time (II) before image subtraction (III). The smoothing in space and time is defined by σ_{xy} and σ_t, respectively, and μ represents the mean value of the distribution. **(B)** Representation of differential TIRF images to visualize polymerization (growth, blue) and depolymerization (shrinkage, red) of FtsZ filaments and automated tracking of treadmilling dynamics with TrackMate (ImageJ). Scale bars = 5μm or 1μm, when indicated. **(C)** Quantitative analysis of FtsZ filament treadmilling. From left to right: Trajectories resultant from the automated tracking of treadmilling dynamics with TrackMate, individual MSD curves for growth (blue lines) and shrinkage (red lines), distribution of velocity values obtained from fitting individual MSD curves and velocity autocorrelation analysis using the definition in the main text.

duration as the error of the MSD curve quickly increases when τ becomes too large. The mean velocity of each sample was estimated from a simple Gaussian fit to the distribution velocities retrieved from each individual MSD curve. The positive curvature of each MSD curve already reveals the existence of directed motion [Qian and Sheetz, 1991], but for a more deep analysis of directionality, we used a second approach termed directional persistence.

This directional analysis measures the autocorrelation of the velocity vectors for all the particles in each track. For this, vector angles of the normalized displacement vectors are compared pairwise as a function of an increasing time interval (τ) and the correlation coefficient (V_{corr}) is given by the cosine of the angle difference.

Accordingly, velocity vectors for a random motion are completely uncorrelated ($V_{corr} = 0$ for all τ), but highly correlated for a directed motion ($V_{corr} > 0$ for all τ).

In contrast to previous methods, this approach can be applied on any time-lapse movie of homogeneously labelled filaments as it does not require specific markers for polymer ends. It surpasses the limitations of kymographs as it allows for a non-biased quantification of dynamic processes in an automated fashion. It allows to quantify both growing and shrinking rates of dynamic cytoskeletal filaments and can be easily extended to more complex analyses, for example to generate spatiotemporal maps of filament dynamics in living cells. In fact, combined with an appropriate detection procedure, this approach could be extended to analyze crawling cells and migrating animals.

4.2 FtsZ Treadmilling Velocities in the Presence of ZapA

In the previous chapter, our experiments revealed that ZapA significantly slows down reorganization of the dynamic FtsZ filament network and increases its spatial order. Next, we considered how ZapA affects the treadmilling velocity of the FtsZ network on a filament level. Previous *in vitro* studies reported that ZapA inhibits the GTPase activity of FtsZ, suggesting that it impairs treadmilling [Small *et al.*, 2007; Galli and Gerdes, 2012; Pacheco-Gómez *et al.*, 2013], even though this effect depends on the buffer conditions [Mohammadi *et al.*, 2009; Woldemeskel *et al.*, 2017]. However, it is unclear how decreased filament turnover is compatible with the function of treadmilling FtsZ filaments to homogeneously distribute wall synthases at the division site. This could perturb the spatiotemporal dynamics of cell wall synthases *in vivo*, as their motion is driven by FtsZ treadmilling. Knocking out individual Zap proteins *in vivo* did not show any significant change in the FtsZ treadmilling velocity [Yang *et al.*, 2017], but due to their overlapping functions it is difficult to rule out the possibility of other FtsZ associated proteins compensating for the loss of crosslinking in these mutants. Accordingly, the direct influence of FtsZ-binding proteins on filament dynamics is unknown.

Due to their ease of use, we have used kymographs routinely to measure growth and shrinkage velocities of treadmilling FtsZ filaments behavior of membrane-bound filaments of FtsZ (Fig. 4.1; [Loose and Mitchison, 2014]).

In this work, we sought for a more accurate and automated manner of studying these processes, which motivated our differential image analysis workflow to track polymerization dynamics, described above. Here, we first constructed differential time-lapse movies using our standard homogeneously labeled FtsZ filaments, either alone or in the presence of 6μM of ZapA (Fig. 4.3A,B; Movie 9 and Movie 10). As explained, this image-processing step removes static objects from the movie while regions where the image changes give rise to either a positive or negative signal, corresponding to areas where the intensity has either increased or decreased between the subsequent frames. These fluctuations correspond to either growing (green) or shrinking (magenta) ends of filament bundles (Fig. 4.3A,B; Movie 9 and Movie 10). Using particle-tracking software to automatically detect and analyze the mean-squared-displacement of these spots along their trajectories (Fig 4.3C,D) and estimate the velocity of the treadmilling filaments (Fig 4.3E,F) we calculated the growth (v^+) and shrinkage (v^-) velocities of thousands of treadmilling tracks simultaneously in both conditions.

In the absence of ZapA, we found v^+ and v^- to be normally distributed with similar mean values ($v^+ = 50.5 \pm 3.0 nm/s$, $n = 10$; $v^- = 53.0 \pm 3.6 nm/s$, $n = 10$), consistent with a treadmilling behavior (Fig. 4.3E, blue). In the presence of 6.0μM ZapA, we found similar values ($v^+ = 47.8 \pm 3.45 nm/s$ and $v^- = 50.4 \pm 4.1 nm/s$, $n = 10$) (Fig. 4.3E, red), as well as for all other ZapA concentrations tested (Fig. 4.3F) and mutants (Fig. 4.3G). Accordingly, we found that ZapA has no effect on the treadmilling velocity of membrane-bound FtsZ filaments.

In addition, we performed a directional autocorrelation analysis on FtsZ treadmilling trajectories, which provides information about the directional persistence of the particles within each track, as described above (Fig. 4.3H-J). In agreement with directional motion, the correlations for treadmilling trajectories were always positive and followed a slow decay (Fig. 4.3I). Interestingly, we observed that the directionality was preserved for longer time delays in the presence of ZapA indicating straighter treadmilling trajectories. This observation is also consistent with the observed decrease in curvature and increase in spatial order (Fig. 3.4). Once again, we confirmed that ZapA R46A and I83E had no effect on the directionality of FtsZ filament bundles (Fig. 4.3J ; $p > 0.05$, Table 6.2).

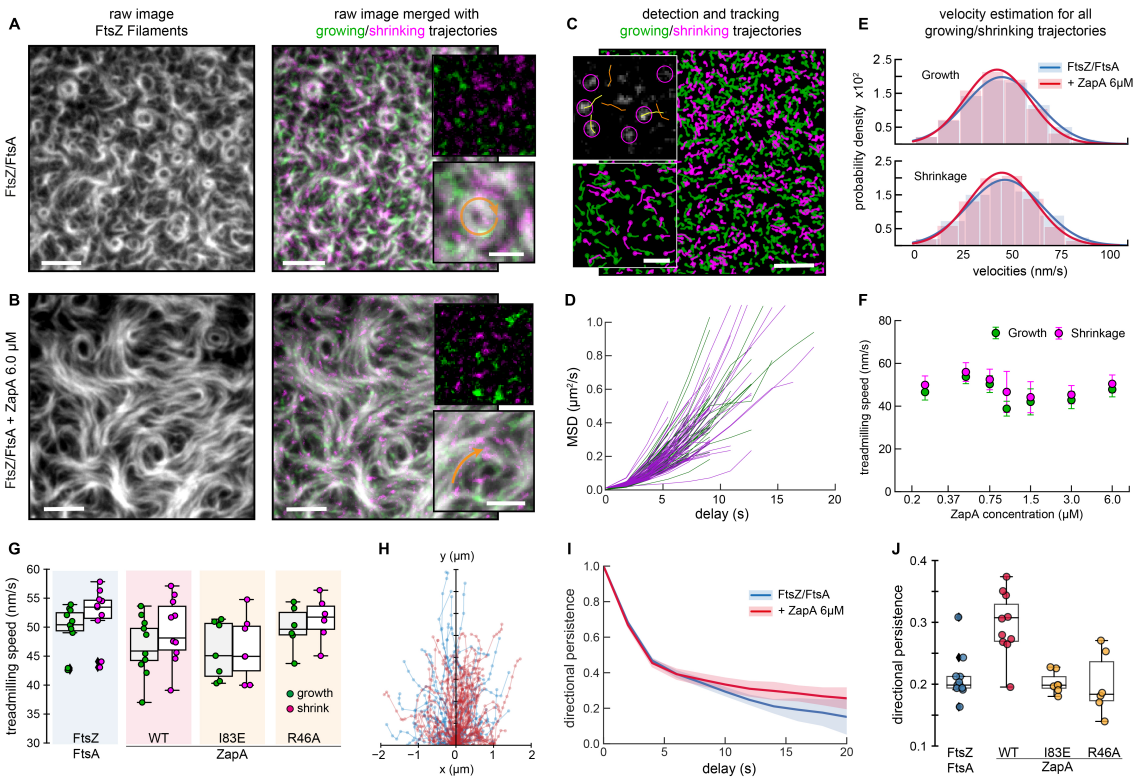

Figure 4.3: ZapA does not change treadmilling speed of FtsZ filaments. Raw image of FtsZ filament network and the corresponding differential image overlaid showing growing (green) and shrinking (magenta) ends without ZapA **(A)** and in the presence of 6.0μM ZapA **(B)**. Orange arrows indicate treadmilling direction. **(C)** Snapshot showing an example of detection (purple circles) and tracking (yellow/orange lines) of fluorescent spots and the respective generated trajectories. First position of each trajectory is indicated with circles. Scale bars, large image = 5μm, small image = 2μm. **(D)** Representation of individual MSD curves for growth and shrinking trajectories generated from a single FtsZ/FtsA sample. **(E)** Velocity distribution of filament growth (upper panel, FtsZ/FtsA, $v^+ = 50.5 \pm 20.1 nm/s$, FtsZ, FtsA + ZapA, $v^+ = 47.8 \pm 18.2 nm/s$) and shrinkage (lower panel, FtsZ/FtsA, $v^- = 53.0 \pm 20.7 nm/s$, FtsZ/FtsA + ZapA, $v^- = 50.4 \pm 18.6 nm/s$). Both show a normal distribution without any significant difference in the mean. **(F,G)** Increasing concentrations of ZapA had no effect on the mean velocity of FtsZ filaments at either end ($p > 0.05$; Table 6.2) as well as the ZapA mutants. **(H)** A couple of individual trajectories of FtsZ/FtsA filaments with (red) and without (blue) 6.0μM ZapA present plotted with the same origin in a Cartesian coordinate system. Particles migrate directionally in both conditions. **(I)** Directional autocorrelation revealed that directionality was increased in the presence of 6μM ZapA (red) when compared to FtsZ/FtsA (blue). **(J)** Autocorrelation values for $\delta t = 14s$: v_{corr}(FtsZ)= 0.21 ± 0.04 ($n = 10$) and v_{corr}(ZapA)= 0.30 ± 0.05 ($n = 10$). ZapA mutants had no effect on this parameter (orange boxplots), showing a similar mean value to FtsZ when alone ($p > 0.05$, Table 6.2).

4.3 FtsZ Filament Polarity in the Presence of ZapA

The observed directional treadmilling of FtsZ filament bundles *in vivo* and *in vitro* is generally compatible with a polar orientation of filaments. However, based on its molecular structure, ZapA was suggested to promote antiparallel alignment [Low *et al.*, 2004]. Accordingly, we wondered how the presence of ZapA changes the relative orientation of FtsZ filaments in our assay.

To obtain information about the relative orientation of FtsZ filaments within the bundles, we looked at the intensity of directionally moving fluorescent spots produced by our differential time-lapse movie analysis (Fig. 4.3A; Movie 9 and Movie 10). A constant intensity along their trajectories is consistent with a predominant polar orientation of filaments within a treadmilling bundle (Fig. 4.4A, left panel). In case of a rearrangement of the filaments into anti-parallel bundles, we expected these fluorescent spots to have different intensities and behavior (Fig. 4.4A, right panel).

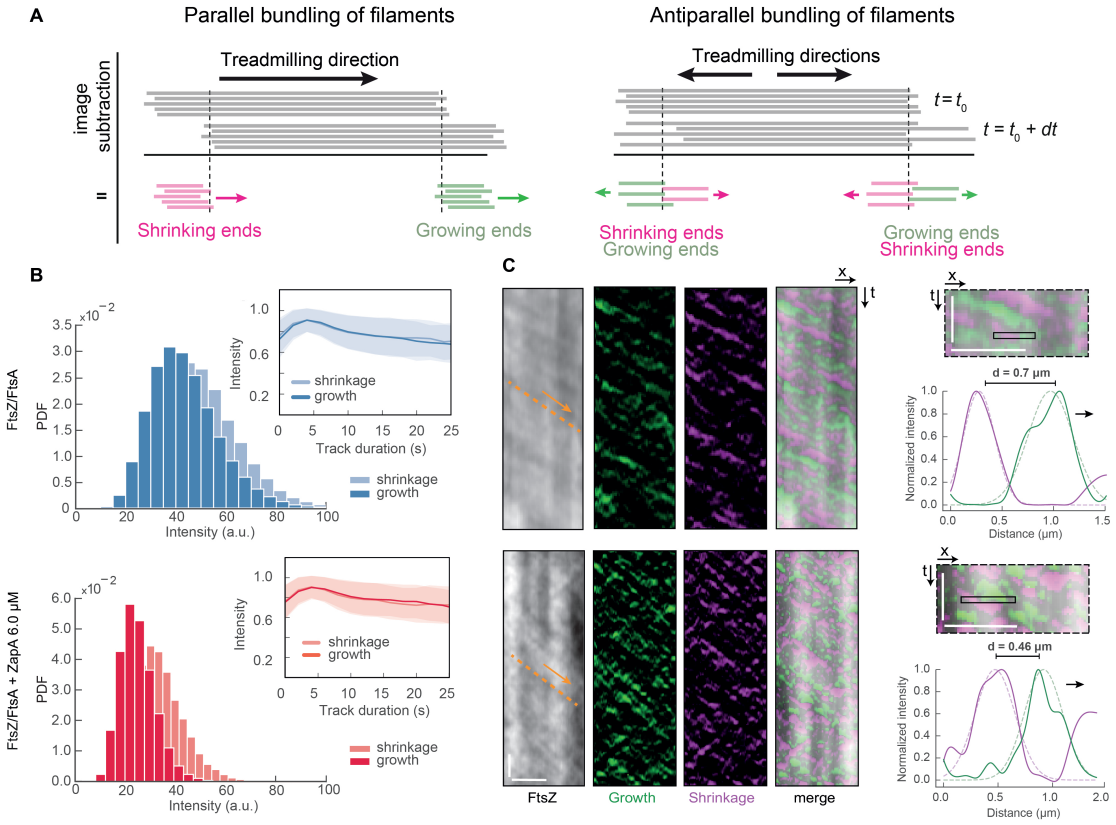

Figure 4.4: ZapA does not change orientation nor length of FtsZ filaments. (A) Illustration of image subtraction step assuming parallel (left panel) or antiparallel filament bundles (right panel). For parallel bundles of treadmilling filaments, image subtraction results in fluorescent spots corresponding to FtsZ binding or detaching from a filament bundle allowing to visualize polymerization (growth, green) and depolymerization (shrinkage, magenta) trajectories. We expect that spots corresponding to growing and shrinking ends have similar intensities and closely follow each other. In contrast, for antiparallel bundles of treadmilling filaments, the spots corresponding to growth and shrinkage would move in opposite directions and cross each other. **(B)** Intensity distribution of fluorescence spots generated from a differential time-lapse movie of FtsZ/FtsA filaments (blues) and with 6.0μM ZapA (reds). Insets depict the mean normalized intensities and standard deviation (shaded error bands) of spots versus trajectory length. The presence of ZapA does not change fluorescent spot intensity and thus filament orientation. **(C)** Kymographs obtained along the orange line in Fig. 4.3A. Images represent the channel with the raw data, the two differential channels (growth and shrinkage trajectories) and the merged image. Arrows indicate treadmilling direction. Scale bars, t = 20s, x = 3μm. For each panel, a zoom in into the kymograph is displayed on the right, and below each is the respective intensity profile along the black line, showing the spot intensities averaged along the treadmilling path.

However, these fluorescent spots showed similar intensity traces along their treadmilling trajectories with (Fig. 4.4B, red) and without 6.0μM ZapA (Fig. 4.4B, blue). Together, these findings show that filaments maintain their parallel, polar orientation even in the presence of ZapA.

Next, we wondered if the increase in spatial order and decrease in curvature with ZapA was due to an increased mean length of FtsZ filaments. Directly measuring the length of individual filaments within dense bundles is not possible by light microscopy, but as the spots for growth and shrinkage of a given bundle correspond to the two different ends of filaments, we reasoned that the distance between them provides an estimate of the mean bundle length. Thus, using our differential time-lapse movies, we draw kymographs of individual bundles along their treadimilling direction and plot the intensity profile of growing and shrinking ends as a function of their spatial position (Fig. 4.4C). The distance between the peaks correspond to the average bundle length of the filament.

Using this approach, we estimated the filament length to be around 400-800 nm independent of the presence of ZapA. Naturally, this is just a rough estimation of filament length as the short duration of our trajectories limit this approach, but this rationale may provide a reliable measurement of filament length for longer and more defined tracks. Neverthless, on the next chapter we provide a more accurate measurement of filament length that corroborates the value estimated here.

4.4 Spatial Regulation of Microtubule Depolymerization

To show that our differential image protocol could be easily extended to other dynamic systems, we used it to measure the polymerization dynamics of microtubules in Xenopus egg extracts - a collaboration work with Bruges lab (MPI, Dresden, Germany). Xenopus egg extracts provide metabolically-active cytoplasm that reconstitutes physiological polymerization dynamic of microtubule asters [Ishihara *et al.*, 2014]. Polymerization events in microtubules are typically tracked by EB1 labelling, but an equivalent probe to measure depolymerization rates is still missing. For that reason, only a handful of studies have looked into these shrinking events, mostly relying on manual tracking of a small number of microtubules at cell periphery [Brouhard and Rice, 2018; Desai and Mitchison, 1997].

In this system, microtubule nucleation induces aster growth and two interesting boundaries exist: the interior region around the microtubule organizing centers (MTOC) and the growing aster periphery. The dynamic behavior of minus ends and whether the microtubule dynamics differ between the interior and periphery is still poorly understood. Here, we used our differential image protocol as method to track and measure spatial regulation of polymerization and depolymerization events to help shed some light on these questions.

In these experiments from Tim Mitchison's lab, asters containing Alexa647-labelled tubulin are assembled under K-casein coated coverslips and imaged with TIRF microscopy, as described elsewhere [Ishihara *et al.*, 2014]. Time-lapses where the field of view (FOV) contains the MTOC in one of the corners is defined as the "interior" region (Fig. 4.5A and Movie 11), while "periphery" regions have the FOV focus on the edge of the growing aster (Movie 12), at least 200 microns from the center of the aster. Plus ends at the periphery polymerize into a microtubule-free environment, while those in the interior polymerize into an environment that is dense in microtubules. Manual tracking of MTs dynamics in these movies is limited and poor in statistics [Ishihara *et al.*, 2014].

Here, we constructed differential time-lapse movies with our approach and hundreds of growing and shrinking microtubule ends were generated in an automated fashion (Fig. 4.5A; Movie 11 and Movie 12). This allowed us to track and measure polymerization and depolymerization events in both regions of the aster (Fig. 4.5A). For tracking with used a LoG (Laplacian Gaussian) detector with an estimated diameter of 1μm to detect the moving spots. To discard potential false positives, we considered only particles with a signal-to-noise ratio lower than 0.8 and a track displacement distance larger than 1μm. To build the final trajectories, we used the "Simple LAP tracker" with a "Max Linking Distance" of 1μm, a "Maximal gap-closing distance" of 1μm and "Max frame Gap" of 5 frames. Later, we only considered for analysis trajectories longer than 5 sec.

For polymerization rates, we found a sharp normal distribution of velocities constant across the field of view, with a mean of 32.0 $\pm$ 4.5 1 μm/min in the aster interior ($n = 6$) and 32.0 $\pm$ 4.0μm/min in the periphery ($n = 6$) (Fig. 4.5C,D). These values of polymerization rates are consistent with EB1 comet tracking [Ishihara *et al.*, 2014]. In contrast, depolymerization rates reveled a striking difference in the aster interior

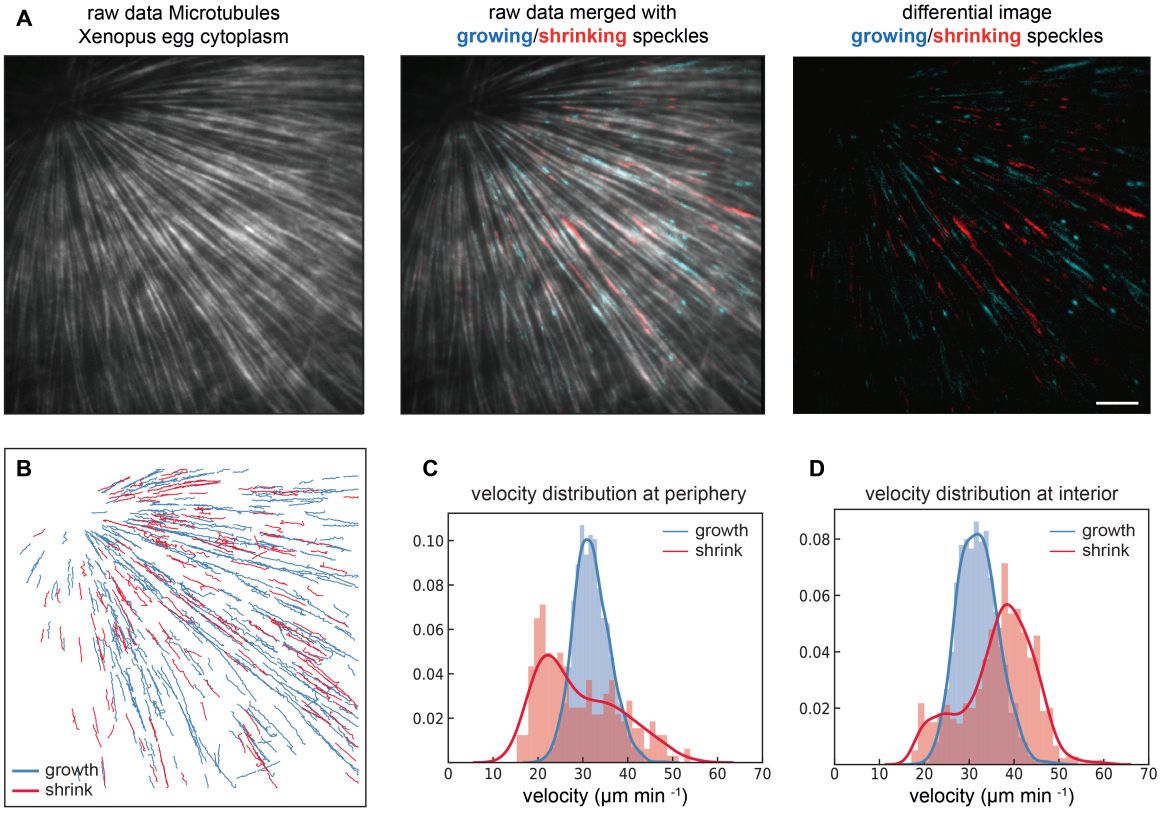

Figure 4.5: Measurement of polymerization and depolymerization rates in large microtubule asters using differential image protocol. (A) Raw image of MTs at the interior of the aster and the corresponding differential image overlaid showing growing (cyan) and shrinking (red) ends. Scale bars: $10\mu m$ **(B)** Map with all growing and shrinking events detected in A. Velocity distribution of growing (blue) and shrinking events (red) at the periphery **(C)** and interior **(D)** of the FOV. Plots represent the distribution of multiple samples pooled together ($n = 6$, interior, $n = 6$, periphery).

versus periphery. The average depolymerization rate was 36.3 ± 7.9 μm/min in the aster interior, compared to 29.2 ± 8.9 μm/min at the aster periphery (Fig. 4.5C,D). The distribution of velocities was quite spread out and had a positive skew in the aster interior and a negative skew in the aster periphery, suggesting some sort of bimodal distribution, probably generated by the transition region between interior and periphery.

Overall, our analysis showed that polymerization rates are kept contant from the interior to the periphery of the aster, while depolymerization rates drop significantly. We also observed a sharp decrease in the number of shrinking events at the periphery when compared to the interor. Together, this work have shown, perhaps for the first time, that plus end depolymerization rates are spatially regulated in large interphase egg asters. Further discussion of these results in the context of tubulin regulation by microtubule assocated proteins (MAPs) can be found in the pre-print (List of Publications).

Chapter 5

Behavior of Single Molecules in Cytoskeletal Networks of FtsZ Filaments

One of the main advantages of combining supported lipid bilayers with TIRF microscopy is the ability to investigate high-resolution transient events down to the single-molecule level. Watching the behavior of single molecules during the reorganization of the filament network can provide us important information about the underlying filament dynamics [Baranova and Loose, 2017]. In fact, this approach has helped to identify that FtsZ reorganization is driven by polymerization dynamics and not filament sliding [Loose and Mitchison, 2014]. In case of filament sliding, FtsZ subunits would move directionally withing the filaments, but they remain static while filaments reorganize in space. By tracking and measuring how long these individual subunits stay bound to membranes, we can obtain a direct measurement of their lifetimes. In this section, we explore the lifetime of FtsZ monomers in the presence of Zaps, as well as the behavior of these crosslinkers down to the single-molecule level.

5.1 Turnover Rate of FtsZ Filaments in the presence of ZapA

To study the lifetime of FtsZ monomers in the treadmilling filaments, we first analyzed the turnover rate of FtsZ in fluorescence recovery after photobleaching (FRAP) experiments (Fig. 6.1A,B and Movie 13; see section 6.4 for details) and found a similar mean recovery half-time of 7.63 ± 1.30 s (blue, $n = 6$) in the absence of ZapA and 6.66 ± 0.64 s or presence 6.0μM ZapA (red, $n = 7$) (Fig. 5.1), in agreement with an unchanged treadmilling speed.

The length of treadmilling filaments can also be estimated by calculating the product of the treadmilling velocity and the lifetime of FtsZ monomers within filaments. Accordingly, as the treadmilling velocity was unchanged, an increase in the filament length should go along with a significant decrease in filament turnover, which was not the case, suggesting that ZapA does not change the filament length ($p = 0.47$, Table 6.2).

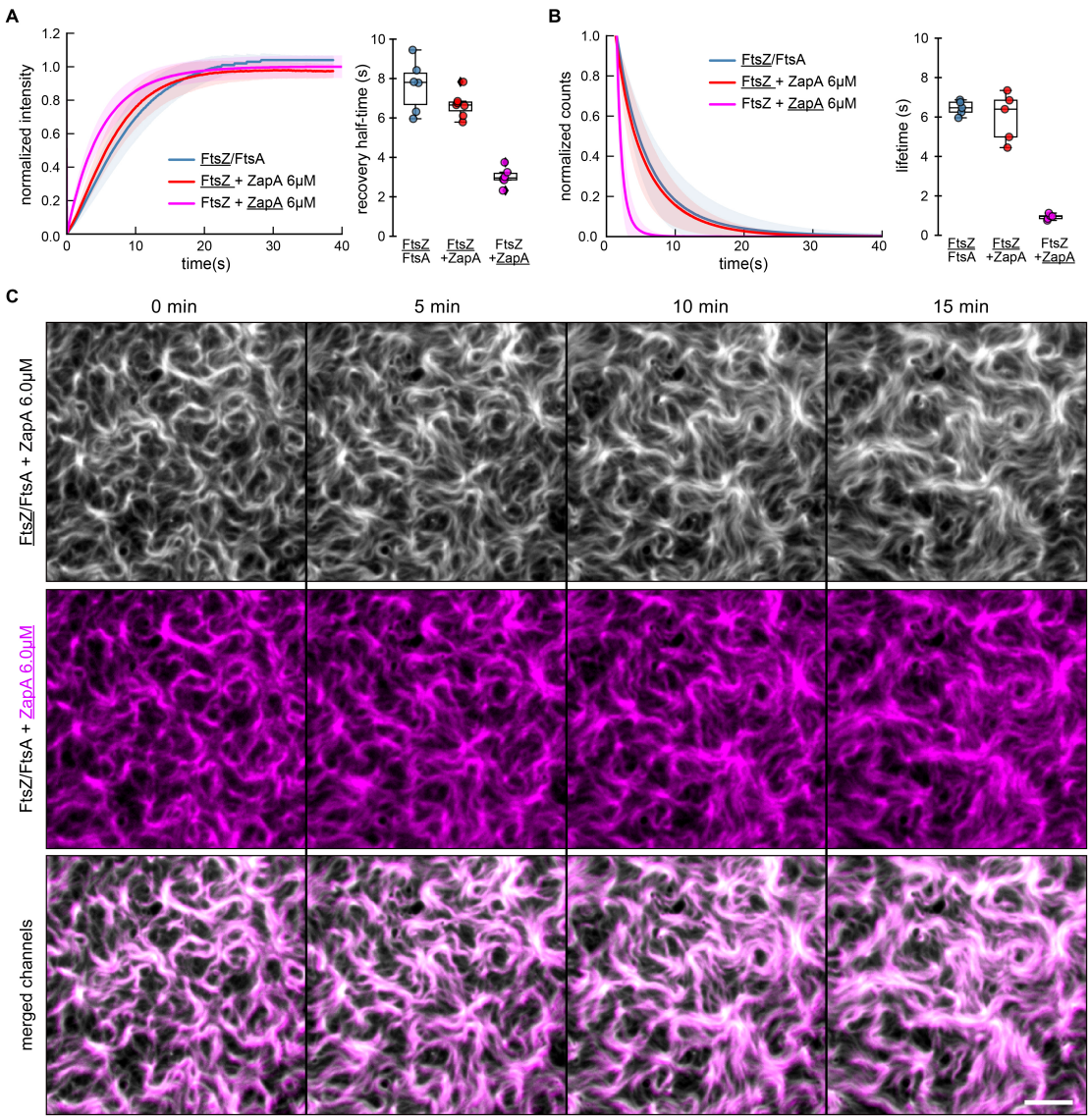

Figure 5.1: ZapA binds only transiently to FtsZ filaments. (A) Half-time recovery of FtsZ was not affected by 6μM ZapA (7.63 ± 1.30 s and 6.66 ± 0.64 s, respectively), while Cy5-labelled ZapA showed a much faster recovery (ZapA $= 3.01 \pm 0.47$, $n = 6$). **(B)** Lifetime distribution of FtsZ does not change significantly with ZapA (FtsZ $= 6.59 \pm 0.28$ s, blue, $n = 5$; FtsZ with ZapA $= 6.01 \pm 1.24$ s, red, $n = 6$). In contrast, the lifetime of ZapA was much shorter (ZapA $= 0.95 \pm 0.14$, $n = 5$). **(C)** Dual-color TIRF micrographs showing co-localization of Alexa488-FtsZ (gray) and ZapA-Cy5 (magenta) (Movie 15). Scale bars = 5μm.

To further corroborate these results, we performed single molecule experiments following the approach described in [Baranova and Loose, 2017], where individual FtsZ monomers are resolved at single molecule level by mixing a sprinkle of Cy5-labelled FtsZ (less than 0.01% v/v) to a background of Alexa488-labelled FtsZ (Fig. 6.2A,B; Movie 14). Since TIRF only excites fluorophores close to the membrane (< 200nm) and FtsZ monomers are not sliding inside the filaments (they treadmill), the time particles appear on the screen corresponds to the residence time between the attachment and detachment of a single monomer from a protofilament.

This allowed us to directly measure the lifetime of FtsZ monomers in the treadmilling filaments (Fig. 5.1B). In agreement with our FRAP experiments, we found no difference ($p = 0.14$, Table 6.2) in the lifetimes of FtsZ with (red, 6.01 ± 1.24 s, $n = 6$) and without ZapA (6.59 ± 0.28 s, $n = 5$).

Together with our quantification of the treadmilling velocity, our findings suggest a mean FtsZ filament length between 341.6 ± 50.0 and 412.0 ± 37.7 nm, when only FtsZ and FtsA were present, and between 302.4 ± 72.9 and 351.8 ± 76.2 nm with 6.0μM ZapA, again showing that ZapA does not change the filament length. These values are similar to the estimated mean length obtained from the distance between growing and shrinkage spots (Fig. 4.4C) and about three times longer than what has been suggested for filaments *in vivo* [Erickson *et al.*, 2010].

Together, these experiments and analyses show that despite its strong effect on the architecture and reorganization dynamics of the FtsZ filament network, ZapA does not slow down or enhance the underlying polymerization dynamics (Table 5.2). Furthermore, the presence of ZapA does not affect the relative orientation of FtsZ filaments towards each other or their length, while it increases the directional persistence of treadmilling.

5.2 Turnover Rate of ZapA when Binding to FtsZ Filaments

Next, we sought to better understand how ZapA could change the architecture of FtsZ filaments without slowing down their treadmilling dynamics. To this end, we prepared a fully functional C-terminally labeled version of ZapA, ZapA-Cy5, which allowed us to image its dynamic behavior simultaneously with FtsZ. Table 5.1 shows all the parameter estimation for the FtsZ network in the presence of this construct, showing that this labeled version of ZapA behaves like the WT.

We found that, as *in vivo*, ZapA co-localized with FtsZ bundles on the membrane (Fig. 5.1C; Movie 15). Having the capacity to image at higher spatiotemporal resolution than in the living cell, we also observed that ZapA showed a more discontinuous appearance (Movie 15) than FtsZ. Also, our dual-color time lapse movies and corresponding differential images revealed that ZapA was able to follow the treadmilling dynamics of FtsZ filaments, but the corresponding trajectories were much shorter.

These results suggest that even though ZapA co-localized with treadmilling FtsZ filaments, ZapA alone does not function as a direct readout for treadmilling dynamics.

We then analyzed the turnover rate of ZapA itself (ZapA-Cy5) with FRAP (Fig. 5.1A, magenta; Movie 13) and single molecule experiments (Fig. 5.1B, magenta; Movie 14) and found a half-recovery rate of 3.01 ± 0.47 s ($n = 6$) and a single-molecule lifetime of 0.94 ± 0.14 s ($n = 5$), respectively. This shows that ZapA transiently binds to membrane-bound FtsZ bundles. ZapA tetramers are incorporated into about 2 to 8 times shorter than FtsZ monomers despite having multiple binding sites for FtsZ.

Table 5.1: Pattern quantification with WT or Cy5-labelled ZapA. Mean and respective std of each parameter in the presence of 6μM WT or Cy5-labelled ZapA.

	FtsZ/FtsA 1.5μM : 0.5μM		
parameter	**+ 6μM WT ZapA**	**+ 6μM ZapA-Cy5**	**pval**
bundle width (μm)	0.77 ± 0.05 ($n = 10$)	0.85 ± 0.06 ($n = 3$)	0.065
correlation length (μm)	1.81 ± 0.26 ($n = 8$)	1.62 ± 0.09 ($n = 4$)	0.081
curvature (μm^{-1})	0.25 ± 0.03 ($n = 10$)	0.28 ± 0.01 ($n = 4$)	0.027
correlation time (min)	6.59 ± 3.92 ($n = 9$)	7.99 ± 4.82 ($n = 3$)	0.551

Together with our observations from the previous chapters, these results show that the strong influence on the large-scale organization of the FtsZ filament network is the result of cooperative, transient binding events between multivalent ZapA tetramers and FtsZ filaments. The fast turnover of components of the Z-ring might help this cytoskeletal structure to continuously adapt to the shrinking diameter of the cell during constriction. We discuss these results more in depth later in Chapter 7.

5.3 Underlying FtsZ Dynamics in the Presence of ZapC

Finally, we combined the single molecule analysis workflow with our treadmilling speed quantification to investigated if the presence of ZapC was also able to conserve the treadmilling velocity of FtsZ filaments as happened in the presence of ZapA (Fig. 4.3).

Table 5.2: Summary of ZapA effect on FtsZ filament network. Weighted mean and respective standard deviation of each parameter for all ZapA concentrations combined, either below 0.75μM (low ZapA) or above 1.5μM (high ZapA). This shows how much the system changed between the two states.

		Low ZapA ($< 0.5\mu$M)			High ZapA ($> 1.5\mu$M)				
parameter	**change**	**mean**	**s.d**	n	**mean**	**s.d**	n	**%**	**Fig.**
bundle width	↑	0.69	0.03	17	0.80	0.02	31	16%	3.2
spatial order	↑	1.33	0.30	13	1.76	0.05	22	33%	3.4
curvature	↓	0.33	0.01	17	0.27	0.01	25	18%	3.4
persistence	↑	1.27	0.30	14	6.61	0.39	25	420%	3.5
growth rate	=	50.6	2.3	17	44.1	2.53	32	n.s	4.3
shrinkage rate	=	53.1	1.9	17	46.6	2.67	32	n.s	4.3
directionality	↑	0.21	0.04	10	0.30	0.05	10	41%	4.3
lifetime	=	6.46	0.37	5	6.01	0.01	5	n.s	5.1
FRAP recovery	=	7.63	1.30	6	6.66	0.64	7	n.s	5.1

Interestingly, after examination of hundreds of treadmilling trajectories of fluorescent spots obtained from our differential image protocol, we found a small reduction in the velocity of treadmilling filaments in the presence of 0.5/1.0μM ZapC (Fig 5.2A, green; $p =< 0.05$).

Furthermore, when we combined 3μM ZapA with 0.5/1.0μM ZapC, this effect was significantly accentuated (Fig 5.2A, orange; $p < 0.01$, Table 6.3) showing a synergetic effect between the two proteins in slowing down the motion of FtsZ filament bundles. These results are in agreement with the suppression of FtsZ GTPase activity observed in other *in vitro* studies [Hale *et al.*, 2011].

To investigate if ZapC co-localizes with FtsZ bundles on the membrane in a different arrangement than the one we observed for ZapA, we prepared a GFP-labeled version of ZapC to image its dynamic behavior simultaneously with FtsZ and in combination with ZapA. As for ZapA experiments, and in agreement with *in vivo* observations [Durand-Heredia *et al.*, 2011], we found that ZapC co-localizes with membrane-bound FtsZ bundles, either alone or in combination with ZapA (Fig. 5.2D).

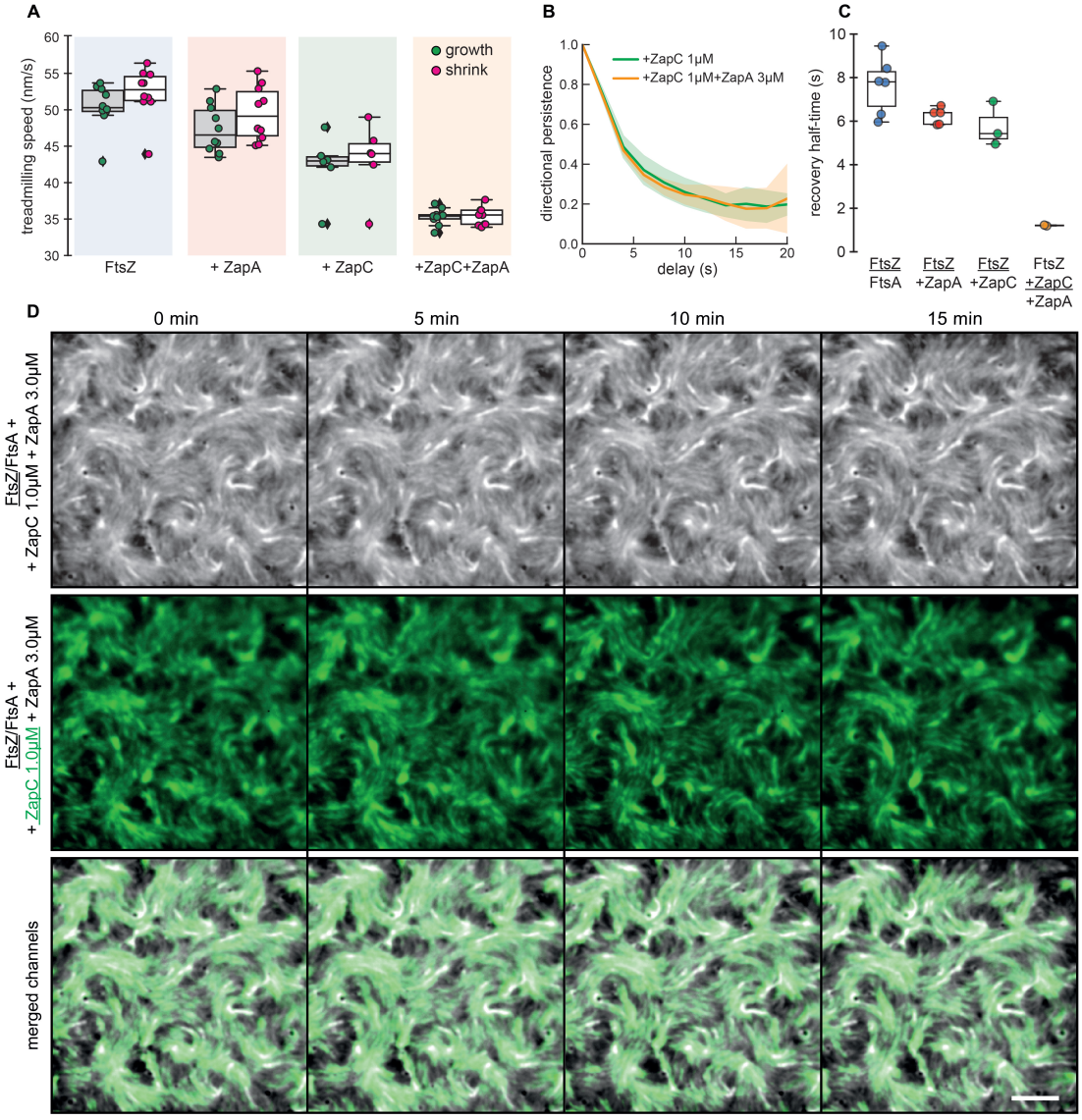

Figure 5.2: ZapC decreases the treadmilling speed of FtsZ bundles. **A** ZapC at 0.5/1.0μM reduced the mean velocity of FtsZ filaments at both ends ($p < 0.05$; Table 6.3) and this effect was further emphasized in combination with 3μM ZapA ($p < 0.01$; Table 6.3). **(B)** Directional autocorrelation analysis shows that directionality is maintained in all conditions. **(C)** Half-time recovery of FtsZ from FRAP experiments was not affected with te presence of ZapC, either alone or in combination with ZapA (FtsZ $= 6.59 \pm 0.28$ s, blue, $n = 5$; FtsZ with ZapC and ZapA $= 5.98 \pm 0.95$ s, green, $n = 3$). In contrast, half-time recovery of ZapC itself was much shorter, either alone or in combination with ZapA (1.33 ± 0.26, $n = 2$; $p < 0.01$, Table 6.3).**(D)** Dual-color TIRF micrographs showing co-localization of FtsZ-Cy5 (gray) and GFP-ZapC (green). Scale bars = 5μm.

Moreover, we also performed experiments using unlabeled FtsZ in combination with 3.0μM Cy5-labelled ZapA and 1.0μM GFP-labelled ZapC to check for possible segregation between the two signals, but they simply overlapped with each other once more (data not shown).

To further examine the underlying dynamics of polymeric FtsZ in these conditions, we used FRAP experiments to analyze the turnover rate of the bundle filaments in the presence of ZapC alone or in combination with ZapA (Fig. 5.2C), as we did before

when studying the effect of ZapA alone (Fig. 5.1; Movie 13). We found a mean recovery half-time of 6.24 ± 0.38s when only ZapC was present (Fig. 5.2C, green box, $n = 5$), and 5.99 ± 0.95s when in combination with 3μM of ZapA ($n = 4$, boxplot not shown), similar to the values obtained for FtsZ alone or in the presence of ZapA (Fig. 5.2C, blue and red boxes, respectively). Additionally, we also analyzed the turnover rate of GFP-labelled ZapC, either alone or combine with ZapA, and in both cases we found a much shorter recovery half-time when compared to FtsZ monomers (Fig. 5.2C, orange) within the same order of magnitude as the one observed for Cy5-labelled ZapA (Fig. 5.1). As discussed before, filament length is proportional to the treadmilling velocity and the lifetime of FtsZ monomers within filaments, which suggests a shrinkage of protofilaments inside the bundles when ZapC is present.

Together with our analysis of filament organization in the presence of ZapC (section 3.4.2) these results show that ZapC has a strong influence on the large-scale architecture of FtsZ filament bundles, has a fast turnover rate and does not change the lifetime of FtsZ subunits, similar to what we observed for ZapA. However, for ZapC, this effect is associated with a decrease in the treadmilling speed of the filaments, an effect that becomes more pronounced in combination with ZapA, suggesting that both proteins work together to modulate FtsZ filament dynamics and organization.

We should point out, that this chapter contains only a limited number of experiments, more data will be necessary to make stronger claims and fully understand the differences between the mechanisms of these regulatory proteins. However, our data provides some support to an attractive hypothesis where different Zap proteins may employ different regulatory mechanisms to modulate FtsZ polymerization and organization. This could be a helpful mechanism perhaps in response to different cues induced by the surrounding environment.

Chapter 6

Material & Methods

6.1 Reagents and Chemicals

Phospholipids used in this paper, DOPC (1,2-dioleoyl-sn-glycero-3-phosphocholine) and DOPG (1,2-dioleoyl-snglycero-3-phospho-(1'-racglycerol)), were purchased from Avanti Polar Lipids (Alabaster, AL) and kept at -20℃ as 25 mg/ml stock solutions in chloroform; Sulfo-Cyanine-5-maleimide (Cy5) was acquired from Lumiprobe and Alexa Fluor® 488 C5-Maleimide (Alexa488) was acquired from ThermoFisher Scientific. Nucleotides were acquired from ThermoFisher Scientific or Jena Bioscience. Precision cover glasses for the homebuilt chambers were obtained from VWR (thickness No. 1.5H, 24 x 50). E.coli strains were obtained from Lucigen. Strep-Tactin resin was acquired from Iba lifesciences and Nickel resins were purchased from ThermoFisher Scientific (HisPurTM Ni-NTA resin) or Macherey-Nagel (Protino Ni-TED resin). All the remaining reactants and salts were obtained from Sigma, Merck, or Invitrogen and were of analytic or spectroscopic grade.

6.2 Protein Biochemistry

6.2.1 Purification of FtsZ

FtsZ (UP P0A9A6) was cloned into a pTB146-derived vector which attached a N-terminal His6-SUMO tag plus seven additional amino acids (AEGCGEL) that provide a cysteine residue for further fluorescent labelling (pML45, His6-SUMO-GCG-FtsZ). E.coli C41 (DE3) cells were transformed with pML45 and grown in TB medium supplemented with ampicillin at 37℃, until cells reached an OD600 of 0.8. After the addition of IPTG to a final concentration of 1mM, cells grew for 5h at 37℃. Cells were harvested by centrifugation, pellets were frozen in liquid nitrogen and kept at -80℃ until further use.

For purification, pellets were thawed and resuspended in FtsZ buffer (50 mM Tris-HCl pH 8.0, 500mM KCl, 2mM β-mercaptoethanol, 10% glycerol) supplemented with 20mM imidazole and cOmplete EDTA-free protease inhibitors cocktail (1 tablet/50ml,

Roche) followed by incubation at 4℃ for 15 min. Cells were lysed using a cell disruptor (Constant Systems) at a pressure 1.36 kbar and incubated with 1 mg/ml DNase I (Sigma-Aldrich) and 2.5 mM MgCl2 for 15min. The lysate was then centrifuged (30min, 60,000 g, 4℃) and the supernatant was incubated with nickel agarose resin (HisPur Ni-NTA resin, Thermo Scientific) for 60min at 4℃. The resin was extensively washed with FtsZ buffer supplemented with 20 mM imidazole and 30 mM imidazole. The fusion protein was eluted with FtsZ buffer supplemented with 250 mM imidazole. Fractions were evaluated by SDS-PAGE (stained with Coomassie Blue) and peak fractions containing His6-SUMO-GCG-FtsZ were pooled and incubated with His6-tagged SUMO protease (His6-Ulp1) during an overnight dialysis into FtsZ cleavage buffer (50mM Tris-HCl pH 8.0, 300 mM KCl and 10% glycerol). The digested sample was passed several times through Ni-NTA resin, to remove His6 containing molecules. The flow through was collected and active protein was enriched by sedimentation of FtsZ filaments. For this, the protein was dialyzed into FtsZ polymerization buffer (50 mM PIPES pH 6.7, 10 mM MgCl2) and incubated with CaCl2 and GTP for 15min at 30℃. The solution was then centrifuged (2min, 20,000xg, RT) and a clear gel-like pellet containing polymeric FtsZ was obtained. The pellet was resuspended into FtsZ storage buffer (50mM Tris-HCl pH 7.4, 50 mM KCl, 1mM EDTA and 10% glycerol) and incubated with 100×molar excess of 7 Tris(2-carboxyethyl)phosphine hydrochloride (TCEP) for 20min at RT for cysteine-labelling. Five times molar excess of a thiol-reactive dye (Alexa488 or Cy5–maleimide) was added to the solution and incubated overnight at 4℃ during dialysis into FtsZ storage buffer. Finally, labelled FtsZ was loaded on a PD10 desalting column to remove CaCl2, GTP and free dye. Purified FtsZ was aliquoted, flash frozen in liquid nitrogen and kept at -80℃ until usage.

6.2.2 Purification of FtsA

The gene coding for FtsA (UP P0ABH0) was cloned into a modified pTB146 vector. The resulting vector, pML60, encodes for FtsA with an N-terminal His6-SUMO-pentaglycine tag. E.coli C41 (DE3) cells were transformed with pML60 and grown in 2xYT medium supplemented with ampicillin, at 37℃, until they reached an OD600 of 0.6-0.8. After the addition of IPTG to a final concentration of 1mM, cells grew overnight at 18℃. Cells were harvested by centrifugation, pellets were frozen in liquid

nitrogen and kept at -80℃ until further use.

For purification, cells were thawed and resuspended in FtsA buffer (50 mM Tris-HCl pH 8.0, 500mM KCl, 10 mM MgCl2) supplemented with 1 mg/ml lysozyme, cOmplete EDTA-free protease inhibitors cocktail (1 tablet/ 50 ml, Roche), 1 mg/ml DNase (Sigma-Aldrich) and 0.5mM DTT. Cells were then lysed using a cell disruptor (Constant Systems) at a pressure of 1.36kbar, centrifuged (60,000xg, 45min at 4℃) and the supernatant was incubated with Nickel agarose beads (Protino Ni-TED, Macherey-Nagel) for 1h at 4℃. The resin was extensively washed with FtsA buffer and FtsA buffer supplemented with 5mM imidazole. The fusion protein was then eluted with FtsA buffer supplemented with 250mM imidazole and fractions were evaluated by SDS-PAGE (stained with Coomassie Blue). Peak fractions containing His-SUMO-GGGGG-FtsA were pooled and the buffer was exchanged into FtsA storage buffer (50 mM Tris-HCl pH 8.0, 500 mM KCl, 10 mM MgCl2, 0.5 mM DTT, 20% glycerol). The His6-SUMO tag was cleaved by incubating His-SUMO-GGGGG-FtsA with His6-Ulp1 for 90min at 30℃. The sample was then passed several times through Protino Ni-TED resin, previously equilibrated with FtsA storage buffer, to remove His6-containing molecules. Protein was aliquoted, flash frozen in liquid nitrogen and kept at -80℃ until usage.

6.2.3 Purification of ZapA and Mutants

ZapA (UP P0ADS2) was cloned into a modified pTB146 vector attached to an N-terminal Twinstrep-SUMO tag (pML130, Twinstrep-SUMO-ZapA). E.coli BL21 (DE3) cells were transformed with pML130 and grown in TB medium supplemented with ampicillin, at 37℃, until cells reached an OD600 of 0.6-0.8. After the addition of IPTG to a final concentration of 1 mM, cells grew for 4h at 37℃. Cultures were harvested, and pellets were frozen in liquid nitrogen and kept at -80℃ until further use.

For purification, cells were thawed and incubated with ZapA buffer (50 mM HEPES pH 7.5, 300mM KCl, 10% glycerol) supplemented with 2mM β-mercaptoethanol and cOmplete EDTA-free protease inhibitor tablets (1 tablet/50 ml, Roche Diagnostics) for 15min at 4℃. Cells were then lysed using a cell disruptor and incubated in the presence of 1 mg/ml of DNase (Sigma-Aldrich) and 2.5 mM MgCl2 for 15min. The

lysate was centrifuged (30min, 60,000 g, 4℃) and the supernatant was incubated with strep-tactin resin (Strep-Tactin® resin, Iba Lifesciences) for 30min at 4℃. Beads were extensively washed with ZapA buffer and the fusion protein was eluted using ZapA buffer supplemented with 50mM biotin. Peak fractions of Twinstrep-SUMO-ZapA were identified by SDS-PAGE (stained with Coomassie Blue) and pooled. The Twinstrep-SUMO tag was cleaved with His6-Ulp1 during an overnight dialysis into ZapA storage buffer (50mM Tris-HCl pH 7.5, 50 mM KCl, 10% Glycerol). The solution was then passed through Ni-NTA and strep-tactin resins to remove His6-Ulp1 and free twinstrep-SUMO tag, respectively. ZapA was aliquoted, flash frozen in liquid nitrogen and kept at -80℃ until usage.

For labeling purposes, ZapA was additionally cloned into a vector which attached 5 residues (LPETG) to the C-terminus of the protein, pMAR16 (TwinStrepSUMO-ZapA-GGGS-LPETG). ZapA-LPETG was expressed and purified as the wildtype protein followed by Sortase-mediated labelling [Theile *et al.*, 2013]. Specifically, ZapA-LPETG was incubated with 0.3 mM of labelled peptide GGGC-Cy5 and 10µM Sortase 7M (purified using pET30b-7M SrtA, a gift from Hidde Ploegh, Addgene plasmid #51141) in a final concentration of 50 µM. The reaction was carried during an overnight dialysis into ZapA storage buffer at 4℃. Sample was further purified from free labelled peptide and Sortase by size-exclusion chromatography using a Hi/Load 16/600 Superdex 75 column (GE Healthcare) previously equilibrated with ZapA storage buffer. Labelled ZapA was collected, aliquoted and flash frozen in liquid nitrogen. ZapA mutants, R46A and I83E, were obtained by site-directed mutagenesis (pMAR9 and pMAR10b, respectively) and purified following the same procedure as the wild type protein.

6.2.4 Purification of ZapB

ZapB (UP A7ZUE3) was cloned into a modified pTB146 vector attached to an N-terminal 6xHis-SUMO tag plus an amino-terminal cysteine residue for further labelling (pML55, His6-SUMO-GCG-ZapB). E.coli BL21 (DE3) cells were transformed with pML55 and grown in TB medium supplemented with ampicillin, at 37℃, until cells reached an OD600 of 0.6-0.8. After the addition of IPTG to a final concentration of 1mM, cells grew for 4h at 37℃. Cultures were harvested, pellets were frozen in liquid nitrogen and kept at -80℃ until further use.

For purification, cells were thawed and incubated with ZapB buffer (50 mM HEPES-KOH at pH 7.5, 500mM KCl, 10% glycerol) supplemented with 1mg/ml lysozyme, 2mM β-mercaptoethanol, 5mM of imidazole, DNase (1 mg/ml, DN25, Sigma-Aldrich), 2.5mM MgCl2 and protease inhibitor (1tablet/50ml, Complete EDTA free, Roche Molecular Biochemicals) for 15min at 4℃. Noteworthy that ZapB formed a jelly solution that made the purification more challenging to handle than for ZapA. Cells were lysed using a cell disrupter (pressure 1.36kbar), centrifuged (30min, 60,000g, 4℃) and the supernatant was incubated with a Ni_2^+-agarose column (HisPur Ni-NTA resin, Thermo Scientific) for 60min at 4°C. Column was extensively washed with ZapB buffer and fusion protein was eluted in small fractions with ZapB buffer supplemented with 2M imidazole. Enriched fractions containing His6-SUMO-GCG-ZapB were evaluated by SDS-PAGE (stained with coomasie Blue), pooled together and incubated with His-Ulp1 during an overnight dialysis into ZapB storage buffer (50mM HEPES-KOH at pH 7.4, 50mM KCl, 10% glycerol and 1mM EDTA). The solution was finally passed through a Ni_2^+-resin previously equilibrated with ZapB storage buffer to remove His6-Ulp1 and free His6-SUMO, aliquoted, flash frozen in liquid nitrogen and kept at -80℃ until usage.

6.2.5 Purification of ZapC

ZapC (UP P75862) was cloned into a modified pTB146 vector attached to an N-terminal Twinstrep-SUMO tag (pML133, Twinstrep-SUMO-ZapC). E.coli BL21 (DE3) cells were transformed with pML133 and grown in TB medium supplemented with ampicillin, at 37℃, until cells reached an OD600 of 0.6-0.8. After the addition of IPTG to a final concentration of 1 mM, cells grew for 4h at 37℃. Cultures were harvested, and pellets were frozen in liquid nitrogen and kept at -80℃ until further use.

For purification, cells were thawed and incubated with ZapC buffer (50 mM HEPES pH 7.5, 500mM KCl, 10% glycerol) supplemented with Lysozime 1mg/mL, 2mM β-mercaptoethanol and cOmplete EDTA-free protease inhibitor tablets (1 tablet/50 ml, Roche Diagnostics) for 15min at 4℃. Cells were then lysed using tip sonication in the presence of 1 mg/ml of DNase (Sigma-Aldrich) and 2.5 mM MgCl2 for 15min. The lysate was centrifuged (30min, 60,000 g, 4℃) and the supernatant was incubated with strep-tactin resin (Strep-Tactin® resin, Iba Lifesciences) for 30min at 4℃. Beads

were extensively washed with ZapC buffer and the fusion protein was eluted using ZapC buffer supplemented with 50mM biotin. Peak fractions of Twinstrep-SUMO-ZapA were identified by SDS-PAGE (stained with Coomassie Blue) and pooled. The Twinstrep-SUMO tag was cleaved with His6-Ulp1 during an overnight dialysis into ZapC storage buffer (20mM HEPES-KOH pH 7.5, 150 mM KCl, 10% Glycerol). The solution was then passed through Ni-NTA and strep-tactin resins to remove His6-Ulp1 and free twinstrep-SUMO tag, respectively. ZapC was aliquoted, flash frozen in liquid nitrogen and kept at -80℃ until usage.

For labelling purposes, ZapC was cloned into a PTB146-derived vector containing a GFP tag attached to the C-terminus of the protein, pMAR7 (6xHis-SUMO-ZapC-GFP). E.coli BL21 (DE3) cells were transformed with pMAR7 and expressed as the wildtype protein. For purification, cells were thawed and incubated with ZapC buffer (50 mM HEPES pH 7.5, 500mM KCl, 10% glycerol) supplemented with Lysozime 1mg/mL, 2mM β-mercaptoethanol, cOmplete EDTA-free protease inhibitor tablets (1 tablet/50 ml, Roche Diagnostics), 1 mg/ml of DNase (Sigma-Aldrich) and 2.5 mM MgCl2 for 15min at 4℃. Cells were then lysed using a cell disruptor (Constant Systems Lda). The lysate was centrifuged (30min, 60,000 g, 4℃) and the supernatant was incubated with nickel agarose resin (HisPur Ni-NTA resin, Thermo Scientific) for 60min at 4℃. The resin was extensively washed with ZapC buffer supplemented with 10 mM imidazole and 30 mM imidazole. The fusion protein was eluted with ZapC buffer supplemented with 250 mM imidazole. Fractions were evaluated by SDS-PAGE (stained with Coomassie Blue) and peak fractions containing His6-SUMO-ZapC-GFP were pooled and incubated with His6-tagged SUMO protease (His6-Ulp1) during an overnight dialysis into ZapC storage buffer (50mM HEPES pH 7.5, 300 mM KCl and 10% glycerol). The digested sample was passed several times through Ni-NTA resin, to remove His6 containing molecules. Zapc-GFP was aliquoted, flash frozen in liquid nitrogen and kept at -80℃ until usage.

6.2.6 Purification of ZapD

The gene encoding ZapD (UP P36680) was cloned into a modified pTB146 vector. The resulting vector, pML142, encodes for ZapD with an N-terminal His6-SUMO tag. E.coli BL21 cells were transformed with pML142 and grown in LB medium supplemented with ampicillin, at 37℃, until they reached an OD600 of 0.6-0.8. After

the addition of IPTG to a final concentration of 1mM, cells grew for 4h at 37℃. Cells were harvested by centrifugation, pellets were frozen in liquid nitrogen and kept at -80℃ until further use.

For purification, pellets were thawed and resuspended in ZapD buffer (20 mM Tris-HCl pH 8.0, 100mM KCl, 1mM EDTA and 10% glycerol) supplemented with 20mM imidazole and cOmplete EDTA-free protease inhibitors cocktail (1 tablet/50ml, Roche). Cells were lysed using a cell disruptor (Constant Systems Lda.) at a pressure 1.36 kbar. The lysate was then centrifuged (30min, 60,000 g, 4℃) and the supernatant was incubated with nickel agarose resin (HisPur Ni-NTA resin, Thermo Scientific) for 60min at 4℃. The resin was extensively washed with ZapD buffer and ZapD buffer supplemented with 20 mM imidazole and 30 mM imidazole (3 washing steps). The fusion protein was eluted with ZapD buffer supplemented with 300 mM imidazole. Fractions were evaluated by SDS-PAGE (stained with Coomassie Blue) and peak fractions containing His6-SUMO-ZapD were pooled and incubated with His6-tagged SUMO protease (His6-Ulp1) during an overnight dialysis into ZapD buffer (50mM Tris-HCl pH 8.0, 300 mM KCl and 10% glycerol). The digested sample was passed several times through Ni-NTA resin, to remove His6 containing molecules. ZapD was quantified by Bradford method, aliquoted, flash frozen in liquid nitrogen and kept at -80℃ until usage.

6.3 Self-organization assay and Imaging

6.3.1 Preparation of small unilamellar vesicles

To prepare small unilamellar vesicles (SUVs), DOPC and DOPG dissolved in chloroform were transferred into a glass vial to a final concentration of 5 mM (70:30 molarity ratio). Using a stream of nitrogen, the mixture was dried to form a thin film of lipids and transferred to a vacuum desiccator for 3h to completely remove any residual chloroform. The lipids were then rehydrated in swelling buffer (50mM Tris-HCl pH 7.5, 300mM KCl) and incubated at 37℃ for 30min. The lipid film was then resuspended by vortexing vigorously to obtain multilamellar vesicles of different sizes. To obtain small unilamellar vesicles (SUVs), the suspension was subjected to 10 freeze-thaw cycles (using either liquid nitrogen or dried ice) followed by tip sonication or extrusion with 100nm filters. Until use, vesicles were kept at 4℃ up to one week or at -20℃ up to two months (in aliquots of 30μl).

6.3.2 Preparation of reaction chamber

To prepare the reaction chamber, glass coverslips were first cleaned by one of two possible methods: (i) coverslips were sonicated for at least 15min in 2% Hellmanex II solution (Hellma) and washed extensively with milliQ H2O to remove all the detergent. This was followed by another two sonication steps ($\geq$ 15min), one in milliQ water and another one in 95% reagent-grade ethanol. After this procedure, coverslips were storaged in 95% reagent-grade ethanol up to one week; (ii) coversplis were covered with piranha solution (30% H2O2 mixed with concentrated H2SO4 in a 1:3 ratio) for 1h, followed by extensive washing and sonication with milliQ water.

Cleaned coverslips were stored in water for no longer than one week. Before use, glass coverslips were blown dry with compressed air and cleaned in an air plasma for 10min. The reaction chamber was prepared by attaching a plastic ring (top of an Eppendorf tube) on a cleaned glass coverslip using ultraviolet glue (Norland optical adhesive 88) activated by exposure to UV light for 5min.

6.3.3 Preparation of supported lipid bilayers and experiments

To form supported lipid bilayers (SLBs), SUVs suspension was diluted to 1mM in swelling buffer and $CaCl_2$ was added to a final concentration of 2mM. From this mix, 50μl were added to each reaction chamber. Vesicles adsorb to the surface, rupture and fuse with the clean hydrophilic glass to form a flat bilayer, assisted by the presence of $CaCl_2$. After 1h of incubation at RT, additional 50μl of swelling buffer were added to each chamber (final volume = 100μl) and rinsed several times with 200μL of reaction buffer (50mM Tris-HCl pH 7.5, 150 mM KCl, 5mM $MgCl_2$).

To prevent oxidative photodamage and increase the lifetime of the dyes we used an oxigen scavenger system based on the activity of glucose oxidase and catalase in the presence of glucose. This system enzymatically consumes molecular oxygen from the buffer increasing the observation time by several orders of magnitude. D-Glucose is oxidized to gluconic acid by glucose oxidase, depleting oxygen in solution and creating hydrogen peroxide as a side product. In a second reaction step, catalase degrades hydrogen peroxide to H2O and O2, restoring half of the oxygen used by glucose oxidase.

Since oxygen can efficiently quench the triplet state, which prevents blinking of the dye, removing the oxigen from solution to reduce photobleaching can increase significantly the lifetime of the triplet state (i.e the lifetime of the dark state). To depopulate the triplet state and reduce blinking of the dye, we added to our buffer the vitamin E analog Trolox (6-hydroxy-2,5,7,8-tetramethylchroman-2-carboxylic acid), which was found to dramatically improve the photochemical properties of several dyes [Baranova and Loose, 2017].

To performed the self-organization assay, all experiments were initiated by first adding this oxygen scavenger system to the reaction chamber: 0.2% d-Glucose, 0.016 mg/ml glucose oxidase, 0.002 mg/ml catalase, 1mM dithiothreitol and 0.25mg/ml trolox. Then, FtsZ (with 30% Cy5- or Alexa488-labeled protein) and FtsA were added to the reaction chamber in a final concentration of 1.5μM and 0.5μM, respectively. To trigger polymerization and membrane recruitment of FtsZ, ATP and GTP were added to the system to a final concentration of 4mM. Zap proteins were added in different concentration ranges (as described for each experiment) before the addition of GTP.

6.3.4 Fluorescence Microscopy

All experiments were performed using a total internal reflection fluorescence (TIRF) setup. Here, the angle of the incident light is adjusted to an angle greater than the critical angle and the reflected light generates an electromagnetic field adjacent to the interface between a higher-index and lower-index medium. The fluorophores close to the glass surface (100-200nm) are selectively excited by interaction with the evanescent field, while everything else in solution are kept out of focus. This increases signal-to-noise ratio significantly and makes possible to detect single-molecule fluorescence in great detail.

All experiments were performed on an Inverted multipoint TIRF microscope (TILL Photonics) equipped with dual camera TIRF objectives (Andor 897straight (X-8449) 512x512 pixel and Andor 897 (X-8533) 512x512 pixel) and an image splitter (Andor Tucam) equipped with a long pass of 580 and 640nm. Alexa488 and Cy5 dyes were excited using 488nm and 642nm laser lines, respectively, and the emitted light was filtered by an Andromeda quad-band bandpass filter. Images were typically obtained every 2s, with 50ms exposure and using a 100x Olympus TIRF (NA = 1.49 DIC) objective.

6.4 Lifetimes Estimation

6.4.1 Fluorescence Recover After Photo Bleaching (FRAP)

For FRAP experiments, we allowed the system to reach the steady state (15min) and a small area of the membrane was bleached using a high laser intensity (Fig. 6.1). FRAP experiments were acquired with an exposure time of 50ms and an acquisition time of one frame every 114 ms or 500 ms. The fluorescence recovery in the region of interest corresponds to a diffusion of the labelled molecules and can be used to characterize its mobility and turnover rate. To obtain the half-time of this recovery, a Jython macro script for ImageJ (Image Processing School 8 Pilsen 2009) was used to fit the fluorescence recovery to $I(t) = a(1 - \exp(-bt))$. Here, $I(t)$ is the intensity value corrected for photobleaching effects, a corresponds to the mobile fraction (curve amplitude until plateau) and the half-time of the recovery is given by $-\exp(\ln 0.5)/b$, which corresponds to the time when the recovery is half of a.

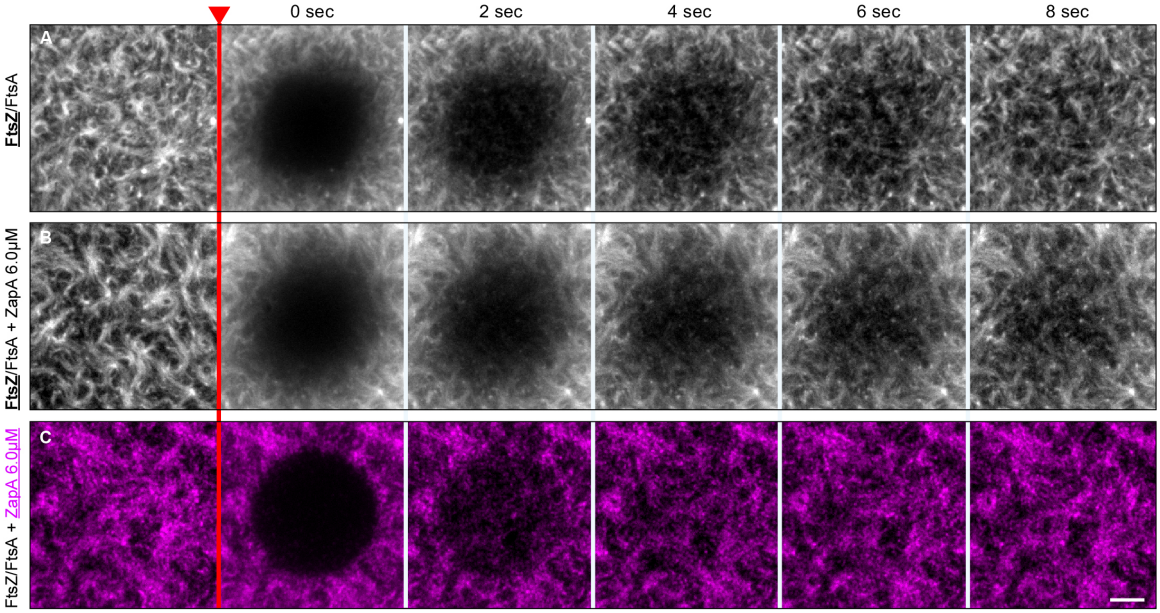

Figure 6.1: FRAP experiments. Snapshots showing typical fluorescence recover after photobleaching (FRAP) experiments for homogeneously-labeled FtsZ filaments without **(A)** and in the presence **(B)** of 6μM ZapA. **(C)** FRAP experiments of Cy5-labelled ZapA pattern showed a faster recovery rate. See Fig. 5.1A and Movie 13. Scale bars = 5μm.

6.4.2 Single Molecule Tracking (SMT)

For tracking of individual subunits, we used the approach described in [Baranova and Loose, 2017]. Briefly, individual FtsZ monomers were resolved at single molecule level by mixing a sprinkle of Cy5-labelled FtsZ (less than 0.01% v/v) to a background of Alexa488-labelled FtsZ (Fig. 6.2). Since TIRF only excites fluorophores close to the membrane ($<$ 200nm) and FtsZ monomers are not sliding inside the filaments (they treadmill), the time particles appear on the screen corresponds to the residence time between the attachment and detachment of a single monomer from a protofilament. The power of the 488nm laser, used to simultaneously visualize the reorganization of the FtsZ filament network, was kept low, while the power of the 642nm laser was increased up to a minimal laser power that could resolve single fluorophores without increasing photobleaching.

These experiments were typically recorded with an exposure time of 50 ms and a varying acquisition time (114ms to 1s) for further photobleaching correction (see [Baranova and Loose, 2017] for more details). For each time-lapse, a minimum of 300 frames was recorded to ensure that a few hundreds of particles were always analyzed per experiment. The residence time of these particles was estimated using the automated particle-tracking plugin TrackMate (https://imagej.net/TrackMate).

For tracking, a maximum particle size of 0.5μm was settled, to prevent classifying two adjacent particles as the same track, and molecules localized for less than two frames were discarded to avoid counting statistically irrelevant molecules. In addition, we allowed two dark frames inside each trajectory to account for rare blinking events of the fluorescent protein at an exposure time of 50ms. The lifetime was quantified by a mono-exponential fit to the residence time distribution of the particles.

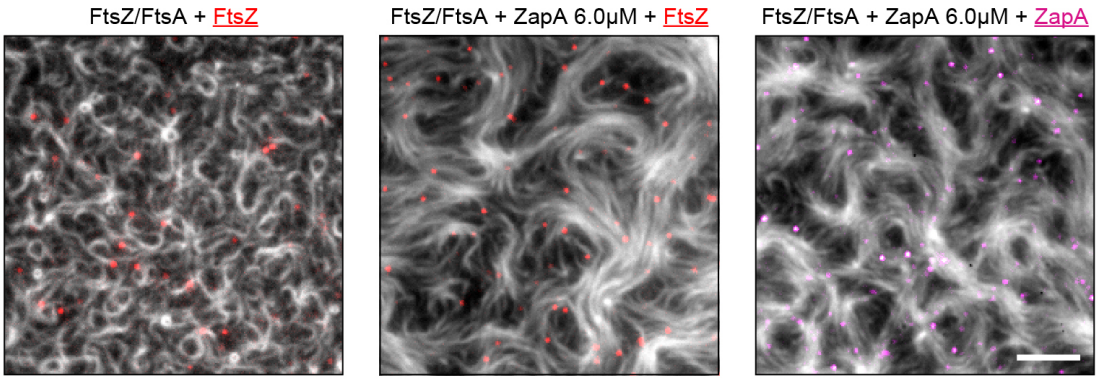

Figure 6.2: Single molecule tracking experiments. Snapshots from a typical single molecule tracking (SMT) experiment of FtsZ (red) with and without 6μM ZapA). Last panel shows the same SMT experiment for Cy5-labeled ZapA (magenta) on a background of 6μM ZapA WT. Lifetime distribution of FtsZ does not change significantly with ZapA, but ZapA itself has a much shorter lifetime. See Fig. 5.1B and Movie 14. Scale bars = 5μm.

6.5 Image Analysis and Code Availability

Prior to each image analysis protocols, acquired time-lapse movies were normalized to create a constant overall intensity and compensate for the increasing intensity over time due to protein binding to the membrane. In addition, all micrographs along the manuscript (except for FRAP snapshots) were constructed using a walking average of every 30 frames (= 1min) for better visualization.

6.5.1 Bundle Width Estimation

To estimate the width of membrane-bound FtsZ bundles (section 3.1, fluorescence images were binarized using the adaptive threshold plugin for ImageJ. This plugin corrects for non-homogeneous background intensities, overcoming the limitation of conventional threshold methods. The background was removed using a local threshold corresponding to the mean intensity of an area of 20x20 pixels without any further subtraction.

The binarized time lapse movie was then denoised using the despeckle filter in ImageJ aiming to remove small particles. Next, we calculated the Euclidean Distance Map (EDM) of every frame using the Distance Mapping function of ImageJ. This transformation resulted in a grey scale image, where the grey value of each pixel represents the shortest distance to the nearest pixel in the background (Fig. 3.2). Accordingly, bundle widths correspond to the local peak intensities multiplied by two. The mean bundle width of each frame was calculated by identifying the peak intensities for each line and column of the image using a costum Matlab script. This value could then be plotted as a function of time.

Later, all these steps were combined into a single custom python script, available for general use here:

https://github.com/paulocaldas/bundle-width-estimator

The script is fully automated, returning all the histograms and a time-plot directly from a time-lapse tif file as input.

6.5.2 Architecture Analysis

To compute the orientation field of each image we used either the OrientationJ plugin for ImageJ (http://bigwww.epfl.ch/demo/orientation/) or a custom python code based on the *scikit-image* package (section 3.2). Correlation length was computed using a custom Matlab script, while curvature heatmaps and all the respective quantifications were computed using a custom python script (Fig. 6.3).

6.5.3 Image Autocorrelation Analysis

To quantify the reorganization dynamics of the membrane-bound FtsZ filament network (section 3.3), we performed a temporal correlation analysis using the ImageCorrelationJ plugin for ImageJ [Chinga and Syverud, 2007]:

https://www.gcsca.net/IJ/ImageCorrelationJ.html

The correlation can be performed based on single pixels or local areas. In our case we set the local area size to 3 pixels and used *increasing sequence* mode to compute the correlation, which correlates images in a stack increasing the distance between the slides. A correlation value R is calculated for each increment.

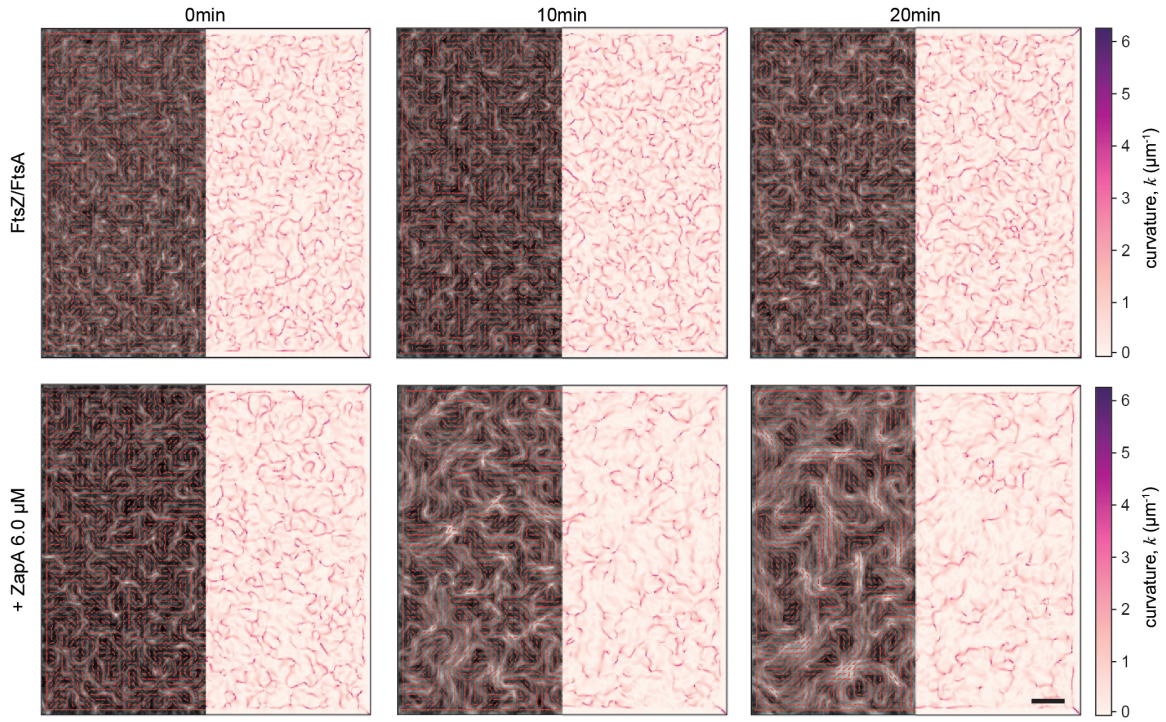

Figure 6.3: Orientation field and curvature of FtsZ filament network. Orientation fields and corresponding curvature maps for FtsZ filament network without (upper panel) or with $6.0\mu M$ ZapA (lower panel) over time. Scale bars = $5\mu m$.

The corresponding correlation curve was fitted to a mono-exponential decay, and the half-time (correlation time, τ) was used to compare a set of individual experiments.

6.5.4 Quantification of Filament Polymerization Dynamics

To analyze multiple time-lapse movies of treadmilling filaments in an automated manner (chapter 4), we have created scripts based on ImageJ plug-ins and Python. These are easy to use, require no programming knowledge and we made them available as supplementary material on Github:

https://github.com/paulocaldas/Treadmilling-Speed-Analysis

The repository is organized into three different computational steps: (i) *extraction*), an ImageJ macro to automatically generate fluorescent speckles from time-lapse movies; (ii) *tracking*, an ImageJ macro that internally uses TrackMate for detection and tracking of fluorescence spots; (iii) *tracking_analysis*, a IPython notebook with detailed analysis of the trajectories generated by TrackMate. All these scrips can be applied for a single time-lapse movie or for multiple files at once in batch processing mode. This creates a highly time-efficient routine to identify and track thousands of speckles at once.

6.6 Modeling and Bootstrapping Confidence Intervals

Using a custom python script based on LMFIT library - Non-Linear Least-Squares (NLS) Minimization and Curve-Fitting for python (https://lmfit.github.io/lmfit-py/) - each ZapA titration curve obtained was best fitted to a modified Hill equation given by:

$$Y = Y_{min} + (Y_{max} - Y_{min})\frac{x^{n_H}}{k^{n_H} + x^{n_H}}$$

where n_H is the hill coefficient and k (or IC_{50}) is the protein concentration that produces 50% of the maximal response. The hill coefficient reflects the behavior of the system, the greater the value of n_H, the more ultrasensitive is the response. Increasing concentrations of ZapA induced a steep transition between two different states and required minimum critical concentration of protein to observe that behavior. Both of these two features support an ultrasensitive/cooperative behavior [Ferrell *et al.*, 2014].

Importantly, while our model shows undoubtedly that nH >> 2 (Fig. 6.4A), the absolute value of the hill coefficient has no biological significance, it simply reflects the sharpness of the switch-like behavior. In fact, due to the steepness of the transition, the standard error of n_H reported by the non-linear regression fit was remarkably large, since a wide range of $n_H >> 8$ can equally explain the data (Fig. 6.4B). In addition, NLS relies on asymptotic approximations, e.g normally distributed data, which generate poor estimations for the variance of non-parametric coefficients. Thus, for a better estimation of the standard errors of the fitting parameters, we used the bootstrap method to construct 95% confidence intervals [Fox, 2018] (Fig. 6.4C-E).

Bootstrapping involves re-sampling a dataset with replacement to create a new sampling distribution of the mean value [Fox, 2018]. It assumes that the variance of the re-sampling statistics will be a good estimator of the real variance. When applied to regression problems, bootstrapping can be used to determine the best-fit estimates of the model parameters. This is done by re-sampling the residuals obtained from the fitting procedure and add them to the observed values to create new hypothetical observed values (bootstrap data set). By fitting our model to each new bootstrap data set (seen as an independent replicate experiment) we obtain a distribution of values for each fitting parameter (n_H and IC_{50} in our model).

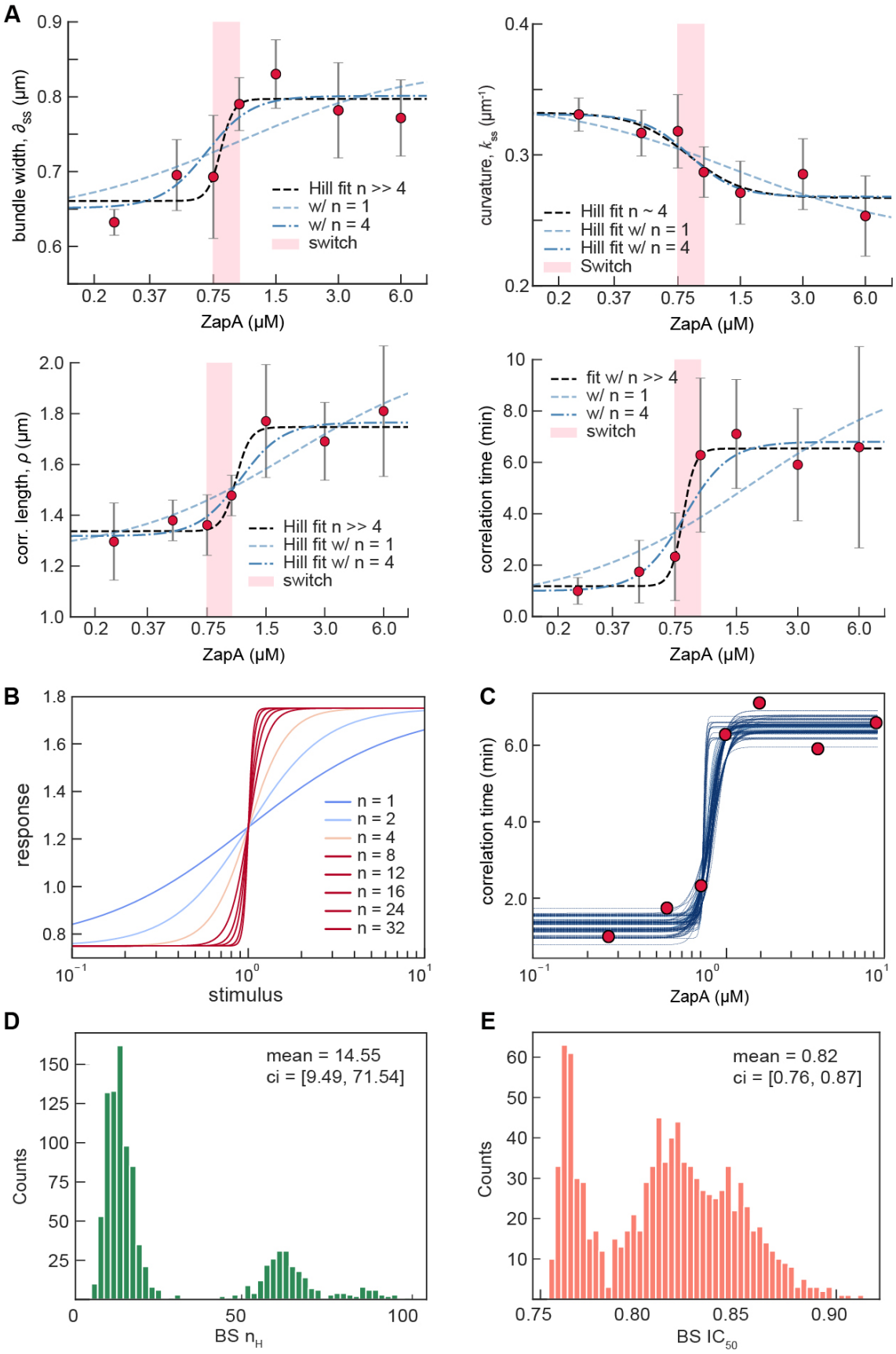

Figure 6.4: Hill coefficients and bootstrapping. **(A)** Plots of Hill equation modeling using Hill coefficients $n_H = 1$, $n_H = 4$ and fitting results. Data points correspond to the mean of the parameter and error bars to the standard deviation.**(B)** simulation of Hill equation with increasing Hill coefficients. **(C)** Typical boostrapping procedure, fitting our model to hundreds of bootstrap data sets generated by re-sampling the residues. This procedure generates a distribution of hypothetical values of **(D)** n_H and **(E)** IC_{50} to estimate more reliable confidence intervals.

The standard deviation of these new distributions (which corresponds to the standard deviation of the mean) can then be used to estimate confidence intervals of each parameter [Fox, 2018].

Note that bootstrapping does not provide any information regarding the mean value of the parameter, but a better estimation of the variance of the parameters when compared to the value obtained directly from the NLS fit. The distributions we obtained for both parametrs were often bimodal (Fig. 6.4D,E), presumably, because the range and number of concentrations used in our titration experiments was limited. Our confidence intervals for n_H and IC_{50} were estimated by bootstrapping the non-linear regression in 1000 iterations (Table 6.1).

Table 6.1: Hill coefficients and bootstrapping parameters for ZapA titrations. Best fitted parameters for each parameter. Confidence intervals were obtained by bootstrapping the parameters obtained from non-linear regression 1000 times. Below is shown the goodness of the fit parameters for a non-linear regression fit using different hill coefficients.

	nH	C.I @90%	IC 50 (μM)	C.I @90%
bundle width	13.86	[13.86, 94.68]	0.81	[0.71, 0.98]
correlation length	12.04	[1.27, 78.81]	1.05	[0.79, 2.03]
curvature	3.28	[1.42, 15.05]	0.84	[0.62, 1.19]
correlation time	14.55	[9.22, 69.27]	0.82	[0.76, 0.87]

6.7 Statistical Analysis

For statistical analyses of box plots data, a two-tailed Student's t-test was performed using a python script based on scipy library. A p-value of < 0.05 was considered as statistically significant. Boxes are represented from 25th to 75th percentiles, the whiskers extend 1.5x the standard deviation and the mean value is plotted as a line in the middle of the box.

Table 6.2: Statistical significance matrix for ZapA quantifications. Each matrix shows the p value for all the pairwise combinations of a two-tailed Student's t-tests.

		FtsZ/A	ZapA	I83E	R46A
bundle width	FtsZ/A	-	4.2E-03	0.130	0.080
	ZapA	***	-	8.6E-05	5.60E-05
	I83E	n.s	***	-	0.470
	R46A	n.s	***	n.s	-
curvature	FtsZ/A	-	1.0E-06	0.01	0.437
	ZapA	***	-	8.5E-05	3.45E-03
	I83E	*	***	-	0.360
	R46A	n.s	***	*	-
correlation length	FtsZ/A	-	1.6E-04	0.160	0.710
	ZapA	***	-	2.1E-03	1.10E-04
	I83E	n.s	***	-	0.130
	R46A	n.s	***	n.s	-
correlation time	FtsZ/A	-	2.9E-03	0.430	0.084
	ZapA	***	-	4.5E-03	1.32E-02
	R46A	n.s	***	-	0.23
	I83E	n.s	***	n.s	-
growth rate	FtsZ/A	-	0.070	0.100	0.985
	ZapA	n.s	-	0.280	0.340
	R46A	n.s	n.s	-	0.130
	I83E	n.s	n.s	n.s	-
shrinkage rate	FtsZ/A	-	0.160	0.050	0.740
	ZapA	n.s	-	0.730	0.130
	R46A	n.s	n.s	-	0.09
	I83E	n.s	n.s	n.s	-
directionality	FtsZ/A	-	6.8E-04	0.870	0.679
	ZapA	***	-	3.8E-04	3.95E-03
	I83E	n.s	***	-	0.730
	R46A	n.s	***	n.s	-

		FtsZ/A	**FtsZ**+ZapA	FtsZ+**ZapA**
lifetime (SPT)	**FtsZ**/A	-	0.470	4.4E-07
	FtsZ+ZapA	n.s	-	7.1E-04
	FtsZ+**ZapA**	***	***	-
lifetime (FRAP)	**FtsZ**/A	-	0.140	1.4E-04
	FtsZ+ZapA	n.s	-	1.7E-07
	FtsZ+**ZapA**	***	***	-

Table 6.3: Statistical significance matrix for ZapC quantifications. Each matrix shows the p value for all the pairwise combinations of a two-tailed Student's t-tests.

		FtsZ/A	ZapA	ZapC	ZapC+ZapA
bundle width	FtsZ/A	-	0.001	0.30	0.013
	ZapA	***	-	0.190	0.230
	ZapC	n.s	***	-	0.550
	ZapC+ZapA	n.s	***	n.s	-
curvature	FtsZ/A	-	4.4E-04	0.22	2.10E-05
	ZapA	***	-	0.019	9.39E-02
	ZapC	n.s	***	-	7.47E-04
	ZapC+ZapA	n.s	***	n.s	-
correlation length	FtsZ/A	-	4.98E-04	0.045	1.37E-04
	ZapA	***	-	0.037	0.0402
	ZapC	n.s	***	-	1.02E-03
	ZapC+ZapA	n.s	***	n.s	-
correlation time	FtsZ/A	-	6.9E-05	1.1E-02	8.5E-04
	ZapA	***	-	0.12	7.70E-03
	ZapC	n.s	***	-	0.12
	ZapC+ZapA	n.s	***	n.s	-
growth rate	FtsZ/A	-	4.6E-02	3.79E-03	7.24E-09
	ZapA	***	-	0.037	1.97E-07
	ZapC	n.s	***	-	0.010
	ZapC+ZapA	n.s	***	n.s	-
shrinkage rate	FtsZ/A	-	0.10	4.07E-03	8.85E-09
	ZapA	***	-	0.026	1.75E-07
	ZapC	n.s	***	-	0.010
	ZapC+ZapA	n.s	***	n.s	-

		FtsZ/A	**FtsZ**+ZapA	**FtsZ**+ZapC	**ZapC**+ZapA
lifetime (FRAP)	**FtsZ**/A	-	0.10	4.07E-03	8.85E-09
	FtsZ+ZapA	***	-	0.026	1.75E-07
	FtsZ+ZapC	n.s	***	-	0.010
	ZapC+ZapA	n.s	***	n.s	-

Chapter 7

Discussion

FtsZ has been established as the main orchestrator of bacterial cell division by playing two essential roles: (i) upon polymerization into a ring-like structure at mid-cell, defines the location of cell division and acts as a scaffold to recruit all the other divisome components; (ii) treadmilling of proto-filaments drive the circumferential motion of peptidoglycan synthases, which is required for the homogeneous distribution of cell wall synthesis at the division site.

In this work, we sought to understand how different FtsZ-associated proteins (Zaps) contribute for these two roles at the molecular level, namely how they modulate FtsZ filament architecture and dynamics in order to increase precision of cell division. These crosslinking proteins have been implicated in the stabilization of the Z-ring *in vivo*, but mechanistic insight was still elusive.

To achieve this, we used an *in vitro* reconstitution approach combined with TIRF microscopy that allowed us to study the dynamic behavior of membrane-bound FtsZ filament bundles directly in the presence of these proteins. In parallel, we set out to develop automatic image analysis methods to quantitatively describe fluctuations in the large-scale architecture of the FtsZ filament network and measure their underlying treadmilling dynamics.

Our image analysis pipelines are mostly data-driven and circumvent the need for user input. Instead, they provide a mathematical description of the biological object which is then interpreted in terms of specific parameters. These methods are easily applied in a high-throughput fashion, enabling a highly time-efficient workflow. We highlight our approach for the computational analysis of membrane-bound treadmilling filaments, which allows to study polymerization dynamics of active filaments in a non-biased, highly automated manner. This automated method can facilitate the analysis of a large variety of dynamic cytoskeletal systems, using standard time-lapse movies obtained from experiments *in vitro* as well as in the living cell (Chapter 4). We demonstrate that our approach can specifically detect, track and analyze growth and shrinkage of polymers, even in dense networks of filaments.

This work was mainly focus in the activity of ZapA, arguably the most relevant of the four bacterial crosslinkers. This protein is the most well studied of the Zaps and is highly conserved, which makes our observations relevant not only for the *Eschericha coli* case but across species. We found that ZapA aligns FtsZ filaments in parallel, which gives rise to a straightening and stabilization of filament bundles and as a consequence increases the spatial order and spatiotemporal persistence of the large-scale filament network. Importantly, this transition from a dynamic state of low spatial order to a persistent state of high order happens within a narrow range of ZapA concentrations and without compromising treadmilling dynamics.

How do we explain the cooperative switch induced by ZapA?

Due to its central four-helix bundle (Fig. 1.8), the ZapA tetramer can be assumed to have a highly rigid structure. We therefore expect that only in the case of straight, parallel filaments all four FtsZ-binding domains of a ZapA tetramer would be in contact with an FtsZ monomer. Accordingly, binding of ZapA aligns and straightens FtsZ filaments, which in turn can increase their affinity to ZapA tetramers. As a result, ZapA stimulates its own recruitment (Fig. 7.1).

How is treadmilling dynamics preserved with an increased bundling?

From a classical point of view, the expectation is that lateral bundling of filaments would stabilize the network and change filament dynamics or length in some manner. Here, even when these filaments are bundled, they treadmill at the same speed and their lifetime does not change. This effect is the result of weak transient interactions between FtsZ filaments and ZapA (chapter 5). These multiple transient interactions with low-activity provide more flexibility than series of stable pair-wise interactions as they allow to reorganize the cytoskeletal filaments without compromising their ability to recycle subunits (Fig. 7.1).

Recently, this effect has also been demonstrated *in vivo* in *Bacillus subtilis* [Squyres *et al.*, 2020]. This work shows that perturbations in the expression of ZapA and other FtsZ binding proteins (SepF and Ezra) have no effect on FtsZ lifetime and treadmmiling velocities due to their transient binding to FtsZ filaments.

Moreover, simply increasing FtsZ to FtsA ratio in our assays also leads to filament bundling, but treadmilling dynamic is impaired as the filaments grow longer [Loose and Mitchison, 2014].

This provides a strong evidence that increasing lateral-lateral interactions via ZapA crosslinker has unique properties regarding filament architecture and dynamics preservation, when compared with a simple overexpression of FtsZ.

How does this system compare to other networks of cytoskeletal filaments? Our experiments show that FtsZ, FtsA and ZapA self-organize into highly ordered cytoskeletal patterns on the membrane. Similar to gels of actin filaments and molecular motors, the structures described here exist out of equilibrium. In contrast to these active gels, however, the FtsZ filament network is driven out of equilibrium due to the continuous consumption of energy during treadmilling and not by the activity of motor proteins. This creates the important distinction that the components of an FtsZ active gel do not necessarily need to move relative to each other in order to rearrange the network.

Actin crosslinkers are known to modulate the architecture and mechanical properties of actin filament networks even when they bind cooperatively and transiently to actin filaments [Lieleg *et al.*, 2008; Schmoller *et al.*, 2011; Li *et al.*, 2012]. However while polymerization and depolymerization rates of FtsZ stay constant even at saturating concentrations of ZapA, actin crosslinkers were found to slow down actin polymerization dynamics [Schmoller *et al.*, 2011]. Accordingly, the switch in FtsZ filament organization that we observed here can also be interpreted as a phase transition that originates from the cumulative effect of multiple weak interactions between multivalent proteins that continuously turn over [Li *et al.*, 2012]

How is FtsZ filament bundling important for division *in vivo*? We believe that this ultrasensitive response plays an important role in the maturation of the cell division machinery as it ensures the correct alignment of FtsZ filaments into a more confined Z-ring prior to cell wall remodeling (Fig. 7.1). The transient binding of ZapA ensures that this occurs without slowing down treadmilling dynamics, which is required for a proper insertion of cell wall around the septum. This might help shaping the signal to recruit downstream proteins and creating a sharper track for the motion of peptoglycan synthases.

In line with this idea, recent *in vivo* work has shown that ZapA and other FtsZ binding proteins are required to compress short sparse FtsZ filaments into a dense Z-ring, which in turn is required for a viable cell division [Squyres *et al.*, 2020; Whitley

et al., 2020]. Here, PG synthases are still active in the absence of these proteins, but Z-ring condensation enhances their recruitment to FtsZ filaments at the division site [Squyres *et al.*, 2020]. Thus, without its bundlers, FtsZ still treadmills and localizes to mid-cell, but cannot condense into Z rings or complete septation.

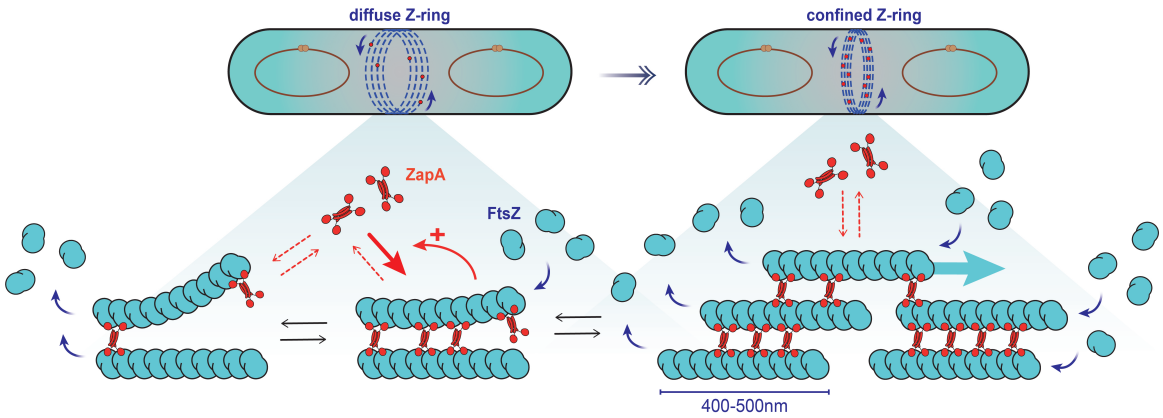

Figure 7.1: A model for the influence of ZapA and its role for Z-ring maturation. Binding of ZapA aligns treadmilling FtsZ filaments, which in turn facilitates its binding, giving rise to cooperativity. At saturation, four molecules of FtsZ bind to one tetramer of ZapA (1:1 monomer ratio) in parallel increasing the bundle width, persistence and alignment of FtsZ filaments. Treadmilling is not affected due to the transient binding of ZapA. Together, ZapA leads to a shift from a network of less ordered and highly dynamic FtsZ filaments into a more well-defined track, acting as an additional fine-tune mechanism for a proper Z-ring alignment without compromising treadmilling dynamics.

Together with our observations, these findings suggest that bundling of FtsZ filaments promotes a more compact Z-ring at mid-cell, which increases the recruitment PG synthases and creates a more defined track for the insertion of new peptidoglycan. This happens without compromising the treadmilling velocity of FtsZ, which enables filaments to find each other efficiently and to distribute PG synthases around the septum. However, how exactly bundling of FtsZ filaments contributes to recruit late division proteins to the division site remains an open question. *In vitro* experiments will certainly provide an ideal platform to explore the interface between these two events.

In addition, ZapA interacts with a large number of divisome proteins that do not interact directly with FtsZ, including FtsQ, FtsL, FtsB, FtsW, and FtsN [Alexeeva *et al.*, 2010; Buss *et al.*, 2015], which might contribute to modulate signal transduction and cell constriction through another bundling-independent mechanism.

Moreover, the switch that we observe here can also have consequences for the mechanical properties of the Z-ring, as ZapA was found to increase the stiffness of FtsZ gels formed *in vitro* [Dajkovic *et al.*, 2010]. Notably, eukaryotic cells have the abil-

ity to divide in the absence or impaired motor proteins [Mendes Pinto *et al.*, 2012; Mendes Pinto *et al.*, 2013]. In this scenario, depolymerization of actin filaments leads to the removal of monomers that are part of a crosslinking site, then thermal fluctuation of the crosslinker allow reattachment to the next monomer within the filament (the new filament end) leading to filament slide. Likewise, shrinking ends during FtsZ filaments treadmilling could create conditions for a similar mechanism to happen and the elastic energy stored could potential contribute to produce force. In the future would be interesting to explore this potential contribution of Zap proteins and bundling in force-generating mechanisms.

What could be the role of the other Zaps in *Escherichia coli*?

We used our self-organization assay to support previous observations that ZapB could disrupt FtsZ-ZapA interaction. The switch-like effect of ZapA towards bundling of membrane-bound FtsZ filaments, suggests a decisive swapping of filaments into a well-aligned ring as soon as the local ZapB concentration is too low to counteract ZapA. Consistent with this idea, other studies have shown that cells lacking SlmA and Min proteins - the two main negative regulators of FtsZ polymerization and responsible for the midcell placement of the Z-ring in *Escherichia coli* - are still able to divide with unexpected precision [Bailey *et al.*, 2014; Buss *et al.*, 2017]. This suggests that the complex formed by ZapA-ZapB, connected to the chromosome by matP (ter-linakge), may provide additional positional cues for Z-ring formation. In fact, mutants for matP constrict at a faster rate than wild type cells over unsegregated chromosomes due to the absence of coordination by this complex [Buss *et al.*, 2015; Coltharp *et al.*, 2016; Männik *et al.*, 2017]

Our experiments showed that ZapC can bundle FtsZ filaments with a slight different architecture than the one observed for ZapA. As discussed previously, ZapC is monomeric, which might engage in a different mechanism to bundle FtsZ when compared with the tetrameric ZapA. Also, treadmilling filaments are still dynamic in the presence of ZapC, but they slowdown significantly when together with ZapA. It is possible that a combination of crosslinkers with variable lengths and binding sites may change interfilamentous spacing and create different bending stiffness regimes.

The ability to rapidly change network morphology using different Zaps might be advantageous in response to different stimuli, either from the environment or from other players during cell cycle. Modulate the space between filaments inside the Z-ring

to accommodate more or less cytoplasmic signaling proteins as cytokinesis proceeds could enhance or decrease Z-ring stability and its cargo capacity. However, it is not clear which scenarios would demand structural organization of the Z-ring and little is known about regulation of Zaps under different conditions.

Clearly, further experiments are needed to probe the differences between these proteins in bundling FtsZ. In the short-term, higher resolution techniques such as EM and AFM, will likely give us substantial details into the inter-filament spacing and rigidity of these different bundles, specially when taking into account what we already know about their structures.

Wrapping up

We believe that the cytoskeletal networks of FtsZ, FtsA and Zap crosslinkers represent a novel and distinct form of active biological matter despite the apparent absence of mechanical stresses that are usually present in gels composed of filaments and molecular motors [Fletcher and Geissler, 2009; Marchetti *et al.*, 2013; Prost *et al.*, 2015]. In particular, we underline our observations for the ZapA system, showing how this protein can increase the precision and robustness of the Z-ring, without sacrificing the performance of the cell division machinery. By transiently binding to FtsZ filaments, ZapA helps to create a more compact structure at the division site, which might contribute to increase the recruitment of late division proteins and contribute to an appropriate insertion of new cell wall. Other Zaps might help change the morphology of the filament network inside the Z-ring, but more studies are needed to understand the importance of these different architectures.

Nevertheless, FtsZ, FtsA and ZapA are highly conserved division proteins, most likely part of core mechanisms common across a wide range of species, thus understanding their underlying dynamics is of great interest for the bacteria field in general. In addition, given the importance of the cell division proteins as primary targets for the development of new broad-spectrum antibacterial inhibitors, this topic should be even more appealing.

Bibliography

[Aarsman *et al.*, 2005] Mirjam E.G. Aarsman, André Piette, Claudine Fraipont, Thessa M.F. Vinkenvleugel, Martine Nguyen-Distèche, and Tanneke Den Blaauwen, "Maturation of the Escherichia coli divisome occurs in two steps," *Mol. Microbiol.*, 55(6):1631–1645, mar 2005.

[Addinall and Lutkenhaus, 1996] Stephen G Addinall and Joe Lutkenhaus, "FtsA is localized to the septum in an FtsZ-dependent manner," *J. Bacteriol.*, 178(24):7167–7172, dec 1996.

[Alexeeva *et al.*, 2010] Svetlana Alexeeva, Theodorus W.J. Gadella, Jolanda Verheul, Gertjan S. Verhoeven, and Tanneke Den Blaauwen, "Direct interactions of early and late assembling division proteins in Escherichia coli cells resolved by FRET," *Mol. Microbiol.*, 77(2):384–398, jul 2010.

[Anderson *et al.*, 2004] David E. Anderson, Frederico J. Gueiros-Filho, and Harold P. Erickson, "Assembly dynamics of FtsZ rings in Bacillus subtilis and Escherichia coli and effects of FtsZ-regulating proteins," *J. Bacteriol.*, 186(17):5775–5781, sep 2004.

[Applegate *et al.*, 2011] Kathryn T. Applegate, Sebastien Besson, Alexandre Matov, Maria H. Bagonis, Khuloud Jaqaman, and Gaudenz Danuser, "PlusTipTracker: Quantitative image analysis software for the measurement of microtubule dynamics," *J. Struct. Biol.*, 176(2):168–184, 2011.

[Ausmees *et al.*, 2003] Nora Ausmees, Jeffrey R. Kuhn, and Christine Jacobs-Wagner, "The bacterial cytoskeleton: An intermediate filament-like function in cell shape," *Cell*, 115(6):705–713, 2003.

[Bagchi *et al.*, 2008] Sonchita Bagchi, Henrik Tomenius, Lyubov M. Belova, and Nora Ausmees, "Intermediate filament-like proteins in bacteria and a cytoskeletal function in Streptomyces," *Mol. Microbiol.*, 70(4):1037–1050, nov 2008.

[Bailey *et al.*, 2014] Matthew W. Bailey, Paola Bisicchia, Boyd T. Warren, David J. Sherratt, and Jaan Männik, "Evidence for Divisome Localization Mechanisms Independent of the Min System and SlmA in Escherichia coli," *PLoS Genet.*, 10(8), 2014.

[Baranova and Loose, 2017] N. Baranova and M. Loose, *Single-molecule measurements to study polymerization dynamics of FtsZ-FtsA copolymers*, volume 137, Elsevier Ltd, 2017.

[Baranova *et al.*, 2020] Natalia Baranova, Philipp Radler, Víctor M. Hernández-Rocamora, Carlos Alfonso, Mar López-Pelegrín, Germán Rivas, Waldemar Vollmer, and Martin Loose, "Diffusion and capture permits dynamic coupling between treadmilling FtsZ filaments and cell division proteins," mar 2020.

[Beech *et al.*, 2000] Peter L. Beech, Thao Nheu, Thomas Schultz, Shane Herbert, Trevor Lithgow, Paul R. Gilson, and Geoffrey I. McFadden, "Mitochondrial FtsZ in a chromophyte alga," *Science (80-.).*, 287(5456):1276–1279, feb 2000.

[Bernhardt and De Boer, 2005] Thomas G. Bernhardt and Piet A.J. De Boer, "SlmA, a nucleoid-associated, FtsZ binding protein required for blocking septal ring assembly over chromosomes in E. coli," *Mol. Cell*, 18(5):555–564, 2005.

[Bi and Lutkenhaus, 1991] Erfei Bi and Joe Lutkenhaus, "FtsZ ring structure associated with division in Escherichia coli," *Nature*, 354(6349):161–164, nov 1991.

[Bisson-Filho *et al.*, 2017] Alexandre W. Bisson-Filho, Yen Pang Hsu, Georgia R. Squyres, Erkin Kuru, Fabai Wu, Calum Jukes, Yingjie Sun, Cees Dekker, Seamus Holden, Michael S. VanNieuwenhze, Yves V. Brun, and Ethan C. Garner, "Treadmilling by FtsZ filaments drives peptidoglycan synthesis and bacterial cell division," *Science (80-.).*, 355(6326):739–743, feb 2017.

[Biteen *et al.*, 2012] Julie S. Biteen, Erin D. Goley, Lucy Shapiro, and W. E. Moerner, "Three-dimensional super-resolution imaging of the midplane protein FtsZ in live Caulobacter crescentus cells using astigmatism," *ChemPhysChem*, 13(4):1007–1012, mar 2012.

[Bramhill and Thompson, 1994] David Bramhill and Chris M. Thompson, "GTP-dependent polymerization of Escherichia coli FtsZ protein to form tubules," *Proc. Natl. Acad. Sci. U. S. A.*, 91(13):5813–5817, jun 1994.

[Brouhard and Rice, 2018] Gary J. Brouhard and Luke M. Rice, "Microtubule dynamics: An interplay of biochemistry and mechanics," jul 2018.

[Buczek *et al.*, 2016] Monika S. Buczek, Andrea L.Cardenas Arevalo, and Anuradha Janakiraman, "CLpXP and ClpAP control the escherichia coli division protein ZaPC by proteolysis," jun 2016.

[Bugyi and Carlier, 2010] Beáta Bugyi and Marie-France Carlier, "Control of Actin Filament Treadmilling in Cell Motility," *Annu. Rev. Biophys.*, 39(1):449–470, apr 2010.

[Busiek *et al.*, 2012] Kimberly K. Busiek, Jesus M. Eraso, Yipeng Wang, and William Margolin, "The Early Divisome Protein FtsA Interacts Directly through Its 1c: Subdomain with the Cytoplasmic Domain of the Late Divisome: Protein FtsN," *J. Bacteriol.*, 194(8):1989–2000, apr 2012.

[Busiek and Margolin, 2015] Kimberly K. Busiek and William Margolin, "Bacterial actin and tubulin homologs in cell growth and division," *Curr. Biol.*, 25(6):R243–R254, 2015.

[Buske and Levin, 2012] Paul J. Buske and Petra Anne Levin, "Extreme C terminus of bacterial cytoskeletal protein FtsZ plays fundamental role in assembly independent of modulatory proteins," *J. Biol. Chem.*, 287(14):10945–10957, mar 2012.

[Buss *et al.*, 2013] Jackson Buss, Carla Coltharp, Tao Huang, Chris Pohlmeyer, Shih-chin Chin Wang, Christine Hatem, and Jie Xiao, "In vivo organization of the FtsZ-ring by ZapA and ZapB revealed by quantitative super-resolution microscopy," *Mol. Microbiol.*, 89(6):1099–1120, 2013.

[Buss *et al.*, 2015] Jackson Buss, Carla Coltharp, Gleb Shtengel, Xinxing Yang, Harald Hess, and Jie Xiao, "A Multi-layered Protein Network Stabilizes the Escherichia coli FtsZ-ring and Modulates Constriction Dynamics," *PLoS Genet.*, 11(4):1–24, 2015.

[Buss *et al.*, 2017] Jackson A. Buss, Nick T. Peters, Jie Xiao, and Thomas G. Bernhardt, "ZapA and ZapB form an FtsZ-independent structure at midcell," *Mol. Microbiol.*, 104(4):652–663, may 2017.

[Cabré *et al.*, 2013] Elisa J. Cabré, Alicia Sánchez-Gorostiaga, Paolo Carrara, Noelia Ropero, Mercedes Casanova, Pilar Palacios, Pasquale Stano, Mercedes Jiménez, Germán Rivas, and Miguel Vicente, "Bacterial division proteins FtsZ and ZipA induce vesicle shrinkage and cell membrane invagination," *J. Biol. Chem.*, 288(37):26625–26634, 2013.

[Caldas *et al.*, 2019] Paulo Caldas, Mar López-Pelegrín, Daniel J.G. Pearce, Nazmi Burak Budanur, Jan Brugués, and Martin Loose, "Cooperative ordering of treadmilling filaments in cytoskeletal networks of FtsZ and its crosslinker ZapA," *Nat. Commun.*, 10(1):5744, dec 2019.

[Caldas *et al.*, 2020] Paulo Caldas, Philipp Radler, Christoph Sommer, and Martin Loose, "Computational analysis of filament polymerization dynamics in cytoskeletal networks," In *Methods Cell Biol.*, volume 158, pages 145–161. Academic Press Inc., feb 2020.

[Chinga and Syverud, 2007] Gary Chinga and Kristin Syverud, "Quantification of paper mass distributions within local picking areas," *Nord. Pulp Pap. Res. J.*, 22(4):441–446, dec 2007.

[Coltharp *et al.*, 2016] Carla Coltharp, Jackson Buss, Trevor M. Plumer, and Jie Xiao, "Defining the rate-limiting processes of bacterial cytokinesis.," *Proc. Natl. Acad. Sci. U. S. A.*, 113(8):E1044–1053, feb 2016.

[Coltharp and Xiao, 2017] Carla Coltharp and Jie Xiao, "Beyond force generation: Why is a dynamic ring of FtsZ polymers essential for bacterial cytokinesis?," *BioEssays*, 39(1):1–11, 2017.

[Corbin *et al.*, 2004] B. D. Corbin, B. Geissler, M. Sadasivam, and W. Margolin, "Z-Ring-Independent Interaction between a Subdomain of FtsA and Late Septation Proteins as Revealed by a Polar Recruitment Assay," *J. Bacteriol.*, 186(22):7736–7744, nov 2004.

[Dajkovic *et al.*, 2008] Alex Dajkovic, Ganhui Lan, Sean X. Sun, Denis Wirtz, and Joe Lutkenhaus, "Article MinC Spatially Controls Bacterial Cytokinesis by Antagonizing the Scaffolding Function of FtsZ," *Curr. Biol.*, 18(4):235–244, feb 2008.

[Dajkovic *et al.*, 2010] Alex Dajkovic, Sebastien Pichoff, Joe Lutkenhaus, and Denis Wirtz, "Cross-linking FtsZ polymers into coherent Z rings," *Mol. Microbiol.*, 78(September):651–668, nov 2010.

[de Boer, 2010] Piet A J de Boer, "Advances in understanding E. coli cell fission.," *Curr. Opin. Microbiol.*, 13(6):730–7, dec 2010.

[de Boer *et al.*, 1989] Piet A.J. de Boer, Robin E. Crossley, and Lawrence I. Rothfield, "A division inhibitor and a topological specificity factor coded for by the minicell locus determine proper placement of the division septum in E. coli," *Cell*, 56(4):641–649, feb 1989.

[Desai and Mitchison, 1997] Arshad Desai and Timothy J. Mitchison, "Microtubule Polymerization Dynamics," *Annu. Rev. Cell Dev. Biol.*, 13(1):83–117, nov 1997.

[Du and Lutkenhaus, 2019] Shishen Du and Joe Lutkenhaus, "At the Heart of Bacterial Cytokinesis: The Z Ring," sep 2019.

[Du *et al.*, 2016] Shishen Du, Sebastien Pichoff, and Joe Lutkenhaus, "FtsEX acts on FtsA to regulate divisome assembly and activity," *Proc. Natl. Acad. Sci. U. S. A.*, 113(34):E5052–E5061, 2016.

[Duman *et al.*, 2013] Ramona Duman, Shu Ishikawa, Ilkay Celik, Henrik Strahl, Naotake Ogasawara, Paulina Troc, Jan Löwe, and Leendert W. Hamoen, "Structural and genetic analyses reveal the protein SepF as a new membrane anchor for the Z ring," *Proc. Natl. Acad. Sci. U. S. A.*, 110(48):E4601–E4610, 2013.

[Durand-Heredia *et al.*, 2012] Jorge Durand-Heredia, Eugene Rivkin, Guoxiang Fan, Jorge Morales, and Anuradha Janakiraman, "Identification of ZapD as a Cell Division Factor That Promotes the Assembly of FtsZ in Escherichia coli," *J. Bacteriol.*, 194(12):3189–3198, 2012.

[Durand-Heredia *et al.*, 2011] Jorge M. Durand-Heredia, Helen H. Yu, Sacha De Carlo, Cammie F. Lesser, and Anuradha Janakiraman, "Identification and characterization of ZapC, a stabilizer of the FtsZ ring in Escherichia coli," *J. Bacteriol.*, 193(6):1405–1413, mar 2011.

[Dworkin, 2009] Jonathan Dworkin, "Cellular polarity in prokaryotic organisms.," 2009.

[Ebersbach *et al.*, 2008] Gitte Ebersbach, Elisa Galli, Jakob Møller-Jensen, Jan Löwe, and Kenn Gerdes, "Novel coiled-coil cell division factor ZapB stimulates Z ring assembly and cell division," *Mol. Microbiol.*, 68(3):720–735, 2008.

[Encinar *et al.*, 2013] Mario Encinar, Andrew V. Kralicek, Ariadna Martos, Marcin Krupka, Sandra Cid, Alvaro Alonso, Ana I. Rico, Mercedes Jiménez, and Marisela Vélez, "Polymorphism of FtsZ filaments on lipid surfaces: Role of monomer orientation," *Langmuir*, 29(30):9436–9446, jul 2013.

[Erickson *et al.*, 1996] H. P. Erickson, D. W. Taylor, K. A. Taylor, and D. Bramhill, "Bacterial cell division protein FtsZ assembles into protofilament sheets and minirings, structural homologs of tubulin polymers.," *Proc. Natl. Acad. Sci. U. S. A.*, 93(1):519–23, jan 1996.

[Erickson *et al.*, 2010] Harold P. Erickson, David E. Anderson, and Masaki Osawa, "FtsZ in Bacterial Cytokinesis: Cytoskeleton and Force Generator All in One," *Microbiol. Mol. Biol. Rev.*, 74(4):504–528, dec 2010.

[Erickson and Osawa, 2010] Harold P. Erickson and Masaki Osawa, "Cell division without FtsZ - A variety of redundant mechanisms," *Mol. Microbiol.*, 78(2):267–270, 2010.

[Espéli *et al.*, 2012] Olivier Espéli, Romain Borne, Pauline Dupaigne, Axel Thiel, Emmanuelle Gigant, Romain Mercier, and Frédéric Boccard, "A MatP-divisome interaction coordinates chromosome segregation with cell division in E. coli," *EMBO Journa*, 31(14):3198–3211, 2012.

[Ferrell *et al.*, 2014] James E Ferrell, Sang Hoon Ha, and Sang Hoon Ha, "Ultrasensitivity part III: cascades, bistable switches, and oscillators.," *Trends Biochem. Sci.*, 39(12):612–8, dec 2014.

[Fletcher and Geissler, 2009] Daniel A. Fletcher and Phillip L. Geissler, "Active Biological Materials," *Annu. Rev. Phys. Chem.*, 60(1):469–486, 2009.

[Fox, 2018] John Fox, *Applied regression analysis and generalized linear models*, SAGE, 2018.

[Fu *et al.*, 2010] Guo Fu, Tao Huang, Jackson Buss, Carla Coltharp, Zach Hensel, and Jie Xiao, "In Vivo Structure of the E . coli FtsZ-ring Revealed by Photoactivated Localization Microscopy (PALM)," *PLoS One*, 5(9):e12680, sep 2010.

[Fujita *et al.*, 2017] Junso Fujita, Ryuhei Harada, Yoko Maeda, Yuki Saito, Eiichi Mizohata, Tsuyoshi Inoue, Yasuteru Shigeta, and Hiroyoshi Matsumura, "Identification of the key interactions in structural transition pathway of FtsZ from Staphylococcus aureus," *J. Struct. Biol.*, 198(2):65–73, may 2017.

[Galli and Gerdes, 2010] Elisa Galli and Kenn Gerdes, "Spatial resolution of two bacterial cell division proteins: ZapA recruits ZapB to the inner face of the Z-ring," *Mol. Microbiol.*, 76(6):1514–1526, apr 2010.

[Galli and Gerdes, 2012] Elisa Galli and Kenn Gerdes, "FtsZ-ZapA-ZapB interactome of Escherichia coli," *J. Bacteriol.*, 194(2):292–302, 2012.

[Gamba *et al.*, 2009] Pamela Gamba, Jan Willem Veening, Nigel J Saunders, Leendert W Hamoen, and Richard A Daniel, "Two-step assembly dynamics of the Bacillus subtilis divisome," *J. Bacteriol.*, 191(13):4186–4194, 2009.

[Garner *et al.*, 2007] Ethan C. Garner, Christopher S. Campbell, Douglas B. Weibel, and R. Dyche Mullins, "Reconstitution of DNA segregation driven by assembly of a prokaryotic actin homolog," *Science (80-.).*, 315(5816):1270–1274, mar 2007.

[Geissler *et al.*, 2003] Brett Geissler, Dany Elraheb, and William Margolin, "A gain-of-function mutation in ftsA bypasses the requirement for the essential cell division gene zipA in Escherichia coli," *Proc. Natl. Acad. Sci. U. S. A.*, 100(7):4197–4202, apr 2003.

[Gerding *et al.*, 2009] Matthew A. Gerding, Bing Liu, Felipe O. Bendezú, Cynthia A. Hale, Thomas G. Bernhardt, and Piet A.J. De Boer, "Self-enhanced accumulation of FtsN at division sites and roles for other proteins with a SPOR domain (DamX, DedD, and RlpA) in Escherichia coli cell constriction," *J. Bacteriol.*, 191(24):7383–7401, dec 2009.

[Gierke *et al.*, 2010] Sarah Gierke, Praveen Kumar, and Torsten Wittmann, *Analysis of Microtubule Polymerization Dynamics in Live Cells*, volume 97, 2010.

[Goehring and Beckwith, 2005] Nathan W. Goehring and Jon Beckwith, "Diverse paths to midcell: Assembly of the bacterial cell division machinery," 2005.

[Goley *et al.*, 2011] Erin D. Goley, Yi Chun Yeh, Sun Hae Hong, Michael J. Fero, Eduardo Abeliuk, Harley H. Mcadams, and Lucy Shapiro, "Assembly of the Caulobacter cell division machine," *Mol. Microbiol.*, 80(6):1680–1698, jun 2011.

[González *et al.*, 2003] José Manuel González, Mercedes Jiménez, Marisela Vélez, Jesús Mingorance, José Manuel Andreu, Miguel Vicente, and Germán Rivas, "Essential Cell Division Protein FtsZ Assembles into One Monomer-thick Ribbons under Conditions Resembling the Crowded Intracellular Environment," *J. Biol. Chem.*, 278(39):37664–37671, sep 2003.

[Guan *et al.*, 2018] Fenghui Guan, Jiayu Jie Jiayu Yu, Jiayu Jie Jiayu Yu, Yang Liu, Ying Li, Xin Hua Feng, Kerwyn Casey Huang, Zengyi Chang, and Sheng Ye, "Lateral interactions between protofilaments of the bacterial tubulin homolog FtsZ are essential for cell division," *Elife*, 7, jun 2018.

[Gueiros-Filho and Losick, 2002] Frederico J. Gueiros-Filho and Richard Losick, "A widely conserved bacterial cell division protein that promotes assembly of the tubulin-like protein FtsZ," *Genes Dev.*, 16(19):2544–2556, oct 2002.

[Haeusser *et al.*, 2007] Daniel P. Haeusser, Anna Cristina Garza, Amy Z. Buscher, and Petra Anne Levin, "The division inhibitor EzrA contains a seven-residue patch required for maintaining the dynamic nature of the medial FtsZ ring," *J. Bacteriol.*, 189(24):9001–9010, 2007.

[Haeusser *et al.*, 2015] Daniel P. Haeusser, Veronica W. Rowlett, and William Margolin, "A mutation in Escherichia coli ftsZ bypasses the requirement for the essential division gene zipA and confers resistance to FtsZ assembly inhibitors by stabilizing protofilament bundling," *Mol. Microbiol.*, 97(5):988–1005, sep 2015.

[Hale *et al.*, 2011] Cynthia A. Hale, Daisuke Shiomi, Bing Liu, Thomas G. Bernhardt, William Margolin, Hironori Niki, and Piet A.J. De Boer, "Identification of Escherichia coli ZapC (YcbW) as a component of the division apparatus that binds and bundles FtsZ polymers," *J. Bacteriol.*, 193(6):1393–1404, mar 2011.

[Hirota *et al.*, 1968] Y. Hirota, A. Ryter, and F. Jacob, "Thermosensitive mutants of E. coli affected in the processes of DNA synthesis and cellular division.," *Cold Spring Harb. Symp. Quant. Biol.*, 33:677–693, 1968.

[Hirota and Matthieu, 1973] Yukinori Hirota and Ricard Matthieu, "Process of cellular division in Escherichia coli growth pattern of E. coli murein.," *J. Mol. Biol.*, 78(1):185–195, 1973.

[Holden *et al.*, 2014] Seamus J. Holden, Thomas Pengo, Karin L. Meibom, Carmen Fernandez Fernandez, Justine Collier, Suliana Manley, C. Fernandez Fernandez, Justine Collier, and Suliana Manley, "High throughput 3D super-resolution microscopy reveals Caulobacter crescentus in vivo," *Proc. Natl. Acad. Sci.*, 111(12):4566–4571, mar 2014.

[Howard *et al.*, 1989] J. Howard, A. J. Hudspeth, and R. D. Vale, "Movement of microtubules by single kinesin molecules," *Nature*, 342(6246):154–158, nov 1989.

[Hu and Lutkenhaus, 1999] Zonglin Hu and Joe Lutkenhaus, "Topological regulation of cell division in Escherichia coli involves rapid pole to pole oscillation of the division inhibitor MinC under the control of MinD and MinE," *Mol. Microbiol.*, 34(1):82–90, oct 1999.

[Huang *et al.*, 2016a] Junqi Huang, Ting Gang Chew, Ying Gu, Saravanan Palani, Anton Kamnev, Douglas S Martin, Nicholas J Carter, Robert Anthony Cross, Snezhana Oliferenko, and Mohan K. Balasubramanian, "Curvature-induced expulsion of actomyosin bundles during cytokinetic ring contraction," *Elife*, 5(October2016):1–14, 2016.

[Huang *et al.*, 2016b] Kuo Hsiang Huang, Aaron Mychack, Lukasz Tchorzewski, and Anuradha Janakiraman, "Characterization of the FtsZ C-Terminal variable (CTV) Region in Z-Ring assembly and interaction with the Z-Ring stabilizer ZapD in E. coli cytokinesis," *PLoS One*, 11(4):e0153337, apr 2016.

[Huecas *et al.*, 2008] Sonia Huecas, Oscar Llorca, Jasminka Boskovic, Jaime Martfn-Benito, Jose Marfa Valpuesta, and Jose Manuel Andreu, "Energetics and geometry of FtsZ polymers: Nucleated self-assembly of single protofilaments," *Biophys. J.*, 94(5):1796–1806, mar 2008.

[Huecas *et al.*, 2017] Sonia Huecas, Erney Ramírez-Aportela, Albert Vergoñós, Rafael Núñez-Ramírez, Oscar Llorca, J. Fernando Díaz, David Juan-Rodríguez, María A. Oliva, Patricia Castellen, and José M. Andreu, "Self-Organization of FtsZ Polymers in Solution Reveals Spacer Role of the Disordered C-Terminal Tail," *Biophys. J.*, 113(8):1831–1844, oct 2017.

[Huecas *et al.*, 2007] Sonia Huecas, Claudia Schaffner-Barbero, Wanius García, Hugo Yébenes, Juan Manuel Palacios, José Fernando Díaz, Margarita Menéndez, and José Manuel Andreu, "The interactions of cell division protein FtsZ with guanine nucleotides," *J. Biol. Chem.*, 282(52):37515–37528, dec 2007.

[Ishihara *et al.*, 2020] Keisuke Ishihara, Franziska Decker, Paulo Caldas, James Pelletier, Martin Loose, Jan Brugues, and Tim Mitchison, "Spatial Variation of Microtubule Depolymerization in Large Asters Suggests Regulation by MAP Depletion," *bioRxiv Cell Biol.*, 2020.

[Ishihara *et al.*, 2014] Keisuke Ishihara, Phuong A. Nguyen, Aaron C. Groen, Christine M. Field, and Timothy J. Mitchison, "Microtubule nucleation remote from centrosomes may explain how asters span large cells," *Proc. Natl. Acad. Sci. U. S. A.*, 111(50):17715–17722, dec 2014.

[Jaiswal *et al.*, 2010] Richa Jaiswal, Ronak Y. Patel, Jayant Asthana, Bhavya Jindal, Petety V. Balaji, and Dulal Panda, "E93R substitution of Escherichia coli FtsZ induces bundling of protofilaments, reduces GTPase activity, and impairs bacterial cytokinesis," *J. Biol. Chem.*, 285(41):31796–31805, oct 2010.

[Kapoor *et al.*, 2019] Varun Kapoor, William G. Hirst, Christoph Hentschel, Stephan Preibisch, and Simone Reber, "MTrack: Automated Detection, Tracking, and Analysis of Dynamic Microtubules," *Sci. Rep.*, 9(1):1–12, 2019.

[Karimova *et al.*, 2005] Gouzel Karimova, Nathalie Dautin, and Daniel Ladant, "Interaction network among Escherichia coli membrane proteins involved in cell division as revealed by bacterial two-hybrid analysis," *J. Bacteriol.*, 187(7):2233–2243, apr 2005.

[Koppelman *et al.*, 2004] Cecile Marie Koppelman, Mirjam E.G. Aarsman, Jarne Postmus, Evelien Pas, Anton O. Muijsers, Dirk Jan Scheffers, Nanne Nanninga, and Tanneke Den Blaauwen, "R174

of Escherichia coli FtsZ is involved in membrane interaction and protofilament bundling, and is essential for cell division," *Mol. Microbiol.*, 51(3):645–657, dec 2004.

[Krupka *et al.*, 2017] Marcin Krupka, Veronica W. Rowlett, Dustin Morado, Heidi Vitrac, Kara Schoenemann, Jun Liu, and William Margolin, "Escherichia coli FtsA forms lipid-bound minirings that antagonize lateral interactions between FtsZ protofilaments," *Nat. Commun.*, 8(1):15957, dec 2017.

[Krupka *et al.*, 2018] Marcin Krupka, Marta Sobrinos-Sanguino, Mercedes Jiménez, Germán Rivas, and William Margolin, "Escherichia coli Zipa organizes FtsZ polymers into dynamic ring-like protofilament structures," *MBio*, 9(3), 2018.

[Lan *et al.*, 2008] Ganhui Lan, Alex Dajkovic, Denis Wirtz, and Sean X. Sun, "Polymerization and Bundling Kinetics of FtsZ Filaments," *Biophys. J.*, 95(8):4045–4056, oct 2008.

[Lan *et al.*, 2009] Ganhui Lan, Brian R. Daniels, Terrence M. Dobrowsky, Denis Wirtz, and Sean X. Sun, "Condensation of FtsZ filaments can drive bacterial cell division," *Proc. Natl. Acad. Sci. U. S. A.*, 106(1):121–126, jan 2009.

[Leisch *et al.*, 2016] Nikolaus Leisch, Nika Pende, Philipp M. Weber, Harald R. Gruber-Vodicka, Jolanda Verheul, Norbert O.E. Vischer, Sophie S. Abby, Benedikt Geier, Tanneke Den Blaauwen, and Silvia Bulgheresi, "Asynchronous division by non-ring FtsZ in the gammaproteobacterial symbiont of Robbea hypermnestra," *Nat. Microbiol.*, 2(1):1–5, oct 2016.

[Li *et al.*, 2012] Pilong Li, Sudeep Banjade, Hui Chun Cheng, Soyeon Kim, Baoyu Chen, Liang Guo, Marc Llaguno, Javoris V. Hollingsworth, David S. King, Salman F. Banani, Paul S. Russo, Qiu Xing Jiang, B. Tracy Nixon, and Michael K. Rosen, "Phase transitions in the assembly of multivalent signalling proteins," *Nature*, 483(7389):336–340, 2012.

[Li *et al.*, 2007] Zhuo Li, Michael J. Trimble, Yves V. Brun, and Grant J. Jensen, "The structure of FtsZ filaments in vivo suggests a force-generating role in cell division," *EMBO J.*, 26(22):4694–4708, nov 2007.

[Lieleg *et al.*, 2008] O. Lieleg, M. M.A.E. Claessens, Y. Luan, and A. R. Bausch, "Transient binding and dissipation in cross-linked actin networks," *Phys. Rev. Lett.*, 101(10), 2008.

[Liu and Fletcher, 2009] Allen P. Liu and Daniel A. Fletcher, "Biology under construction: in vitro reconstitution of cellular function," *Nat. Rev. Mol. Cell Biol.*, 10(9):644–650, sep 2009.

[Loose *et al.*, 2008] Martin Loose, Fischer-F, Elisabeth Riedrich, Jonas Ries, Karsten Kruse, and Petra Schwille, "Spatial Regulators for Bacterial Cell," *Science (80-.).*, 320(May):789–792, 2008.

[Loose and Mitchison, 2014] Martin Loose and Timothy J. Mitchison, "The bacterial cell division proteins FtsA and FtsZ self-organize into dynamic cytoskeletal patterns," *Nat. Cell Biol.*, 16(1):38–46, jan 2014.

[Loose and Schwille, 2009] Martin Loose and Petra Schwille, "Biomimetic membrane systems to study cellular organization," *J. Struct. Biol.*, 168(1):143–151, 2009.

[Low *et al.*, 2004] Harry H. Low, Martin C. Moncrieffe, and Jan Löwe, "The crystal structure of ZapA and its modulation of FtsZ polymerisation," *J. Mol. Biol.*, 341(3):839–852, 2004.

[Löwe and Amos, 1998] Jan Löwe and Linda A. Amos, "Crystal structure of the bacterial cell-division protein FtsZ," *Nature*, 391(6663):203–206, jan 1998.

[Löwe and Amos, 1999] Jan Löwe and Linda A. Amos, "Tubulin-like protofilaments in Ca2+-induced FtsZ sheets," *EMBO J.*, 18(9):2364–2371, may 1999.

[Löwe and Amos, 2000] Jan Löwe and Linda A. Amos, "Helical Tubes of FtsZ from Methanococcus jannaschii," *Biol. Chem.*, 381(9-10):993–999, jan 2000.

[Lu *et al.*, 2000] Chunlin Lu, Mary Reedy, and Harold P. Erickson, "Straight and curved conformations of FtsZ are regulated by GTP hydrolysis," *J. Bacteriol.*, 182(1):164–170, jan 2000.

[Lutkenhaus *et al.*, 1980] J F Lutkenhaus, H Wolf-Watz, and W D Donachie, "Organization of genes in the ftsA-envA region of the Escherichia coli genetic map and identification of a new fts locus (ftsZ).," *J. Bacteriol.*, 142(2):615–20, may 1980.

[Lutkenhaus, 2007] Joe Lutkenhaus, "Assembly Dynamics of the Bacterial MinCDE System and Spatial Regulation of the Z Ring," *Annu. Rev. Biochem.*, 76(1):539–562, jun 2007.

[Lyu *et al.*, 2016] Zhixin Lyu, Carla Coltharp, Xinxing Yang, and Jie Xiao, "Influence of FtsZ GTPase activity and concentration on nanoscale Z-ring structure in vivo revealed by three-dimensional Superresolution imaging," *Biopolymers*, 105(10):725–734, oct 2016.

[Ma *et al.*, 1996] Xiaolan Ma, David W Ehrhardt, and William Margolin, "Colocalization of cell division proteins FtsZ and FtsA to cytoskeletal structures in living Escherichia coli cells by using green fluorescent protein," *Proc. Natl. Acad. Sci. U. S. A.*, 93(23):12998–13003, nov 1996.

[Ma and Margolin, 1999] Xiaolan Ma and William Margolin, "Genetic and functional analyses of the conserved C-terminal core domain of Escherichia coli FtsZ," *J. Bacteriol.*, 181(24):7531–7544, dec 1999.

[Maggi *et al.*, 2008] Silvia Maggi, Orietta Massidda, Giuseppe Luzi, Daniela Fadda, Luciano Paolozzi, and Patrizia Ghelardini, "Division protein interaction web: Identification of a phylogenetically conserved common interactome between Streptococcus pneumoniae and Escherichia coli," *Microbiology*, 154(10):3042–3052, 2008.

[Männik *et al.*, 2017] Jaana Männik, Matthew W. Bailey, Jordan C. O'Neill, and Jaan Männik, "Kinetics of large-scale chromosomal movement during asymmetric cell division in Escherichia coli," *PLoS Genet.*, 13(2):e1006638, feb 2017.

[Marchetti *et al.*, 2013] M. C. Marchetti, J. F. Joanny, S. Ramaswamy, T. B. Liverpool, J. Prost, Madan Rao, and R. Aditi Simha, "Hydrodynamics of soft active matter," *Rev. Mod. Phys.*, 85(3):1143–1189, 2013.

[Margolin, 2005] William Margolin, "FtsZ and the division of prokaryotic cells and organelles.," *Nat. Rev. Mol. Cell Biol.*, 6(11):862–871, 2005.

[Martos *et al.*, 2012] Ariadna Martos, Mercedes Jiménez, Germán Rivas, and Petra Schwille, "Towards a bottom-up reconstitution of bacterial cell division," *Trends Cell Biol.*, 22(12):634–643, 2012.

[Matov *et al.*, 2010] Alexandre Matov, Kathryn Applegate, Praveen Kumar, Claudio Thoma, Wilhelm Krek, Gaudenz Danuser, and Torsten Wittmann, "Analysis of microtubule dynamic instability using a plus-end growth marker," *Nat. Methods*, 7(9):761–768, 2010.

[Matsui *et al.*, 2014] Takashi Matsui, Xuerong Han, Jian Yu, Min Yao, and Isao Tanaka, "Structural change in FtsZ induced by Intermolecular interactions between Bound GTP and the T7 Loop," *J. Biol. Chem.*, 289(6):3501–3509, feb 2014.

[McQuillen and Xiao, 2020] Ryan McQuillen and Jie Xiao, "Insights into the Structure, Function, and Dynamics of the Bacterial Cytokinetic FtsZ-Ring.," *Annu. Rev. Biophys.*, 2020.

[Meier *et al.*, 2016] Elizabeth L. Meier, Shiva Razavi, Takanari Inoue, and Erin D. Goley, "A novel membrane anchor for FtsZ is linked to cell wall hydrolysis in Caulobacter crescentus," *Mol. Microbiol.*, 00:n/a–n/a, 2016.

[Mendes Pinto *et al.*, 2012] Inês Mendes Pinto, Boris Rubinstein, Andrei Kucharavy, Jay R. Unruh, and Rong Li, "Actin Depolymerization Drives Actomyosin Ring Contraction during Budding Yeast Cytokinesis," *Dev. Cell*, 22(6):1247–1260, 2012.

[Mendes Pinto *et al.*, 2013] Inês Mendes Pinto, Boris Rubinstein, and Rong Li, "Force to divide: Structural and mechanical requirements for actomyosin ring contraction," 2013.

[Mercier *et al.*, 2008] Romain Mercier, Marie Agnès Petit, Sophie Schbath, Stéphane Robin, Meriem El Karoui, Frédéric Boccard, and Olivier Espéli, "The MatP/matS Site-Specific System Organizes the Terminus Region of the E. coli Chromosome into a Macrodomain," *Cell*, 135(3):475–485, oct 2008.

[Mingorance *et al.*, 2001] Jesús Mingorance, Sonsoles Rueda, Paulino Gómez-Puertas, Alfonso Valencia, and Miguel Vicente, "Escherichia coli FtsZ polymers contain mostly GTP and have a high nucleotide turnover," *Mol. Microbiol.*, 41(1):83–91, dec 2001.

[Mitchison and Kirschner, 1984] Tim Mitchison and Marc Kirschner, "Dynamic instability of microtubule growth," *Nature*, 312(5991):237–242, 1984.

[Mohammadi *et al.*, 2009] Tamimount Mohammadi, Ginette E.J. Ploeger, Jolanda Verheul, Anouskha D. Comvalius, Ariadna Martos, Carlos Alfonso, Jan Van Marle, German Rivas, and Tanneke Den Blaauwen, "The GTPase activity of Escherichia coli FtsZ determines the magnitude of the FtsZ polymer bundling by ZapA in vitro," *Biochemistry*, 48(46):11056–11066, 2009.

[Mosyak, 2000] L Mosyak, "The bacterial cell-division protein ZipA and its interaction with an FtsZ fragment revealed by X-ray crystallography," *EMBO J.*, 19(13):3179–3191, jul 2000.

[Mukherjee and Lutkenhaus, 1998] Amit Mukherjee and Joe Lutkenhaus, "Dynamic assembly of FtsZ regulated by GTP hydrolysis," *EMBO J.*, 17(2):462–469, jan 1998.

[Nogales *et al.*, 1998] Eva Nogales, Sharon G. Wolf, and Kenneth H. Downing, "Structure of the $\alpha\beta$ tubulin dimer by electron crystallography," *Nature*, 391(6663):199–203, jan 1998.

[Oliva *et al.*, 2004] Maria A Oliva, Suzanne C Cordell, and Jan Löwe, "Structural insights into FtsZ protofilament formation.," *Nat. Struct. Mol. Biol.*, 11(12):1243–1250, 2004.

[Oliva *et al.*, 2003] María A. Oliva, Sonia Huecas, Juan M. Palacios, Jaime Martín-Benito, José M. Valpuesta, and José M. Andreu, "Assembly of archaeal cell division protein FtsZ and a GTPase-inactive mutant into double-stranded filaments," *J. Biol. Chem.*, 278(35):33562–33570, aug 2003.

[Ortiz *et al.*, 2015] Cristina Ortiz, Paolo Natale, Laura Cueto, and Miguel Vicente, "The keepers of the ring: Regulators of FtsZ assembly," *FEMS Microbiol. Rev.*, 40(1):57–67, 2015.

[Osawa *et al.*, 2008] Masaki Osawa, David E. Anderson, and Harold P. Erickson, "Reconstitution of contractile FtsZ rings in liposomes.," *Science*, 320(5877):792–794, may 2008.

[Osawa *et al.*, 2009] Masaki Osawa, David E Anderson, and Harold P Erickson, "Curved FtsZ protofilaments generate bending forces on liposome membranes," *EMBO J.*, 28(22):3476–3484, 2009.

[Osawa and Erickson, 2013] Masaki Osawa and Harold P Erickson, "Liposome division by a simple bacterial division machinery.," *Proc. Natl. Acad. Sci. U. S. A.*, 110(27):11000–4, 2013.

[Osteryoung and Vierling, 1995] Katherine W. Osteryoung and Elizabeth Vierling, "Conserved cell and organelle division," aug 1995.

[Ozyamak *et al.*, 2013] Ertan Ozyamak, Justin M. Kollman, and Arash Komeili, "Bacterial actins and their diversity," *Biochemistry*, 52(40):6928–6939, oct 2013.

[Pacheco-Gómez *et al.*, 2013] Raúl Pacheco-Gómez, Xi Cheng, Matthew R. R Hicks, Corinne J. J I. Smith, David I. I Roper, Stephen Addinall, Alison Rodger, and Timothy R. R Dafforn, "Tetramerization of ZapA is required for FtsZ bundling," *Biochem. J.*, 449(3):795–802, feb 2013.

[Pazos *et al.*, 2018] Manuel Pazos, Katharina Peters, Mercedes Casanova, Pilar Palacios, Michael VanNieuwenhze, Eefjan Breukink, Miguel Vicente, and Waldemar Vollmer, "Z-ring membrane anchors associate with cell wall synthases to initiate bacterial cell division," *Nat. Commun.*, 9(1):1–12, dec 2018.

[Perez *et al.*, 1999] Franck Perez, Georgios S. Diamantopoulos, Romaine Stalder, and Thomas E. Kreis, "CLIP-170 highlights growing microtubule ends in vivo," *Cell*, 96(4):517–527, 1999.

[Pichoff and Lutkenhaus, 2001] S. Pichoff and J. Lutkenhaus, "Escherichia coli division inhibitor mincd blocks septation by preventing Z-ring formation," *J. Bacteriol.*, 183(22):6630–6635, nov 2001.

[Pichoff *et al.*, 2018] Sebastien Pichoff, Shishen Du, and Joe Lutkenhaus, "Disruption of divisome assembly rescued by FtsN–FtsA interaction in Escherichia coli," *Proc. Natl. Acad. Sci. U. S. A.*, 115(29):E6855–E6862, 2018.

[Pichoff and Lutkenhaus, 2002] Sebastien Pichoff and Joe Lutkenhaus, "Unique and overlapping roles for ZipA and FtsA in septal ring assembly in Escherichia coli," *EMBO J.*, 21(4):685–693, 2002.

[Popp *et al.*, 2009] David Popp, Mitsusada Iwasa, Akihiro Narita, Harold P. Erickson, and Yuichiro Maéda, "FtsZ condensates: An in vitro electron microscopy study," *Biopolymers*, 91(5):340–350, may 2009.

[Prost *et al.*, 2015] J. Prost, F. Jülicher, and J. F. Joanny, "Active gel physics," feb 2015.

[Qian and Sheetz, 1991] Hong Qian and Michael P Sheetz, "Analysis of diffusion and flow in two-dimensional systems," *Biophys. J.*, 60(October):910–921, 1991.

[Ramirez-Diaz *et al.*, 2018] Diego A. Ramirez-Diaz, Daniela A. García-Soriano, Ana Raso, Jonas Mücksch, Mario Feingold, Germán Rivas, and Petra Schwille, "Treadmilling analysis reveals new insights into dynamic FtsZ ring architecture," *PLoS Biol.*, 16(5):e2004845, may 2018.

[Rico *et al.*, 2004] Ana Isabel Rico, Maria García-Ovalle, Jesús Mingorance, and Miguel Vicente, "Role of two essential domains of Escherichia coli FtsA in localization and progression of the division ring," *Mol. Microbiol.*, 53(5):1359–1371, jul 2004.

[Roach *et al.*, 2014] Elyse J. Roach, Matthew S. Kimber, and Cezar M. Khursigara, "Crystal structure and site-directed mutational analysis reveals key residues involved in Escherichia coli ZapA function," *J. Biol. Chem.*, 289(34):23276–23286, aug 2014.

[Rodrigues and Harry, 2012] Christopher D.A. Rodrigues and Elizabeth J. Harry, "The min system and nucleoid occlusion are not required for identifying the division site in bacillus subtilis but ensure its efficient utilization," *PLoS Genet.*, 8(3):e1002561, mar 2012.

[Romberg *et al.*, 2001] Laura Romberg, Martha Simon, and Harold P. Erickson, "Polymerization of FtsZ, a bacterial homolog of tubulin. Is assembly cooperative?," *J. Biol. Chem.*, 276(15):11743–11753, apr 2001.

[Roseboom *et al.*, 2018] Winfried Roseboom, Madhvi G. Nazir, Nils Y. Meiresonne, Tamimount Mohammadi, Jolanda Verheul, Hansuk Buncherd, Alexandre M.J.J. Bonvin, Leo J. de Koning, Chris G. de Koster, Luitzen De Jong, and Tanneke Den Blaauwen, "Mapping the contact sites of the escherichia coli division-initiating proteins FtsZ and ZapA by BAMG cross-linking and site-directed mutagenesis," *Int. J. Mol. Sci.*, 19(10):2928, sep 2018.

[Roth *et al.*, 2019] Sophie Roth, Ioana Gârlea, Mathijs Vleugel, Bela Mulder, and Marileen Dogterom, "Reconstitution of basic mitotic spindles in cell-like confinement," *bioRxiv*, page 770602, sep 2019.

[Rowlett and Margolin, 2014] Veronica Wells Rowlett and William Margolin, "3D-SIM Super-resolution of FtsZ and its membrane tethers in Escherichia coli cells," *Biophys. J.*, 107(8):L17–L20, oct 2014.

[Ruhnow *et al.*, 2011] Felix Ruhnow, David Zwicker, and Stefan Diez, "Tracking single particles and elongated filaments with nanometer precision," *Biophys. J.*, 100(11):2820–2828, 2011.

[Schaller *et al.*, 2010] Volker Schaller, Christoph Weber, Christine Semmrich, Erwin Frey, and Andreas R. Bausch, "Polar patterns of driven filaments," *Nature*, 467(7311):73–77, sep 2010.

[Schmoller *et al.*, 2011] Kurt M. Schmoller, Christine Semmrich, and Andreas R. Bausch, "Slow down of actin depolymerization by cross-linking molecules," *J. Struct. Biol.*, 173(2):350–357, feb 2011.

[Schoenemann and Margolin, 2017] Kara M. Schoenemann and William Margolin, "Bacterial Division: FtsZ Treadmills to Build a Beautiful Wall," *Curr. Biol.*, 27(8):R301–R303, 2017.

[Schumacher *et al.*, 2017] Maria A. Schumacher, Kuo-hsiang Huang, Wenjie Zeng, and Anuradha Janakiraman, "Structure of the Z ring associated protein , ZapD , bound to the C-terminal domain of the tubulin-like protein , FtsZ , suggests mechanism of Z ring stabilization through FtsZ crosslinking," *J. Biol. Chem.*, 292(9):1–25, mar 2017.

[Schumacher *et al.*, 2016] Maria A Schumacher, Wenjie Zeng, Kuo Hsiang Huang, Lukasz Tchorzewski, and Anuradha Janakiraman, "Structural and functional analyses reveal insights into the molecular properties of the Escherichia coli Z ring stabilizing protein, ZapC," *J. Biol. Chem.*, 291(5):2485–2498, jan 2016.

[Sherratt *et al.*, 2010] David J. Sherratt, Lidia K. Arciszewska, Estelle Crozat, James E. Graham, and Ian Grainge, "The Escherichia coli DNA translocase FtsK," apr 2010.

[Si *et al.*, 2013] Fangwei Si, Kimberly Busiek, William Margolin, and Sean X. Sun, "Organization of FtsZ filaments in the bacterial division ring measured from polarized fluorescence microscopy," *Biophys. J.*, 105(9):1976–1986, nov 2013.

[Singla, 2014] Nishu Singla, "Motion Detection Based on Frame Difference Method," *Int. J. Inf. Comput. Technol.*, 4(15):1559–1565, 2014.

[Small *et al.*, 2007] Elaine Small, Rachel Marrington, Alison Rodger, David J. Scott, Katherine Sloan, David Roper, Timothy R. Dafforn, and Stephen G. Addinall, "FtsZ Polymer-bundling by the Escherichia coli ZapA Orthologue, YgfE, Involves a Conformational Change in Bound GTP," *J. Mol. Biol.*, 369(1):210–221, may 2007.

[Söderström *et al.*, 2016] Bill Söderström, Kiavash Mirzadeh, Stephen Toddo, Gunnar von Heijne, Ulf Skoglund, and Daniel O Daley, "Coordinated disassembly of the divisome complex in Escherichia coli.," *Mol. Microbiol.*, pages 1–43, 2016.

[Soderstrom *et al.*, 2014] Bill Soderstrom, Karl Skoog, Hans Blom, David S. Weiss, Gunnar von Heijne, and Daniel O. Daley, "Disassembly of the divisome in Escherichia coli: Evidence that FtsZ dissociates before compartmentalization," *Mol. Microbiol.*, 92(1):1–9, 2014.

[Sossong *et al.*, 1999] Thomas M. Sossong, Michael R. Brigham-Burke, Preston Hensley, and Kenneth H. Pearce, "Self-activation of guanosine triphosphatase activity by oligomerization of the bacterial cell division protein FtsZ," *Biochemistry*, 38(45):14843–14850, 1999.

[Squyres *et al.*, 2020] Georgia R Squyres, Matthew J Holmes, Sarah R Barger, Betheney R Pennycook, Joel Ryan, Victoria T Yan, and Ethan C Garner, "Dynamics of bacterial cell division: Z ring condensation is essential for cytokinesis," *bioRxiv*, page 2020.06.30.180737, 2020.

[Stricker and Erickson, 2003] Jesse Stricker and Harold P. Erickson, "In vivo characterization of Escherichia coli ftsZ mutants: Effects on Z-ring structure and function," *J. Bacteriol.*, 185(16):4796–4805, aug 2003.

[Stricker *et al.*, 2002] Jesse Stricker, Paul Maddox, E. D. Salmon, and Harold P. Erickson, "Rapid assembly dynamics of the Escherichia coli FtsZ-ring demonstrated by fluorescence recovery after photobleaching," *Proc. Natl. Acad. Sci. U. S. A.*, 99(5):3171–3175, 2002.

[Szwedziak *et al.*, 2014] Piotr Szwedziak, Qing Wang, Tanmay A M Bharat, Matthew Tsim, and Jan Löwe, "Architecture of the ring formed by the tubulin homologue FtsZ in bacterial cell division.," *Elife*, 3:e04601, dec 2014.

[Theile *et al.*, 2013] Christopher S Theile, Martin D Witte, Annet E M Blom, Lenka Kundrat, Hidde L Ploegh, and Carla P Guimaraes, "Site-specific N-terminal labeling of proteins using sortase-mediated reactions.," *Nat. Protoc.*, 8(9):1800–7, sep 2013.

[Treuner-Lange and Søgaard-Andersen, 2014] Anke Treuner-Lange and Lotte Søgaard-Andersen, "Regulation of cell polarity in bacteria," 2014.

[Van De Putte *et al.*, 1964] P. Van De Putte, Jeannette Van Dillewijn, and A. Rörsch, "The selection of mutants of escherichia coli with impaired cell division at elevated temperature," *Mutat. Res. - Fundam. Mol. Mech. Mutagen.*, 1(2):121–128, jul 1964.

[Van den Ent *et al.*, 2002] Fusinita Van den Ent, Jakob Møller-Jensen, Linda A. Amos, Kenn Gerdes, and Jan Löwe, "F-actin-like filaments formed by plasmid segregation protein ParM," *EMBO J.*, 21(24):6935–6943, 2002.

[van Ginkel *et al.*, 1999] M. van Ginkel, J. van de Weijer, L.J. van Vliet, and P.W. Verbeek, "Curvature estimation from orientation fields," In *Proc. Scand. Conf. Image Anal.*, pages 545–551, 1999.

[Wagstaff *et al.*, 2017] James M. Wagstaff, Matthew Tsim, María A. Oliva, Alba García-Sanchez, Danguole Kureisaite-Ciziene, José Manuel Andreu, and Jan Löwe, "A polymerization-associated structural switch in ftsz that enables treadmilling of model filaments," *MBio*, 8(3), 2017.

[Wang *et al.*, 1997] Xunde Wang, Jian Huang, Amit Mukherjee, Chune Cao, and Joe Lutkenhaus, "Analysis of the interaction of FtsZ with itself, GTP, and FtsA," *J. Bacteriol.*, 179(17):5551–5559, sep 1997.

[Watanabe and Mitchison, 2002] Naoki Watanabe and Timothy J. Mitchison, "Single-molecule speckle analysis of actin filament turnover in lamellipodia," *Science (80-.).*, 295(5557):1083–1086, 2002.

[Waterman-Storer *et al.*, 1998] Clare M. Waterman-Storer, Arshad Desai, J. Chloe Bulinski, and E. D. Salmon, "Fluorescent speckle microscopy, a method to visualize the dynamics of protein assemblies in living cells," *Curr. Biol.*, 8(22):1227–1230, nov 1998.

[Whitley *et al.*, 2020] Kevin D Whitley, Calum Jukes, Nicholas Tregidgo, Eleni Karinou, Pedro Almada, Cees Dekker, and Séamus Holden, "FtsZ treadmilling is essential for Z-ring condensation and septal constriction initiation in bacterial cell division," *bioRxiv*, page 2020.07.01.182006, jul 2020.

[Woldemeskel *et al.*, 2017] Selamawit Abi Woldemeskel, Ryan McQuillen, Alex M. Hessel, Jie Xiao, and Erin D. Goley, "A conserved coiled-coil protein pair focuses the cytokinetic Z-ring in Caulobacter crescentus," *Mol. Microbiol.*, 105(5):721–740, sep 2017.

[Wu and Errington, 2004] Ling Juan Wu and Jeff Errington, "Coordination of cell division and chromosome segregation by a nucleoid occlusion protein in Bacillus subtilis," *Cell*, 117(7):915–925, 2004.

[Wu *et al.*, 2009] Ling Juan Wu, Shu Ishikawa, Yoshikazu Kawai, Taku Oshima, Naotake Ogasawara, and Jeff Errington, "Noc protein binds to specific DNA sequences to coordinate cell division with chromosome segregation," *EMBO J.*, 28(13):1940–1952, jul 2009.

[Xiao and Goley, 2016] Jie Xiao and Erin D Goley, "Redefining the roles of the FtsZ-ring in bacterial cytokinesis," *Curr. Opin. Microbiol.*, 34:90–96, 2016.

[Yang *et al.*, 2017] Xinxing Yang, Zhixin Lyu, Amanda Miguel, Ryan Mcquillen, Kerwyn Casey Huang, and Jie Xiao, "GTPase activity–coupled treadmilling of the bacterial tubulin FtsZ organizes septal cell wall synthesis," *Science (80-.).*, 355(6326):744–747, feb 2017.

[Yao *et al.*, 2017] Qing Yao, Andrew I Jewett, Yi-Wei Chang, Catherine M Oikonomou, Morgan Beeby, Cristina V Iancu, Ariane Briegel, Debnath Ghosal, and Grant J Jensen, "Short FtsZ filaments can drive asymmetric cell envelope constriction at the onset of bacterial cytokinesis," *EMBO J.*, 36(11):e201696235, jun 2017.